

**A THEORETICAL STUDY ON SALT-BRIDGE
IN AQUEOUS SOLUTION**

Police Captain Supaporn Chaiyapongs

**A Thesis Submitted in Partial Fulfillment of the Requirements
for the Degree of Doctor of Philosophy in Chemistry**

Suranaree University of Technology

Academic Year 2004

ISBN 974-533-423-5

การศึกษาสะพานเกลือในสารละลายน้ำโดยวิธีทางทฤษฎี

ร้อยตำรวจเอกหญิง สุภาพร ไชยพงษ์

วิทยานิพนธ์นี้เป็นส่วนหนึ่งของการศึกษาตามหลักสูตรปริญญาวิทยาศาสตรดุษฎีบัณฑิต

สาขาวิชาเคมี

มหาวิทยาลัยเทคโนโลยีสุรนารี

ปีการศึกษา 2547

ISBN 974-533-423-5

**A THEORETICAL STUDY ON SALT-BRIDGE
IN AQUEOUS SOLUTION**

Suranaree University of Technology has approved this thesis submitted in partial fulfillment of the requirements for the Degree of Doctor of Philosophy.

Thesis Examining Committee

M. Tangsathitkulchai

(Asst. Prof. Dr. Malee Tangsathitkulchai)

Chairperson

K. Sagarik

(Prof. Dr. Kritsana Sagarik)

Member (Thesis Advisor)

S. Hannongbua

(Assoc. Prof. Dr. Supot Hannongbua)

Member

A. Tongraar

(Assoc. Prof. Dr. Anan Tongraar)

Member

Visit Vao

(Asst. Prof. Dr. Visit Vao-Soongnern)

Member

P. Suebka

(Assoc. Prof. Dr. Prasart Suebka)

S. Sujitjorn

(Assoc. Prof. Dr. Sarawut Sujitjorn)

Vice Rector for Academic Affairs

Dean of Institute of Science

สุภาพร ไชยพงษ์ : การศึกษาสะพานเกลือในสารละลายน้ำโดยวิธีทางทฤษฎี
(A THEORETICAL STUDY ON SALT-BRIDGE IN AQUEOUS
SOLUTION) อาจารย์ที่ปรึกษา : ศาสตราจารย์ ดร.กฤษณะ สาคริก, 102 หน้า.
ISBN 974-533-423-5

การศึกษาโครงสร้างและเสถียรภาพของสะพานเกลือ (salt-bridge) ในสารละลายน้ำ ดำเนินการโดยใช้สารประกอบเชิงซ้อน (complex) ที่เกิดจากการรวมตัวของไอออนกวานิดีนียม (guanidinium ion; Gdm^+) และไอออนฟอร์มเมต (formate ion; FmO^-) เป็นแบบจำลอง โดยเริ่มจากการสร้างและทดสอบศักย์ระหว่างโมเลกุลเทสท์พาร์ทิเคิล (Test-particle model; T-model) เพื่อใช้อธิบายอันตรกิริยาในสารประกอบเชิงซ้อน $Gdm^+ - H_2O$ $FmO^- - H_2O$ และ $Gdm^+ - FmO^-$ จากนั้นประยุกต์ศักย์ระหว่างโมเลกุลที่คำนวณได้กับการจำลองโมเลกุลพลวัต (molecular dynamics (MD) simulations) ในสารละลายน้ำที่อุณหภูมิ 298 K สมบัติของสารละลายที่สนใจได้แก่โครงสร้างสามมิติและการกระจายพลังงานที่โครงข่ายพันธะไฮโดรเจน (H-bond networks) ของน้ำในชั้นไฮเดรชันที่ 1 (the first hydration shell) ที่อยู่ล้อมรอบไอออน Gdm^+ FmO^- และสารประกอบเชิงซ้อน $Gdm^+ - FmO^-$ ในงานวิจัยชิ้นนี้มีการสร้างแผนภาพการแจกแจงความน่าจะเป็น (probability distribution (PD) map) ในเชิงโครงสร้างและพลังงานของโครงข่ายพันธะไฮโดรเจน ซึ่งใช้อธิบายและวิเคราะห์เสถียรภาพตลอดจนพฤติกรรมพลวัต (dynamic behavior) ของโมเลกุลน้ำในชั้นไฮเดรชันที่ 1 ที่ล้อมรอบตัวถูกละลาย (solute) ผลการศึกษาพบว่าโมเลกุลน้ำในชั้นไฮเดรชันที่ 1 สร้างโครงข่ายพันธะไฮโดรเจนล้อมรอบสารประกอบเชิงซ้อน $Gdm^+ - FmO^-$ ชนิดชิดกัน (close-contact) เสริมให้เกิดเสถียรภาพในการรวมตัวเป็นคู่อิออน (ion-pair) เพิ่มขึ้น ในขณะที่โครงข่ายพันธะไฮโดรเจนของน้ำหากแทรกอยู่ระหว่างไอออนของสารประกอบเชิงซ้อน $Gdm^+ - FmO^-$ ชนิดแยกโดยตัวทำละลาย (solvent-separated) จะทำให้เสถียรภาพการรวมตัวเป็นคู่อิออนลดลงทำให้ไอออนเกิดการแยกตัวออกจากกันเป็นไอออนอิสระในที่สุด ผลการศึกษานี้แสดงให้เห็นด้วยว่าหากต้องการความเข้าใจอย่างลึกซึ้งเกี่ยวกับโครงสร้างและเสถียรภาพของคู่อิออนในสารละลายน้ำ แบบจำลองที่นำมาใช้ในการคำนวณต้องพิจารณาโมเลกุลน้ำทุกตัวที่เกี่ยวข้องในระบบ (explicit water molecules) เสมอ

สาขาวิชาเคมี
ปีการศึกษา 2547

ลายมือชื่อนักศึกษา สุภาพร ไชยพงษ์
ลายมือชื่ออาจารย์ที่ปรึกษา กฤษณะ สาคริก

SUPAPORN CHAIYAPONGS : A THEORETICAL STUDY ON SALT-
BRIDGE IN AQUEOUS SOLUTION. THESIS ADVISOR : PROF.
KRITSANA SAGARIK, Ph.D. 102 PP. ISBN 974-533-423-5

GUANIDINIUM/FORMATE/SALT-BRIDGE/ION-PAIR/HYDRATION

Structures and stability of salt-bridges in aqueous solutions were investigated using a complex formed from the guanidinium (Gdm^+) and formate (FmO^-) ions as a model system. The Test-particle model (T-model) potentials to describe the interactions in the Gdm^+ - H_2O , FmO^- - H_2O and Gdm^+ - FmO^- complexes were constructed, tested and applied in molecular dynamics (MD) simulations of the aqueous solutions at 298 K. The three-dimensional structures and energetic of the hydrogen-bond (H-bond) networks of water in the first hydration shells of the Gdm^+ and FmO^- ions, as well as the Gdm^+ - FmO^- complex, were visualized and analyzed using various probability distribution (PD) maps. The structures of the average potential energy landscapes at the H-bond networks were employed to characterize the stability and dynamic behavior of water molecules in the first hydration shells of the solutes. It was observed that water molecules in the first hydration shell of the close-contact Gdm^+ - FmO^- complex form associated H-bond networks, which introduce a net stabilization effect to the ion-pair, whereas those in the interstitial H-bond network destabilize and break the solvent-separated Gdm^+ - FmO^- complex. The present results showed that, in order to provide complete insights into the structures and stability of ion-pairs in aqueous solutions, explicit water molecules have to be included in the model calculations.

School of Chemistry

Academic Year 2004

Student's Signature

Advisor's Signature

S. Chaiyapongs

K. Sagarik

ACKNOWLEDGEMENTS

I would like to express my sincerest gratitude to my thesis advisor, Prof. Dr. Kritsana Sagarik for his guidance, valuable suggestions, encouragement and kind help throughout the course of my study.

I would like to express my special thanks Ramkhamhaeng University (RU) for allowing me to continue my advanced study.

I would like to acknowledge the financial support from the Commission on Higher Education (CHE), Thailand's Ministry of Education.

Special thanks are extended to the School of Chemistry, Suranaree University of Technology (SUT) for providing computer facilities.

I wish to express my sincere thanks to Assoc. Prof. Dr. Anan Tongraar and Asst. Prof. Dr. Visit Vao-soongnern for their kindness and help throughout the study.

I also would like to express my sincere thanks to the thesis examining committee for their valuable suggestions and comments.

Thanks to all of my friends in the computational chemistry research group for their friendship and help.

Finally, I would like to take this opportunity to express my deepest gratitude to my parents, sisters and brothers for their love, understanding, and encouragement.

Supaporn Chaiyapongs

CONTENTS

	Page
ABSTRACT IN THAI.....	I
ABSTRACT IN ENGLISH.....	II
ACKNOWLEDGEMENTS.....	III
CONTENTS.....	IV
LIST OF TABLES.....	VI
LIST OF FIGURES.....	VII
LIST OF ABBREVIATION.....	IX
CHAPTERS	
I INTRODUCTION.....	1
II RESEARCH METHODOLOGY.....	10
2.1 The T-model potentials.....	10
2.2 MD simulations.....	13
2.3 Computer softwares and facilities.....	19
III RESULTS AND DISCUSSION.....	20
3.1 Equilibrium structures in the gas phase.....	20
3.1.1 The $\text{Gdm}^+ \text{-H}_2\text{O}$ complex.....	20
3.1.2 The $\text{FmO}^- \text{-H}_2\text{O}$ complex.....	23
3.1.3 The $\text{Gdm}^+ \text{-FmO}^-$ complex.....	25

CONTENTS (Continued)

	Page
3.2 MD simulations.....	28
3.2.1 [Gdm ⁺] _{aq}	31
3.2.2 [FmO ⁻] _{aq}	38
3.2.3 [Gdm ⁺ – FmO ⁻] _{aq}	43
IV CONCLUSION	60
REFERENCES	64
APPENDICES	
Appendix A Twenty Common Amino Acids.....	73
Appendix B Supplementary Diagrams for Research Methodology.....	74
Appendix C Supplementary Results.....	76
Appendix D Article in Proceeding of ANSCSE-8.....	97
CURRICULUM VITAE	102

LIST OF TABLES

Table		Page
3.1	MD simulations parameters and the results for $[\text{Gdm}^+]_{\text{aq}}$, $[\text{FmO}^-]_{\text{aq}}$ and $[\text{Gdm}^+ - \text{FmO}^-]_{\text{aq}}$	29
3.2	$\tau_{\text{type X, max}}$ and some $\langle \Delta E_{\text{aq}}^{\text{T}} \rangle$ obtained from MD simulations of $[\text{Gdm}^+]_{\text{aq}}$, $[\text{FmO}^-]_{\text{aq}}$ and $[\text{Gdm}^+ - \text{FmO}^-]_{\text{aq}}$	30
C.1	Optimized geometries of the Gdm^+ , FmO^- ions.....	76
C.2	The T-model parameters for Gdm^+ , FmO^- and water.....	77

LIST OF FIGURES

Figure		Page
1.1	Equilibrium structures of the $\text{MGdm}^+ - \text{AcO}^-$ complexes.....	3
1.2	Structures of the $\text{Gdm}^+ - \text{FmO}^-$ complexes.....	4
2.1	Atom numbering systems of the $\text{Gdm}^+ - \text{FmO}^-$ 1 : 1 complex.....	15
3.1	Equilibrium structures and interaction energies of the $\text{Gdm}^+ - \text{H}_2\text{O}$ 1 : 1 complex in the gas phase computed from the T-model potentials..	22
3.2	Equilibrium structures and interaction energies of the $\text{FmO}^- - \text{H}_2\text{O}$ 1 : 1 complex in the gas phase computed from the T-model potentials..	24
3.3	Equilibrium structures and interaction energies of the $\text{Gdm}^+ - \text{FmO}^-$ 1 : 1 complex in the gas phase computed from the T-model potentials..	26
3.4	Selected structure and energetic results obtained from MD- $[\text{Gdm}^+]_{\text{aq}}$..	32
3.5	Selected structure and energetic results obtained from MD- $[\text{FmO}^-]_{\text{aq}}$..	39
3.6	Selected structure and energetic results obtained from MD- $[\text{Gdm}^+ - \text{FmO}^-]_{\text{aq, frozen}}^{\text{R}=3.9}$ and MD- $[\text{Gdm}^+ - \text{FmO}^-]_{\text{aq, free}}^{\text{R}=3.9}$..	44
3.7	Selected structure and energetic results obtained from MD- $[\text{Gdm}^+ - \text{FmO}^-]_{\text{aq, frozen}}^{\text{R}=6.3}$..	53
A.1	Twenty common amino acids.....	73
B.1	Basic steps in the construction of the T-model potential.....	74
B.2	Schematic diagram for MD simulations of N-particle system.....	75

LIST OF FIGURES (Continued)

Figure	Page
C.1 $g(R)$ obtained from MD- $[Gdm^+]_{aq}$	78
C.2 The PDO, PDH, AWPD, WWPD and AW-WWPD maps obtained from MD- $[Gdm^+]_{aq}$	79
C.3 $g(R)$ obtained from MD- $[FmO^-]_{aq}$	81
C.4 The PDO, PDH, AWPD, WWPD and AW-WWPD maps obtained from MD- $[FmO^-]_{aq}$	82
C.5 $g(R)$ obtained from MD- $[Gdm^+ - FmO^-]_{aq, frozen}^{R=3.9}$	84
C.6 The PDO, PDH, AWPD, WWPD and AW-WWPD maps obtained from MD- $[Gdm^+ - FmO^-]_{aq, frozen}^{R=3.9}$	86
C.7 $g(R)$ obtained from MD- $[Gdm^+ - FmO^-]_{aq, free}^{R=3.9}$	88
C.8 $g(R)$ obtained from MD- $[Gdm^+ - FmO^-]_{aq, frozen}^{R=6.3}$	91
C.9 The PDO, PDH, AWPD, WWPD and AW-WWPD maps obtained from MD- $[Gdm^+ - FmO^-]_{aq, frozen}^{R=6.3}$	93
C.10 $g(R)$ obtained from MD- $[Gdm^+ - FmO^-]_{aq, free}^{R=6.3}$	95

LIST OF ABBREVIATIONS

°	=	degree
Å	=	angström
kJ/mol	=	kilo Joule/mole
D	=	Debye
K	=	Kelvin
ps	=	pico second
Arg	=	Arginine
Asp	=	Aspartate
Glu	=	Glutamate
Lys	=	Lysine
DNA	=	Deoxyribonucleic acid
PDB	=	Protein Data Bank
AcO ⁻	=	Acetate
COO ⁻	=	Carboxylate
FmO ⁻	=	Formate
Gdm ⁺	=	Guanidinium
MAm ⁺	=	Methylammonium
MGdm ⁺	=	Methylguanidinium
Na ⁺	=	Sodium ion
Cl ⁻	=	Chloride ion

LIST OF ABBREVIATIONS (Continued)

CCl ₄	=	Carbon tetrachloride
DMSO	=	Dimethyl sulfoxide
H ₂ O	=	Water
BA	=	Benzoic acid
(BA) ₂	=	Benzoic acid dimer
NH ₂ OH	=	Hydroxylamine
(NH ₂ OH) ₂	=	Hydroxylamine dimer
TBA · AcO ⁻	=	Tetrabutylammonium acetate
AM1	=	Austin Model 1
TIP3P	=	Transferable Intermolecular Potential with 3-Point model
OPLS	=	Optimized Potentials for Liquid Simulations
H-bond	=	Hydrogen bond
NMR	=	Nuclear Magnetic Resonance
PES	=	Potential Energy Surface
PMF	=	Potential of Mean Force
SCRf	=	Self-Consistent Reaction Field
SCF	=	Self-Consistent Field
CHelpG	=	CHarges from ELectrostatic Potentials using a Grid based method
BSSE	=	Basis Set Superposition Error

LIST OF ABBREVIATIONS (Continued)

HF	=	Hartree-Fock
HF/6-311++G(d,p)	=	Hartree-Fock approximation with 6-311++G (d,p) basis set
MP2	=	Second-order Møller-Plesset
MP2/6-311++G(d,p)	=	Second-order Møller-Plesset theory with 6-311++G(d,p) basis set
MP2CP	=	MP2 calculations with the counterpoise corrections
ΔE_{MP2}	=	MP2 interaction energy
ΔE_{MP2CP}	=	MP2CP interaction energy
T-model	=	Test-particle model
$\Delta E_{\text{T-model}}$	=	T-model interaction energy
ΔE_{SCF}^1	=	First-order interaction energy
ΔE^r	=	Higher-order energy term
ΔE_{REP}	=	Exchange repulsion energy
ΔE_{ES}	=	Electrostatic energy
B(T)	=	Second virial coefficient
$[\text{Gdm}^+ - \text{TBA} \cdot \text{AcO}^-]_{\text{DMSO}}$	=	$\text{Gdm}^+ - \text{TBA} \cdot \text{AcO}^-$ in DMSO solution
$[\text{MGdm}^+ - \text{AcO}^-]_{\text{aq}}$	=	$\text{MGdm}^+ - \text{AcO}^-$ in aqueous solution
$[\text{NaCl}]_{\text{aq}}$	=	NaCl in aqueous solution

LIST OF ABBREVIATIONS (Continued)

$[\text{Gdm}^+]_{\text{aq}}$	=	Gdm^+ in aqueous solution
$[\text{FmO}^-]_{\text{aq}}$	=	FmO^- in aqueous solution
$[\text{Gdm}^+ - \text{FmO}^-]_{\text{aq}}$	=	$\text{Gdm}^+ - \text{FmO}^-$ in aqueous solution
L	=	Simulation box length
MC	=	Monte Carlo
MD	=	Molecular Dynamics
NVE-MD	=	Microcanonical Ensemble-MD simulations
MD- $[\text{Gdm}^+]_{\text{aq}}$	=	MD simulations of Gdm^+ in aqueous solution
MD- $[\text{FmO}^-]_{\text{aq}}$	=	MD simulations of FmO^- in aqueous solution
MD- $[\text{Gdm}^+ - \text{FmO}^-]_{\text{aq}}$	=	MD simulations of $\text{Gdm}^+ - \text{FmO}^-$ in aqueous solution
$R_{\text{C}\dots\text{C}}$	=	Distance between the carbon atoms of Gdm^+ and FmO^-
MD- $[\text{Gdm}^+ - \text{FmO}^-]_{\text{aq, frozen}}^{\text{R}=\text{X}}$	=	MD- $[\text{Gdm}^+ - \text{FmO}^-]_{\text{aq}}$ with $R_{\text{C}\dots\text{C}} = \text{X}$
MD- $[\text{Gdm}^+ - \text{FmO}^-]_{\text{aq, free}}^{\text{R}=\text{X}}$	=	MD- $[\text{Gdm}^+ - \text{FmO}^-]_{\text{aq}}$ with $R_{\text{C}\dots\text{C}} = \text{X}$ only in the first equilibration step
$g(\text{R})$	=	Atom-atom pair correlation function
$n(\text{R})$	=	Average running coordination number
R_{max}	=	Position of the maximum of the main peak of $g(\text{R})$
$n(R_{\text{max}})$	=	Running coordination number of $g(\text{R})$ at R_{max}

LIST OF ABBREVIATIONS (Continued)

PD	=	Probability distribution
PDO	=	The oxygen probability distribution of water
PDH	=	The hydrogen probability distribution of water
AWPD	=	The average solute-solvent interaction energy probability distribution
WWPD	=	The average solvent-solvent interaction energy probability distribution
AW-WWPD	=	The total-average interaction energy probability distribution
$\langle E_{\text{aq}}^{\text{pot}} \rangle$	=	The average potential energy of aqueous solutions
$\langle E_{\text{aq}}^{\text{solv-solv}} \rangle$	=	The average solute-solvent interaction energies
$\langle E_{\text{aq}}^{\text{solv-solv}} \rangle$	=	The average solvent-solvent interaction energies
$\langle E_{\text{aq}}^{\text{solv-solv}} \rangle$	=	The average solute-solute interaction energies
$\langle E_{\text{aq}}^{\text{L}} \rangle$	=	The transition energy barrier of the longitudinal profile line
$\langle E_{\text{aq}}^{\text{T}} \rangle$	=	The transition energy barrier of the transverse profile line
A-H...B	=	H-bond between the proton donor A and acceptor B
$\tau_{\text{A-H}\cdots\text{B}, \text{max}}$	=	The longest H-bond lifetime between the proton donor A and acceptor B
$\tau_{\text{type X}, \text{max}}$	=	The longest H-bond lifetime of water molecule at the H-bond network type X

CHAPTER I

INTRODUCTION

Proteins are important polymer molecules in living organisms. They are assembled from amino acids which are connected together by peptide bonds. There are twenty naturally occurring amino acids (see Figure A.1 in Appendix A) which are distinguished by the chemical nature of their side-chains (Van Holde, Johnson, and Ho, 1998). Salt-bridge or ion-pair interaction is defined as the interaction between ionized functional groups with opposite charges. They contact each other approximately at their van der Waals radii. The resulting salt-bridge is stabilized by attractive electrostatic force which may have some hydrogen bond (H-bond) characters (Nakamura, 1999). In proteins, for example salt-bridges are formed when a positively charged side-chain of arginine (Arg) or lysine (Lys) interacts with a negatively charged side-chain of aspartate (Asp) or glutamate (Glu) (Barlow and Thornton, 1983).

Salt-bridges or ion-pairs have been of interest since, on average, one-third of the charged residues in proteins are involved in ion-pairs, and about 76 % of these play important roles in stabilization of the protein secondary and tertiary structures (Barlow and Thornton, 1983; Gandini, Gogioso, Bolognesi, and Bordo, 1996). Due to strong electrostatic interaction, salt-bridges have been recognized to have other specific functions to perform, especially in globular proteins (Barlow and Thornton, 1983). They were suggested, for example, to act as active mediator for molecular

recognition in enzymes and proteins (Riordan, McElvany, and Borders, 1977; Kirsch et al., 1984; Tormo et al., 1994). About 40 % of ion-pairs within proteins involve arginine-carboxylate (Arg-COO⁻) interactions (Barlow and Thornton, 1983; Singh, Thornton, Snarey, and Campbell, 1987), *e.g.*, the arginine-glutamate (Arg-Glu) and arginine-aspartate (Arg-Asp) side-chain interactions. Therefore, the guanidinium (Gdm⁺) and formate (FmO⁻) ions (Fülscher and Mehler, 1988; Zheng and Ornstein, 1996), as well as the methylguanidinium (MGdm⁺) and acetate (AcO⁻) ions (Barril, Alemán, Orozco, and Luque, 1998; Melo et al., 1999), have been frequently chosen as model systems in the studies of ion-pair interactions between side-chains of proteins.

According to a systematic geometric analysis of the Brookhaven Protein Data Bank (PDB), the stereochemistry of the side-chain H-bonds of proteins was pointed out to be characterized by at least three factors; (a) the electronic configuration of the H-bond acceptor atoms; (b) the steric accessibility of the H-bond donor atoms and; (c) the conformation of amino acid side-chains (Ippolito, Alexander, and Christianson, 1990). Singh et al. (1987) categorized the geometries of Arg-COO⁻ interactions by observing the frequencies that the interacting pairs adopt in 37 high-resolution protein structures. They found that the most preferential structure for Arg-COO⁻ interaction is a planar structure, in which a single N-H···O-C H-bond is the most common type of interaction; whereas double N-H···O-C H-bonds are also frequently found. Moreover, the “side-on” doubly H-bonded structures seem to be more favorable than the “end-on” structures. Mitchell, Thornton, Singh, and Price (1992) evaluated intramolecular and intermolecular Arg-Asp interactions by extracting structural information from protein coordinate data, in comparison with the results of the

electrostatic modeling of $\text{MGdm}^+ - \text{AcO}^-$ complex. The results showed that the side-on configuration is more favored for the intramolecular interactions. Whereas the end-on configuration is more preferred for the intermolecular interactions. The geometrical constraints were suggested to be the main reason for the discrepancy. Additionally, it was also reported that, the side-on structure is slightly lower in energy than the end-on structure. Equilibrium structures of the $\text{MGdm}^+ - \text{AcO}^-$ complexes are shown in Figure 1.1.

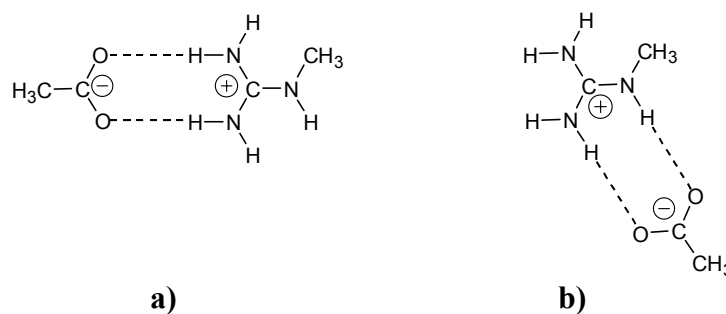


Figure 1.1 Equilibrium structures of the $\text{MGdm}^+ - \text{AcO}^-$ complexes.

a) The end-on structure.

b) The side-on structure.

Several theoretical investigations were conducted on model salt-bridges in the gas phase, aqueous and non-aqueous solutions, using both continuum (Zheng and Ornstein, 1996; Barril et al., 1998) and explicit solvent models (Saigal and Pranata, 1997; Rozanska and Chipot, 2000). The stability of the side-on and end-on configurations in the gas phase was examined by *ab initio* calculations, using the $\text{MGdm}^+ - \text{AcO}^-$ complex as an example (Barril et al., 1998; Melo et al., 1999). It was reported that the side-on structure is more stable than the end-on structure (Barril et al., 1998; Melo et al., 1999).

Due to the possibility of proton transfer in H-bonds, the Arg-Glu and Arg-Asp complexes can take both neutral and zwitterionic forms. In order to obtain information on the relative stability of these two structures in the gas phase as well as in polar and nonpolar solvents, Zheng and Ornstein (1996) applied *ab initio* calculations, in combination with reaction field theory, on the $\text{Gdm}^+ - \text{FmO}^-$ complex. Figure 1.2 shows the neutral and zwitterionic H-bond complexes.

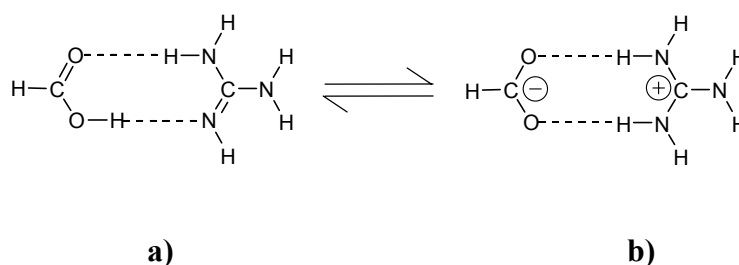


Figure 1.2 Structures of the $\text{Gdm}^+ - \text{FmO}^-$ complexes.

a) The neutral H-bond complex.

b) The zwitterionic H-bond complex.

The results of *ab initio* calculations (Zheng and Ornstein, 1996) revealed that the neutral H-bond complex is considerably more stable than the zwitterionic H-bond complex in the gas phase and only slightly more stable in nonpolar solvent, such as CCl_4 . In contrast, the zwitterionic H-bond complex is significantly more stable in polar solvents, such as dimethyl sulfoxide (DMSO) and water. Based on the results of *ab initio* calculations with the self-consistent reaction field (SCRF) on the $\text{MGdm}^+ - \text{AcO}^-$ complex, it was confirmed that, in the gas phase, the neutral form is more stable than the zwitterionic one (Barril et al., 1998; Melo et al., 1999). It was also illustrated that, the preference of the ion-pairs over the neutral complexes in polar

solvents is considerably reduced or even reversed in very low dielectric media, such as chloroform (Barril et al., 1998). Through an explicit water model, molecular dynamics (MD) free energy calculations were performed on the MGdm⁺-AcO⁻ complex in aqueous solution ($[MGdm^+ - AcO^-]_{aq}$), using various approaches to take into account long-range electrostatic interaction (Rozanska and Chipot, 2000). The potential of mean force (PMF) for the doubly N-H...O-C H-bond configuration showed minima which are the characteristics of both close-contact and solvent-separated ion-pairs (Rozanska and Chipot, 2000). Saigal and Pranata (1997) presented the free energy profiles of the Gdm⁺-AcO⁻ and methylammonium (MAM⁺)-AcO⁻ complexes in aqueous solutions using Monte Carlo (MC) simulations. The Gdm⁺-FmO⁻ and MAM⁺-AcO⁻ complexes serve as models to represent salt-bridges in the Arg-Asp (or Glu) and Lys-Asp (or Glu) complexes, respectively. The PMF showed the close-contact ion-pair distances in the Gdm⁺-AcO⁻ and MAM⁺-AcO⁻ complexes to be 3.8 and 3.6 Å, respectively. In both cases, the free energy wells were found to be rather shallow. This implies that, in aqueous solution, the attractive interactions between the ions are not particularly strong. Saigal and Pranata (1997) described the existence of double minima on the free energy profile as a result of the constraint imposed on the relative orientation of the ions in the PMF calculations.

Although in principle, *ab initio* calculations with continuum model such as the SCRF method could provide useful information on molecular association in continuum solvent characterized by a dielectric constant, more and more theoretical and experimental evidences showed the necessity to include the details of solvent

molecules in model calculations, especially for H-bond systems (Keith and Frisch, 1994). This is due to the fact that, continuum models neglect specific short-range solute-solvent interaction, as well as the behavior and structures of solvent molecules in the first solvation shell of solute. Continuum models were pointed out to be suitable only for the systems, in which solvents act only as perturbation on the gas-phase property of the system (Keith and Frisch, 1994).

According to literature survey, at least four remarks could be made in the field of salt-bridge interactions in solutions; (a) previous theoretical and experimental investigations tend to focus attention only on the effects of solute-solute and solute-solvent interactions; (b) the detail information on the solvent structures especially in the first solvation shell of solute has been neglected in many investigations; (c) due to the limitation of computer resources, there has been an increasing number of theoretical studies made based on continuum models; (d) there were few theoretical and experimental investigations which combine structural and energetic effects, as well as the dynamic behavior of solvent molecules in the first solvation shell of solute, in the study of ion-pairs in solutions *etc.*

Intermolecular potentials to describe the interactions between molecules are primary input for statistical mechanical simulations, such as MC and MD simulations. Both MC and MD simulations provide information at the microscopic scale which can be used to predict macroscopic properties of chemical systems. MC simulations generate information by sampling configurations of molecules in statistical ensembles and provide statistical averaged properties, such as thermodynamic and structural properties. Whereas MD simulations solve the equations of motion by calculations of instantaneous forces on molecules. The trajectories recorded in the course of MD

simulations also yield dynamic properties such as transport coefficients (Allen and Tildesley, 1994; Leach, 1996) and reorientational correlation time (Sagarik, Ahlrichs, and Brode, 1986).

An alternative theoretical approach to compute intermolecular potentials has been proposed (Böhm and Ahlrichs, 1982, 1985; Hoinkis, Ahlrichs, and Böhm, 1983; Böhm, Ahlrichs, Scharf, and Schiffer, 1984; Böhm, Meissner, and Ahlrichs, 1984). It is called the Test-particle model or briefly T-model since the main contributions to the interaction energy are derived separately by probing the molecules of interest with suitable test particles. The major advantage of the T-model over the *ab initio* supermolecular approach is that, the T-model is derived by probing molecules of interest with a spherical test particle. This reduces the degree of freedom to describe the relative position and orientation of a pair of molecule from six to three. Therefore, the T-model requires less computer resources compared to *ab initio* supermolecular approach; thus the T-model can be applied to larger chemical systems. Moreover, the T-model incorporates the effects of electron correlation in an approximate way. This enables the T-model to be applied on large aromatic systems, such as pyridine (Sagarik and Spohr, 1995), phenol (Sagarik and Asawakun, 1997), and benzoic acid (Sagarik and Rode, 2000; Sagarik, Chaiwongwattana, and Sisot, 2004). The intermolecular potentials derived from the T-model have been tested successfully on various chemical systems, ranging from small molecules (Sagarik et al., 1986; Sagarik and Ahlrichs, 1986, 1987; Sagarik, Pongpituk, Chaiyapongs, and Sisot, 1991; Sagarik, 1999) to the base pairs of DNA (Sagarik et al., 1991).

In the present study, the structures and energetic of a model salt-bridge formed from Gdm^+ and FmO^- were studied, both in the gas phase and aqueous solutions. The

theoretical investigation started with construction of intermolecular potentials to describe the interactions in the $\text{Gdm}^+ \text{-H}_2\text{O}$, $\text{FmO}^- \text{-H}_2\text{O}$ and $\text{Gdm}^+ \text{-FmO}^-$ complexes, using the T-model. The T-model potentials were applied in the calculations of the equilibrium structures and interaction energies of the $\text{Gdm}^+ \text{-H}_2\text{O}$, $\text{FmO}^- \text{-H}_2\text{O}$ and $\text{Gdm}^+ \text{-FmO}^-$ complexes in the gas phase. Selected lowest-lying minimum energy geometries of these H-bond complexes were checked by *ab initio* calculations at the MP2 level of theory. This is to ensure that the computed T-model potentials give reasonable results when applied in MD simulations. The computed T-model potentials were applied in MD simulations of $[\text{Gdm}^+]_{\text{aq}}$, $[\text{FmO}^-]_{\text{aq}}$ and $[\text{Gdm}^+ \text{-FmO}^-]_{\text{aq}}$ at 298 K.

In order to obtain information on the preferential hydration sites, the three-dimensional structures and stability, as well as energetic of H-bond networks in the first hydration shells of solutes, the MD results were visualized and analyzed using various probability distribution (PD) maps (Clementi, 1980). The hydration structures of the complexes were inferred from the oxygen (PDO) and hydrogen probability distribution (PDH) maps, as well as atom-atom pair correlation function ($g(R)$). The energetic of H-bond networks of water in the vicinities of the solutes were analyzed based on the solute-solvent (AWPD) and solvent-solvent interaction energy probability distribution (WWPD) maps, together with the total-average interaction energy probability distribution (AW-WWPD) maps. Dynamic behavior and stability of water molecules in the first hydration shell of solutes were characterized using cross section plots derived from average energy landscapes and H-bond lifetimes.

The results were discussed in comparison with available theoretical and experimental results of the same and similar systems.

The results obtained from the present study will lead to a better understanding of salt-bridge interactions in proteins. It is also expected that the T-model potentials can be further applied on larger molecules in biological systems.

CHAPTER II

RESEARCH METHODOLOGY

In the present work, the optimized geometries of the Gdm^+ and FmO^- ions were obtained from *ab initio* calculations at MP2/6-311++G(d,p) and MP2/6-311++G(3df,3pd) levels of theory, respectively. They were kept constant throughout the calculations. The optimal bond lengths and angles of the ions are listed in Table C.1 (see Appendix C).

2.1 The T-model potentials

The derivation of the T-model has been discussed in detail elsewhere (Böhm and Ahlrichs, 1982, 1985; Hoinkis et al., 1983; Böhm, Ahlrichs, Scharf, and Schiffer, 1984; Böhm, Meissner, and Ahlrichs 1984). Here only some relevant aspects of the T-model are summarized.

Within the framework of the T-model, the interaction energy ($\Delta E_{\text{T-model}}$) between molecules A and B is written as a sum of the first-order interaction energy (ΔE_{SCF}^1) and a higher-order energy term (ΔE^r).

$$\Delta E_{\text{T-model}} = \Delta E_{\text{SCF}}^1 + \Delta E^r \quad (1)$$

ΔE_{SCF}^1 accounts for the exchange repulsion and electrostatic energies. It is computed from *ab initio* SCF calculations and takes the following analytical form:

$$\Delta E_{\text{SCF}}^1 = \sum_{i \in A} \sum_{j \in B} \left[\exp\left(\frac{-R_{ij} + \sigma_i + \sigma_j}{\rho_i + \rho_j}\right) + \frac{q_i q_j}{R_{ij}} \right] \quad (2)$$

i and j in Eq.(2) label the sites of molecules A and B . σ_i , ρ_i and q_i are the site parameters. R_{ij} is the site-site distance. The first term in Eq.(2) relates to the size and shape of interacting molecules A and B . The exponential parameters in Eq.(2) are derived by probing molecule A , as well as B , in various directions with an uncharged spherical test particle. A nitrogen (N) atom in its average of terms state has been proved to be the most suitable (Böhm and Ahlrichs, 1982). The repulsion energies between A and N, as well as B and N, are calculated using *ab initio* calculations at Hartree-Fock level of theory. These repulsion energies are employed to determine the exponential parameters σ_i , and ρ_i , by means of least squares fits and combination rules. The point charges, q_i and q_j , are computed from the requirement that a point-charge model reproduces the electrostatic potentials of molecule of interest. The CHelpG charges (Breneman and Wiberg, 1990) in Gaussian 98 (Frisch et al., Computer software, 1998) were shown to be applicable and quite practical (Sagarik, 1999; Sagarik and Rode, 2000). Therefore, in the present study, the point charges for Gdm^+ and FmO^- were determined by a fit of the electrostatic potentials at points selected according to the CHelpG scheme (Breneman and Wiberg, 1990). For the Gdm^+ and FmO^- ions, the electrostatic potentials employed in the fit were computed from *ab initio* calculations at the HF/6-311++G(d,p) and HF/6-311++G(3df,3pd) levels of theory, respectively. Due to the symmetry, the dipole moment for Gdm^+ is 0 D; whereas that for FmO^- is 1.90 D, which is in good agreement with those reported by Cummins and Gready (1994) between 1.6 to 1.7 D.

ΔE^r in Eq.(1) represents the dispersion and polarization contributions to the T-model potential. ΔE^r could be determined from both theoretical and experimental

data. A calibration of the incomplete potential to the properties related to intermolecular interactions, such as the second virial coefficients (B(T)), dimerization energies or potential energy of liquid *etc.*, seems to be the most appropriate choice.

ΔE^r takes the following form:

$$\Delta E^r = - \sum_{i \in A} \sum_{j \in B} C_{ij}^6 F_{ij}(R_{ij}) R_{ij}^{-6} \quad (3)$$

where

$$F_{ij}(R_{ij}) = \exp \left\{ - \left(1.28 R_{ij}^0 / R_{ij} - 1 \right)^2 \right\}, \text{ if } R_{ij} < 1.28 R_{ij}^0 \\ = 1, \text{ elsewhere} \quad (4)$$

and

$$C_{ij}^6 = C_6 \frac{3}{2} \frac{\alpha_i \alpha_j}{(\alpha_i / N_i)^{1/2} + (\alpha_j / N_j)^{1/2}} \quad (5)$$

R_{ij}^0 in Eq.(4) is the sum of van der Waals radii of interacting atoms. Eq.(5) is the Slater-Kirkwood relation. α_i and N_i in Eq.(5) denote the atomic polarizability and the number of valence electrons of the corresponding atom, respectively. $F_{ij}(R_{ij})$ in Eq.(4) is a damping function, introduced to correct the behavior of R_{ij}^{-6} at short R_{ij} distance. Only C_6 in Eq.(5) is unknown.

The values of C_6 could be varied within a wide range and careful variation of C_6 seems not lead to significant changes in the potential energy surface (PES). For some microsolvated systems, the values of C_6 were determined by adjusting the C_6 parameters to reproduce the interaction energies computed from *ab initio* calculations. This includes, for example, the phenol-H₂O 1 : 1 complex (Sagarik and Asawakun, 1997), benzoic acid dimer ((BA)₂), the BA-H₂O 1 : 1 complex (Sagarik and Rode,

2000) and $(\text{NH}_2\text{OH})_2$ (Sagarik, 1999). The calibration procedure employed in the present work consists of three basic steps as follows; (a) the T-model parameters for the Gdm^+ and FmO^- ions, with $C_6 = 1.0$, were applied in the calculations of the equilibrium structures and interaction energies of the $\text{Gdm}^+ - \text{H}_2\text{O}$, $\text{FmO}^- - \text{H}_2\text{O}$ and $\text{Gdm}^+ - \text{FmO}^-$ 1 : 1 complexes in the gas phase; (b) all the global minimum energy geometries predicted by the T-model potentials were reoptimized using *ab initio* calculations at the MP2/6-311++G(d,p) level for the $\text{Gdm}^+ - \text{H}_2\text{O}$ and $\text{Gdm}^+ - \text{FmO}^-$ complexes, and at the MP2/6-311++G(2d,2p) level for the $\text{FmO}^- - \text{H}_2\text{O}$ complex. The interaction energies of the reoptimized geometries were corrected using conventional single point counterpoise correction of the basis set superposition error (BSSE) (Boys and Bernardi, 1970); (c) the C_6 parameters for the complexes were readjusted, using the corresponding MP2 interaction energies as guide lines. The computed C_6 parameters for the $\text{Gdm}^+ - \text{H}_2\text{O}$, $\text{FmO}^- - \text{H}_2\text{O}$ and $\text{Gdm}^+ - \text{FmO}^-$ complexes are 1.13, 1.54 and 2.48, respectively. The T-model parameters for water were taken from Sagarik et al. (1991). The T-model parameters for Gdm^+ , FmO^- and water are summarized in Table C.2 (see Appendix C). The basic steps in the construction of T-model potential are illustrated in Figure B.1 (see Appendix B).

2.2 MD simulations

In order to provide insights into the structures and energetic of the H-bond networks of water in the first hydration shell of the Gdm^+ and FmO^- ions, as well as the $\text{Gdm}^+ - \text{FmO}^-$ complex, the T-model potentials computed in the previous section were applied in NVE-MD simulations of $[\text{Gdm}^+]_{\text{aq}}$, $[\text{FmO}^-]_{\text{aq}}$ and

$[\text{Gdm}^+ - \text{FmO}^-]_{\text{aq}}$ at 298 K. In MD simulations in general, an ion or an ion-pair was put at the center a cubic box subject to periodic boundary conditions. The solute was surrounded by five hundred water molecules, with the density of the aqueous solutions maintained at 1.0 g/cm^3 . The cutoff radius was half of the box length. The Ewald summation was applied to account for the long-range Coulomb interaction. Fifty thousand MD steps of 0.0005 ps were devoted to equilibration and one hundred thousand steps to property calculations. The schematic diagram showing all important steps in MD simulations is illustrated in Figure B.2 (see Appendix B).

The primary energetic results obtained from MD simulations were the average solute-solvent interaction energies ($\langle E_{\text{aq}}^{\text{solv-solv}} \rangle$) and the average solvent-solvent interaction energies ($\langle E_{\text{aq}}^{\text{solv-solv}} \rangle$), as well as the average potential energy of aqueous solutions ($\langle E_{\text{aq}}^{\text{pot}} \rangle$). These energy values were the results of the average over the MD steps and the number of solvent molecules. They are summarized in Table 3.1, together with all the MD simulations conditions employed in the present study.

To fulfill all the major objectives, six series of MD simulations were performed in the present study. MD- $[\text{Gdm}^+]_{\text{aq}}$ and MD- $[\text{FmO}^-]_{\text{aq}}$ represent MD simulations, in which single ions and water molecules were considered. In MD simulations of $[\text{Gdm}^+ - \text{FmO}^-]_{\text{aq}}$, the most stable configuration of the $\text{Gdm}^+ - \text{FmO}^-$ 1 : 1 complex in the gas phase, similar to the structure **b** in Figure 1.2, was chosen as a representative ion-pair. The atom numbering systems of $\text{Gdm}^+ - \text{FmO}^-$ are given in Figure 2.1.

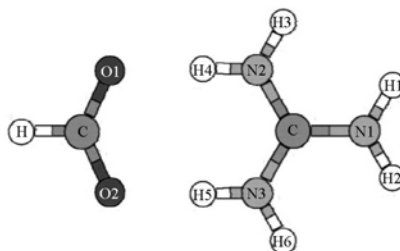


Figure 2.1 Atom numbering systems of the $\text{Gdm}^+ - \text{FmO}^-$ 1 : 1 complex.

It should be mentioned that, for the dimerization of alanine dipeptide in aqueous solutions (Su and Gallicchio, 2004), a relatively large free energy barrier corresponding to the intermediate state is characterized by a single hydration layer of interstitial water molecules which separates the close-contact dimer from the solvent-separated structure. It is, therefore, of interest to study the hydration structures and stability of such an intermediate state in $[\text{Gdm}^+ - \text{FmO}^-]_{\text{aq}}$. Since the preliminary PMF calculations on $[\text{Gdm}^+ - \text{FmO}^-]_{\text{aq}}$ (Sagarik and Chaiyapongs, 2004) revealed two shallow minima at $R_{\text{C}\dots\text{C}} \approx 3.9$ and 6.3 \AA on the free energy profile, these two configurations were adopted in the present MD simulations. They correspond to the close-contact and solvent-separated $\text{Gdm}^+ - \text{FmO}^-$ structures, respectively; the two minima are separated by a very low free energy barrier. In the present study, $\text{MD}-[\text{Gdm}^+ - \text{FmO}^-]_{\text{aq, frozen}}^{\text{R}=\text{X}}$ symbolizes the MD simulations, in which the $\text{Gdm}^+ - \text{FmO}^-$ complex with $R_{\text{C}\dots\text{C}} = \text{X}$ was frozen in the course of MD simulations. Therefore, $\text{MD}-[\text{Gdm}^+ - \text{FmO}^-]_{\text{aq, frozen}}^{\text{R}=\text{X}}$ with $R_{\text{C}\dots\text{C}} = 3.9$ and 6.3 \AA could assimilate, respectively, the initial and intermediate states, in which the H-bonds in the close-contact ion-pair are disrupted by water molecules in the interstitial H-bond network.

The stability of the close-contact and solvent-separated $\text{Gdm}^+ - \text{FmO}^-$ complexes in aqueous solutions was discussed based on the results of MD- $[\text{Gdm}^+ - \text{FmO}^-]_{\text{aq, free}}^{\text{R=X}}$. In MD- $[\text{Gdm}^+ - \text{FmO}^-]_{\text{aq, free}}^{\text{R=X}}$, two consecutive equilibration steps were carried out before property calculations took place. In the first equilibration step, the $\text{Gdm}^+ - \text{FmO}^-$ complex with $\text{R}_{\text{C}\dots\text{C}} = \text{X}$ was treated as a supermolecule, in which both Gdm^+ and FmO^- ions were not allowed to move in the course of MD simulations. After water molecules were well-equilibrated, all molecules inside the simulation box, including the Gdm^+ and FmO^- ions, were allowed to freely move in the second equilibration.

The hydration structures in $[\text{Gdm}^+]_{\text{aq}}$, $[\text{FmO}^-]_{\text{aq}}$ and $[\text{Gdm}^+ - \text{FmO}^-]_{\text{aq}}$ were primarily analyzed using the atom-atom pair correlation functions ($g(\text{R})$) and the average running coordination number ($n(\text{R})$). The three-dimensional structures of the H-bond networks of water in the aqueous solutions were visualized using the PDO and PDH maps. In the present case, they represent static pictures of the H-bond networks of water in the first hydration shells of solutes. In the constructions of the PDO and PDH maps, the molecular plane of solute was assumed to coincide with the XY plane of the simulation box (with $Z = 0 \text{ \AA}$). The volumes above and below the molecular plane of solute were divided into layers, with the thickness of 1 \AA . In each layer, the PDO and PDH maps were computed at 61×61 grid intersections, by following the trajectories of oxygen and hydrogen atoms of water in the course of MD simulations. The PDO and PDH maps were represented by contour lines. SURFER program (Golden Software, Computer software, 1997) was employed in the construction of the contour maps. For simplicity the maximum and minimum values

of the contour lines, as well as the contour interval were chosen to be the same for all the PDO and PDH maps.

In order to obtain insights into the interaction energy distributions in $[\text{Gdm}^+]_{\text{aq}}$, $[\text{FmO}^-]_{\text{aq}}$ and $[\text{Gdm}^+ - \text{FmO}^-]_{\text{aq}}$, a similar approach was adopted to construct the AWP, WWP and AW-WWP maps. The AWP maps were derived from the average interaction energies between the water molecules at the grid intersections and the ion or ion-pair, whereas the WWP maps were computed based on the average interaction energies between the water molecules at the grid intersections and all other water molecules in aqueous solutions. In the present study, the AW-WWP maps represent the average potential energy landscapes of the H-bond networks of water. They were computed by combination of the AWP and WWP maps (Sagarik and Dokmaisrijan, 2005). Only the negative interaction energies were displayed in the AWP, WWP and AW-WWP maps.

Since the dynamic behavior of water molecules in the H-bond networks was one of the main objectives, additional MD analyses were made. Due to the fact that the mobility of water molecules depends on the transition energy barriers, which could be estimated from the average potential energy landscapes, the AWP, WWP and AW-WWP maps were examined in details. Various cross section plots of the average potential energy landscapes were generated by taking vertical slices along predefined profile lines, through the surfaces of the AW-WWP maps, as well as the AWP and WWP maps (Sagarik and Dokmaisrijan, 2005). In the present study, the cross section plots computed from the longitudinal profile lines could be associated with the transition energy barriers to water exchange within, as well as between, the H-bond networks ($\langle E_{\text{aq}}^L \rangle$). Whereas those derived from the transverse profile lines

are related to the transition energy barriers to water exchange between the H-bond networks and the outsides ($\langle E_{\text{aq}}^{\text{T}} \rangle$).

It should be augmented that, when a particular water molecule leaves the first hydration shell, its place is occupied nearly simultaneously by another water molecule. Therefore, the residence time has been frequently used in the discussion of the dynamic behavior of water molecules in the first hydration shells of solutes (Wüthrich, 1995). The measured residence times seem to be very sensitive to the methods used, and could be approximated in general by MD simulations and NMR experiments (Odelius and Laaksonen, 1999). However, both approaches have advantages and disadvantages (Wüthrich, 1995; Brunne, Liepinsh, Otting, Wüthrich, and van Gunsteren, 1993). For examples, due to the fact that the H-bond formations and disruptions take place very often and very fast in the first hydration shell of solutes, the residence times derived from MD simulations could vary in a wide range (Brunner et al., 1993), depending on the path taken by individual water molecule; whereas NMR experiments can more effectively detect the long-lived hydration water (Wüthrich, 1995). From literature survey, there have been various approaches to calculate the residence times from MD simulations (Odelius and Laaksonen, 1999; Brunne et al., Impey, Madden, and McDonald, 1983). The one proposed by McDonald (Impey et al., 1983) seems to be relatively straight forward and widely used, especially for spherical symmetric solutes such as monovalent ions (Impey et al.; Smith and Dang, 1994). Since the ions and ion-pair considered here are more complicated and the intention is only to characterize the mobility of water molecules in the H-bond networks in terms of the average potential energy landscapes. Therefore, the H-bond lifetime proposed by Sagarik (Sagarik and Dokmaisrijan,

2005) was employed in the present study. The so-called “the longest H-bond lifetime” ($\tau_{A-H \cdots B, \max}$) was approximated from the percentage of the MD steps, during which a specific pair of H-bond donor and acceptor coming close enough to continuously engage in H-bond. The H-bond donor and acceptor were considered to engage in H-bond when the donor-acceptor distance was shorter than 4 Å (Barlow and Thornton, 1983; Case et al., Computer software, 1999). Attention was focused on cyclic-bifurcated H-bonding features, since preliminary MD simulations showed that they dominated in $[\text{Gdm}^+]_{\text{aq}}$, $[\text{FmO}^-]_{\text{aq}}$ and $[\text{Gdm}^+ - \text{FmO}^-]_{\text{aq}}$.

2.3 Computer softwares and facilities

All calculations in the present study were performed at the School of Chemistry, Institute of Science, SUT. The following computers and standard computational chemistry softwares were used.

- Compaq alpha1000 XP1000 and Compaq alpha DS20.
- DEC alpha 600/5-266.
- COLUMBUS system programs developed by Ahlrichs et al. (1985).
- Gaussian 98 package (Frisch et al., Computer software, 1998).
- Moldy MD simulations program (Refson, Computer software, 1996).
- SURFER contouring program (Golden Software, Computer software, 1997).
- AMBER version 6 (Case et al., Computer software, 1999) etc.

CHAPTER III

RESULTS AND DISCUSSION

3.1 Equilibrium structures in the gas phase

Since the main objectives of the present study were to investigate hydration structures and stability of the ions and the ion-pair in aqueous solutions, the analysis of the equilibrium structures and interaction energies in the gas phase was made only to sample check the potential energy surfaces, as well as to test the applicability and reliability of the computed T-model potentials. This is to ensure that the T-model potentials will give reasonable results when applied in MD simulations. Due to the fact that different theoretical approaches yield different results, comparisons with available theoretical and experimental data were not made rigorously in the following subsections.

The absolute and some low-lying minimum energy geometries for the $\text{Gdm}^+ \text{-H}_2\text{O}$, $\text{FmO}^- \text{-H}_2\text{O}$ and $\text{Gdm}^+ \text{-FmO}^-$ complexes, computed from the T-model potentials, are illustrated in Figures 3.1 to 3.3, respectively. $\Delta E_{\text{T-model}}$ and some characteristic H-bond distances and angles, together with the corresponding results from MP2 calculations, are included in the figures for comparison.

3.1.1 The $\text{Gdm}^+ \text{-H}_2\text{O}$ complex

In general, the results on the $\text{Gdm}^+ \text{-H}_2\text{O}$ 1 : 1 complex are as expected namely, a cyclic-bifurcated $\text{N-H}\cdots\text{Ow}$ H-bond structure, structure **a** in Figure 3.1,

represents the global minimum energy geometry in the gas phase. Both N-H...Ow H-bonds in structure **a** are identical, with two N-H groups of Gdm⁺ acting as proton donors toward the oxygen atom of water. The Gdm⁺ and H₂O molecular planes are perpendicular, with the N-H...Ow H-bond distance and $\Delta E_{T\text{-model}}$ of 2.93 Å and -72.9 kJ/mol, respectively. Starting from structure **a**, MP2/6-311++G(d,p) yielded the same structure. The BSSE corrected interaction energy of structure **a**, ΔE_{MP2CP} in Figure 3.1, is -68.0 kJ/mol. The T-model predicted structure **b** to be 9.3 kJ/mol less stable than structure **a**. For structure **b**, the Gdm⁺ and H₂O molecular planes are coplanar, with the cyclic-bifurcated N-H...Ow H-bond distance and $\Delta E_{T\text{-model}}$ of 3.01 Å and -63.6 kJ/mol, respectively. The relative orientations of water molecules in structures **a** and **c**, as well as in structures **b** and **d**, are similar. However, the water molecules in structures **c** and **d** are H-bonded to the Gdm⁺ ion through a single N-H...Ow H-bond, with the Gdm⁺ and H₂O molecular planes perpendicular and coplanar with each other, respectively. $\Delta E_{T\text{-model}}$ of structures **c** and **d** are almost the same, -59.0 and -58.4 kJ/mol, respectively. The N-H...Ow H-bond distance in structure **d** is slightly longer than structure **c**. Structure **e** represents another type of cyclic-bifurcated H-bond in the Gdm⁺-H₂O 1 : 1 complex, with $\Delta E_{T\text{-model}}$ and the N-H...Ow H-bond distance of -46.9 kJ/mol and 2.75 Å, respectively.

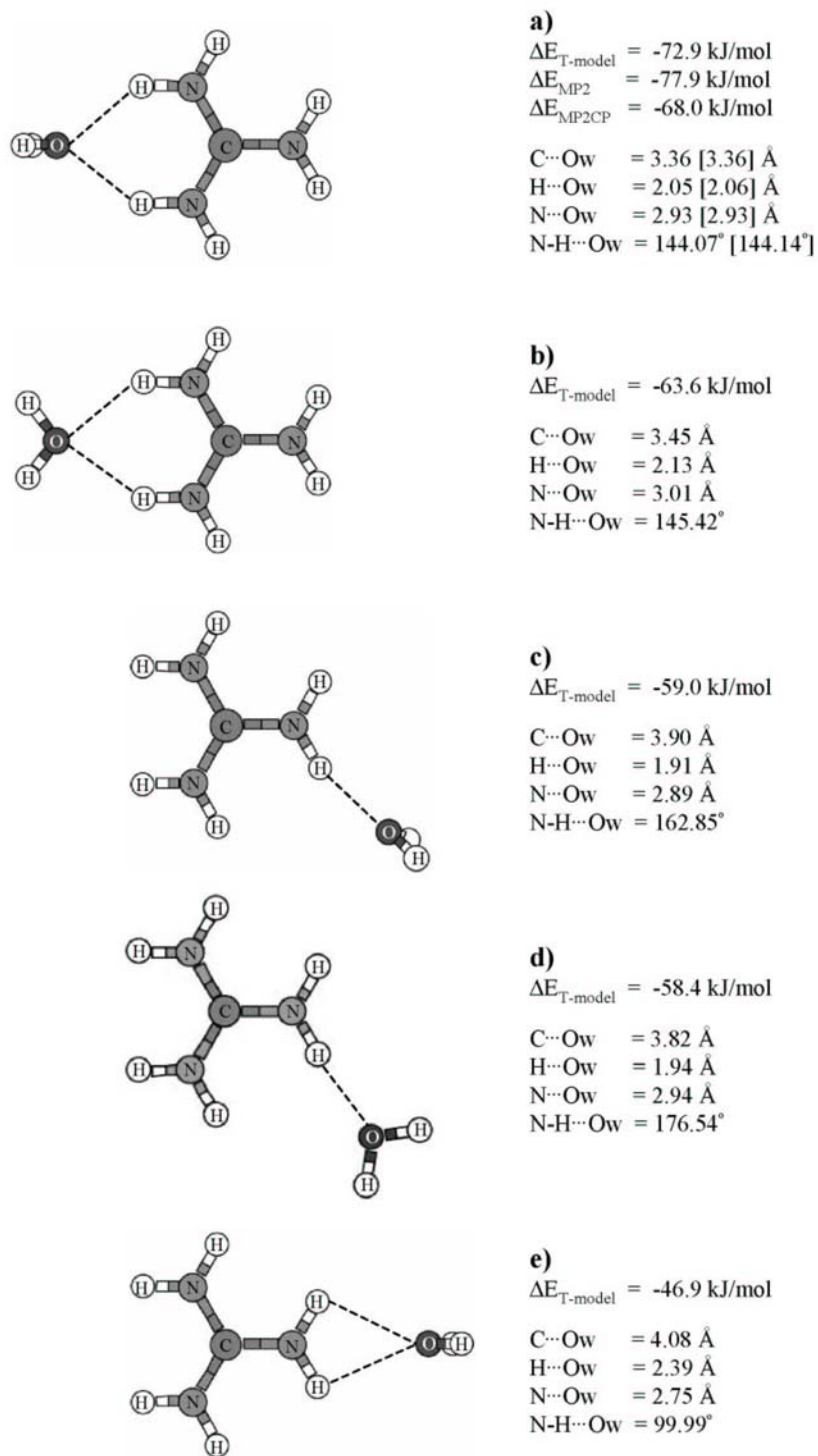


Figure 3.1 Equilibrium structures and interaction energies of the $Gdm^+ - H_2O$

1 : 1 complex in the gas phase computed from the T-model potentials.

[...] the values obtained from MP2/6-311++G(d,p).

Only limited number of low-lying minimum energy geometries of the $\text{Gdm}^+ \text{-H}_2\text{O}$ 1 : 1 complex were reported in the literature (Jorgensen and Tirado-Rives, 1988; Gao, 1994; Field, Bash, and Karplus, 1990). Based on the OPLS potentials and *ab initio* calculations with the 6-31G(d) basis set (Field et al., 1990), structure **a** possesses the interaction energies of -74.4 and -76.1 kJ/mol, respectively. Whereas the AM1/TIP3P (Gao, 1994) and *ab initio* calculations (Field et al., 1990) predicted the C \cdots Ow distances to be 3.22 and 3.41 Å, respectively. Structure **d** was inferred from the OPLS potentials and *ab initio* calculations to be an additional minimum energy geometry, with the interaction energies of -66.0 and -57.7 kJ/mol, respectively (Field et al., 1990).

3.1.2 The $\text{FmO}^- \text{-H}_2\text{O}$ complex

The T-model potential predicted a cyclic-bifurcated Ow-Hw \cdots O H-bond structure, structure **a** in Figure 3.2, to be the absolute minimum energy geometry for the $\text{FmO}^- \text{-H}_2\text{O}$ 1 : 1 complex. Structure **a** consists of two symmetric Ow-Hw \cdots O H-bonds, with water molecule acting as proton donors toward the COO^- group. Both Ow-Hw \cdots O H-bond distances are 2.91 Å, with $\Delta E_{\text{T-model}}$ of -75.2 kJ/mol. MP2/6-311++G(2d,2p) geometry optimization predicted the same structure, with slightly shorter Ow-Hw \cdots O H-bond distance. ΔE_{MP2CP} for structure **a** is -69.7 kJ/mol. The second and third low-lying minimum energy geometries for the $\text{FmO}^- \text{-H}_2\text{O}$ 1 : 1 complex are represented by a single Ow-Hw \cdots O H-bond formation, with $\Delta E_{\text{T-model}}$ of -62.6 and -55.6 kJ/mol, respectively; the Ow-Hw \cdots O H-bond distances are 2.90 and 2.81 Å, respectively.

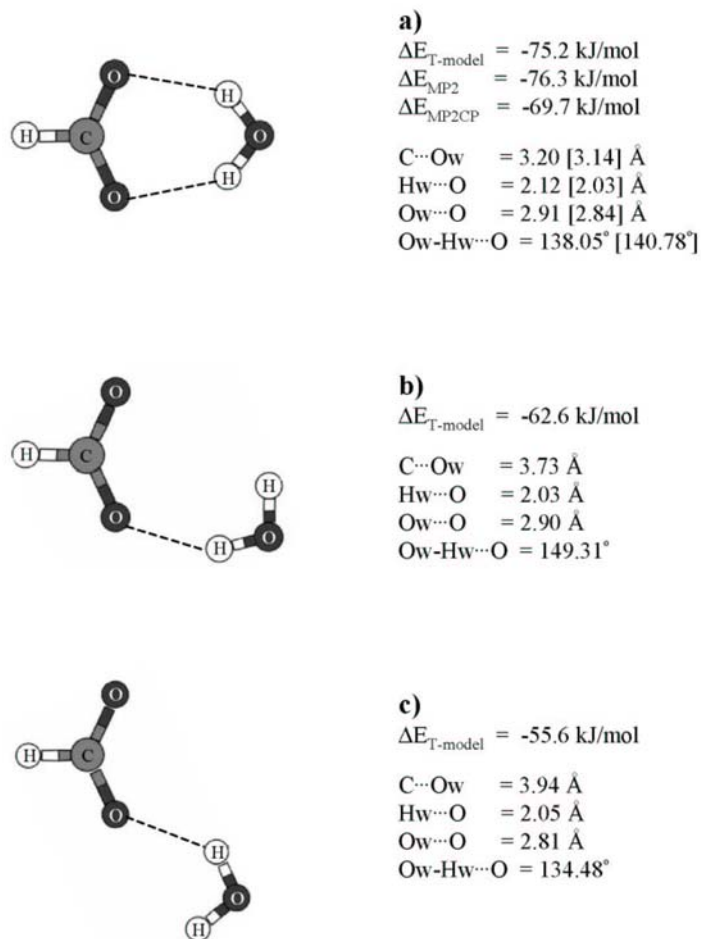


Figure 3.2 Equilibrium structures and interaction energies of the $\text{FmO}^- \text{-H}_2\text{O}$

1 : 1 complex in the gas phase computed from the T-model potentials.

[...] the values obtained from MP2/6-311++G(2d,2p).

Three low-lying minimum energy geometries similar to those of the present study were reported for the FmO^- - H_2O (Lukovits, Karpfen, Lischka, and Schuster, 1979; Jorgensen and Gao, 1986; Gao, Garner, and Jorgensen, 1986; Luque, Reuter, Cartier, and Ruiz-López, 2000) and AcO^- - H_2O 1 : 1 complexes (Gao, 1994). The interaction energy of structure **a** was estimated by *ab initio* calculations at the HF/6-31G(d,p) level, plus the counterpoise and dispersion corrections, to be -83.6 kJ/mol (Jorgensen and Gao, 1986), whereas the structures similar to structures **b** and **c** were about -71.1 kJ/mol (Jorgensen and Gao, 1986). The C...Ow distances for these structures are in good agreement with the T-model results, 3.23, 3.91 and 3.92 Å, respectively (Lukovits et al., 1979). *Ab initio* calculations at the HF/6-31+G(d) level (Gao et al., 1986) yielded the interaction energies of -76.1 , -64.0 and -61.0 kJ/mol, respectively.

3.1.3 The Gdm^+ - FmO^- complex

Only two equilibrium geometries for the Gdm^+ - FmO^- 1 : 1 complex were generated from the T-model potential. The absolute minimum energy geometry is represented by a coplanar cyclic arrangement of the N-H...O H-bonds, structure **a** in Figure 3.3. The two N-H...O H-bonds are identical, with the N-H groups of the Gdm^+ ion acting as proton donors toward the COO^- group of FmO^- . $\Delta E_{\text{T-model}}$ of structure **a** is -480.8 kJ/mol, with the N-H...O H-bond distances of 2.74 Å. Starting from structure **a**, MP2/6-311++G(d,p) geometry optimization yielded the same structure, with the BSSE corrected interaction energy of -480.1 kJ/mol; the N-H...O H-bond distances are slightly smaller than the T-model result. Structure **a** is similar to a bidentate H-bonding structure reported by Shimoni, Glusker, and Bock (1996), in

which *ab initio* calculations at MP2/6-31+G(d,p)//MP2/6-31+G(d,p) level predicted the interaction energy to be -542.6 kJ/mol and the N-H \cdots O H-bond distances of 2.6 Å. Another type of cyclic-bifurcated N-H \cdots O H-bonds was predicted by the T-model potential, structure **b** in Figure 3.3. Structure **b** possesses the interaction energy and the N-H \cdots O H-bond distances of -431.4 kJ/mol and 2.62 Å, respectively.

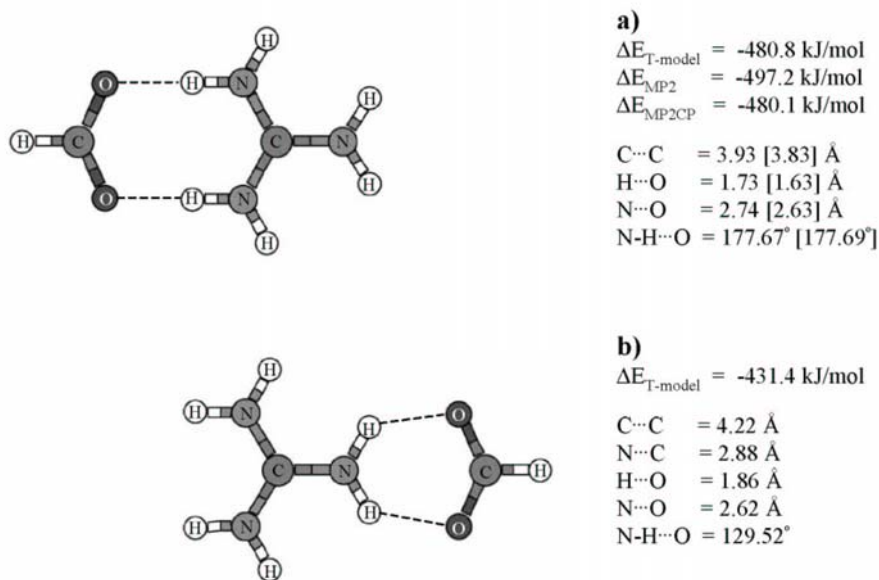


Figure 3.3 Equilibrium structures and interaction energies of the $\text{Gdm}^+ - \text{FmO}^-$

1 : 1 complex in the gas phase computed from the T-model potentials.

[...] the values obtained from MP2/6-311++G(d,p).

In order to provide insight into the accuracy of the MP2 results reported in this section, geometry optimizations on the ions and the 1 : 1 complexes were performed at the HF level with the same basis sets. It was found that, at the HF level, the covalent bond lengths were systematically shorter, 0.03 Å at most, whereas the bond angles did not change significantly. For all the 1 : 1 complexes, the H-bond distances obtained from *ab initio* calculations at the HF level were systematically longer, 0.16 Å at most. The latter represents general trend when the effects of electron correlation were neglected; additional attractive interaction is obtained when *ab initio* calculations take into account the dispersion interaction properly. This also implies that the basis sets employed in the present MP2 calculations are quite reasonable, leading to correct effects of electron correlation. It should also be stressed that the T-model employed in the present work takes into account the effects of electron correlation in an approximate way, using the Slater-Kirkwood relation and the C_6 parameter. This considerably reduces computational efforts, especially for large H-bond and aromatic systems, in which the effects of electron correlation cannot be neglected (Sagarik and Asawakun, 1997; Sagarik and Rode, 2000; Sagarik et al., 2004). The T-model has been proved to be an appropriate choice for the situations, in which the numerical accuracy and the computational facility are to be balanced.

3.2 MD simulations

$\langle E_{\text{aq}}^{\text{pot}} \rangle$, $\langle E_{\text{aq}}^{\text{solu-solv}} \rangle$, $\langle E_{\text{aq}}^{\text{solv-solv}} \rangle$ and $\langle E_{\text{aq}}^{\text{solu-solu}} \rangle$ are included in Table 3.1, together with the conditions employed in MD simulations. Only some selected PDO, AWPD and AW-WWPD maps, as well as the corresponding cross section plots, are illustrated in this section. The rest are accumulated in Appendix C. Characteristic high-density contour areas on the PDO, AWPD and AW-WWPD maps are labeled with letters. To compare the transition energy barriers to water exchanges ($\langle E_{\text{aq}}^{\text{L}} \rangle$ and $\langle E_{\text{aq}}^{\text{T}} \rangle$) at various H-bond networks, the lowest energy minima on the AW-WWPD cross section plots were set to 0 kJ/mol (Sagarik and Dokmaisrijan, 2005).

Since the ions and the ion-pair considered in the present work possess symmetries, some H-bond networks are equivalent. To simplify the discussion, equivalent H-bond networks were categorized and analyzed. $\tau_{\text{A-H}\cdots\text{B}, \text{max}}$ obtained from MD- $[\text{Gdm}^+]_{\text{aq}}$, MD- $[\text{FmO}^-]_{\text{aq}}$ and MD- $[\text{Gdm}^+ - \text{FmO}^-]_{\text{aq}, \text{frozen}}^{\text{R=X}}$ are summarized in Table 3.2, together with some characteristic $\langle E_{\text{aq}}^{\text{T}} \rangle$.

Table 3.1 MD simulations parameters and the results for $[\text{Gdm}^+]_{\text{aq}}$, $[\text{FmO}^-]_{\text{aq}}$ and $[\text{Gdm}^+ - \text{FmO}^-]_{\text{aq}}$.

MD	L	$\langle E_{\text{aq}}^{\text{pot}} \rangle$	$\langle E_{\text{aq}}^{\text{solv-solv}} \rangle$	$\langle E_{\text{aq}}^{\text{solv-solv}} \rangle$	$\langle E_{\text{aq}}^{\text{solv-solv}} \rangle$
$[\text{Gdm}^+]_{\text{aq}}$	24.6865	-30.99 ± 0.16	-0.9	-29.6	-
$[\text{FmO}^-]_{\text{aq}}$	24.6729	-31.35 ± 0.16	-1.1	-29.6	-
$[\text{Gdm}^+ - \text{FmO}^-]_{\text{aq, frozen}}^{\text{R}=3.9}$	24.7273	-31.90 ± 0.17	-0.9	-29.4	-480.8*
$[\text{Gdm}^+ - \text{FmO}^-]_{\text{aq, free}}^{\text{R}=3.9}$	24.7273	-31.94 ± 0.16	-1.0	-29.5	-457.0
$[\text{Gdm}^+ - \text{FmO}^-]_{\text{aq, frozen}}^{\text{R}=6.3}$	24.7273	-31.98 ± 0.17	-1.5	-29.2	-256.5*
$[\text{Gdm}^+ - \text{FmO}^-]_{\text{aq, free}}^{\text{R}=6.3}$	24.7273	-31.96 ± 0.17	-0.6	-29.1	-120.4

L = simulation box lengths.

$\langle E_{\text{aq}}^{\text{pot}} \rangle$ = average potential energy of aqueous solution.

$\langle E_{\text{aq}}^{\text{solv-solv}} \rangle$ = average solute-solvent interaction energy.

$\langle E_{\text{aq}}^{\text{solv-solv}} \rangle$ = average solvent-solvent interaction energy.

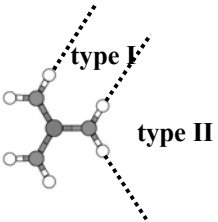
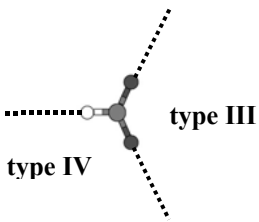
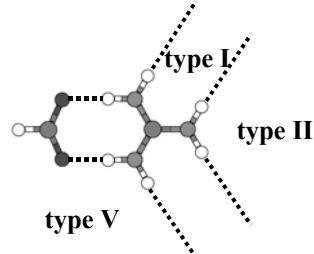
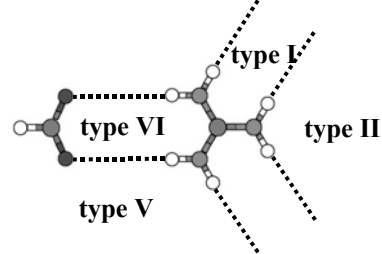
$\langle E_{\text{aq}}^{\text{solv-solv}} \rangle$ = average solute-solute interaction energy.

* = $\Delta E_{\text{T-model}}$ for the $\text{Gdm}^+ - \text{FmO}^-$ 1 : 1 complex in the gas phase.

Energies in kJ/mol and distances in Å.

Table 3.2 $\tau_{\text{type } X, \text{ max}}$ and some $\langle \Delta E_{\text{aq}}^{\text{T}} \rangle$ obtained from MD simulations of $[\text{Gdm}^+]_{\text{aq}}$, $[\text{FmO}^-]_{\text{aq}}$ and $[\text{Gdm}^+ - \text{FmO}^-]_{\text{aq}}$.

Energies in kJ/mol and time in ps.

X	MD- $[\text{Gdm}^+]_{\text{aq}}$		MD- $[\text{FmO}^-]_{\text{aq}}$		MD- $[\text{Gdm}^+ - \text{FmO}^-]_{\text{aq, frozen}}^{\text{R}=3.9}$		MD- $[\text{Gdm}^+ - \text{FmO}^-]_{\text{aq, frozen}}^{\text{R}=6.3}$	
	$\langle \Delta E_{\text{aq}}^{\text{T}} \rangle$	$\tau_{\text{type } X, \text{ max}}$	$\langle \Delta E_{\text{aq}}^{\text{T}} \rangle$	$\tau_{\text{type } X, \text{ max}}$	$\langle \Delta E_{\text{aq}}^{\text{T}} \rangle$	$\tau_{\text{type } X, \text{ max}}$	$\langle \Delta E_{\text{aq}}^{\text{T}} \rangle$	$\tau_{\text{type } X, \text{ max}}$
I	101.8	8.52	-	-	86.3	6.92	101.5	10.04
II	76.8	11.11	-	-	34.8	6.98	84.3	14.29
III	-	-	86.7	1.84	-	-	-	-
IV	-	-	26.5	1.17	-	-	-	-
V	-	-	-	-	24.3	1.41	23.7	8.96
VI	-	-	-	-	-	-	102.2-103.8	18.14
								

3.2.1 $[\text{Gdm}^+]_{\text{aq}}$

Figure 3.4 shows $g(R)$ and $n(R)$ directly related to the H-bonds in $[\text{Gdm}^+]_{\text{aq}}$, together with the PDO, AWPD and AW-WWPD maps and the cross section plots. All the results on MD- $[\text{Gdm}^+]_{\text{aq}}$, are summarized in Appendix C. The H-bond networks at **A**, **B** and **C** in Figures 3.4b and 3.4c are equivalent due to the symmetry of the Gdm^+ ion. Therefore, only two types of H-bond networks are to be discussed in $[\text{Gdm}^+]_{\text{aq}}$. The representative examples are the H-bond networks in the areas between H4 and H5 and between H1 and H2 in Figure 3.1. They are regarded as the H-bond network types **I** and **II**, respectively.

The main peak of $g(R_{\text{C}\cdots\text{Ow}})$ in Figure 3.4a is split into two peaks, corresponding to the H-bond network types **I** and **II**, respectively. The peak height of $g(R_{\text{C}\cdots\text{Ow}})$ at $R_{\text{max}} = 3.43 \text{ \AA}$ is slightly lower than that at $R_{\text{max}} = 4.09 \text{ \AA}$. The first peak could be attributed to the H-bonding features in structures **a** and **b**, whereas the second one accounts for structures **c**, **d** and **e** in Figure 3.1. The N-H \cdots Ow H-bonds in $[\text{Gdm}^+]_{\text{aq}}$ seem to be quite strong, as seen from the structures of the main peaks of $g(R_{\text{N}\cdots\text{Ow}})$ and $g(R_{\text{H}\cdots\text{Ow}})$ in Figure 3.4a. $g(R_{\text{N}\cdots\text{Ow}})$ indicates that, at $R_{\text{max}} = 2.90 \text{ \AA}$, there is about one (1.2) water molecule in close-contact or H-bonded to each N-H group of Gdm^+ , and about eight (7.8) water molecules in the first hydration shell at 4.09 \AA .

Figure 3.4 Selected structure and energetic results obtained

from MD- $[\text{Gdm}^+]_{\text{aq}}$.

- a) $g(R)$; characteristic distances are given,
with $n(R)$ in parentheses.
- b) – d) the PDO, AWPD and AW-WWPD maps.
- e) – h) cross section plots computed from longitudinal and
transverse profile lines.

————— the AW-WWPD cross section plot.

----- the AWPD cross section plot.

..... the WWPD cross section plot.

X-, Y- and Z-axis in Å; energies in kJ/mol.

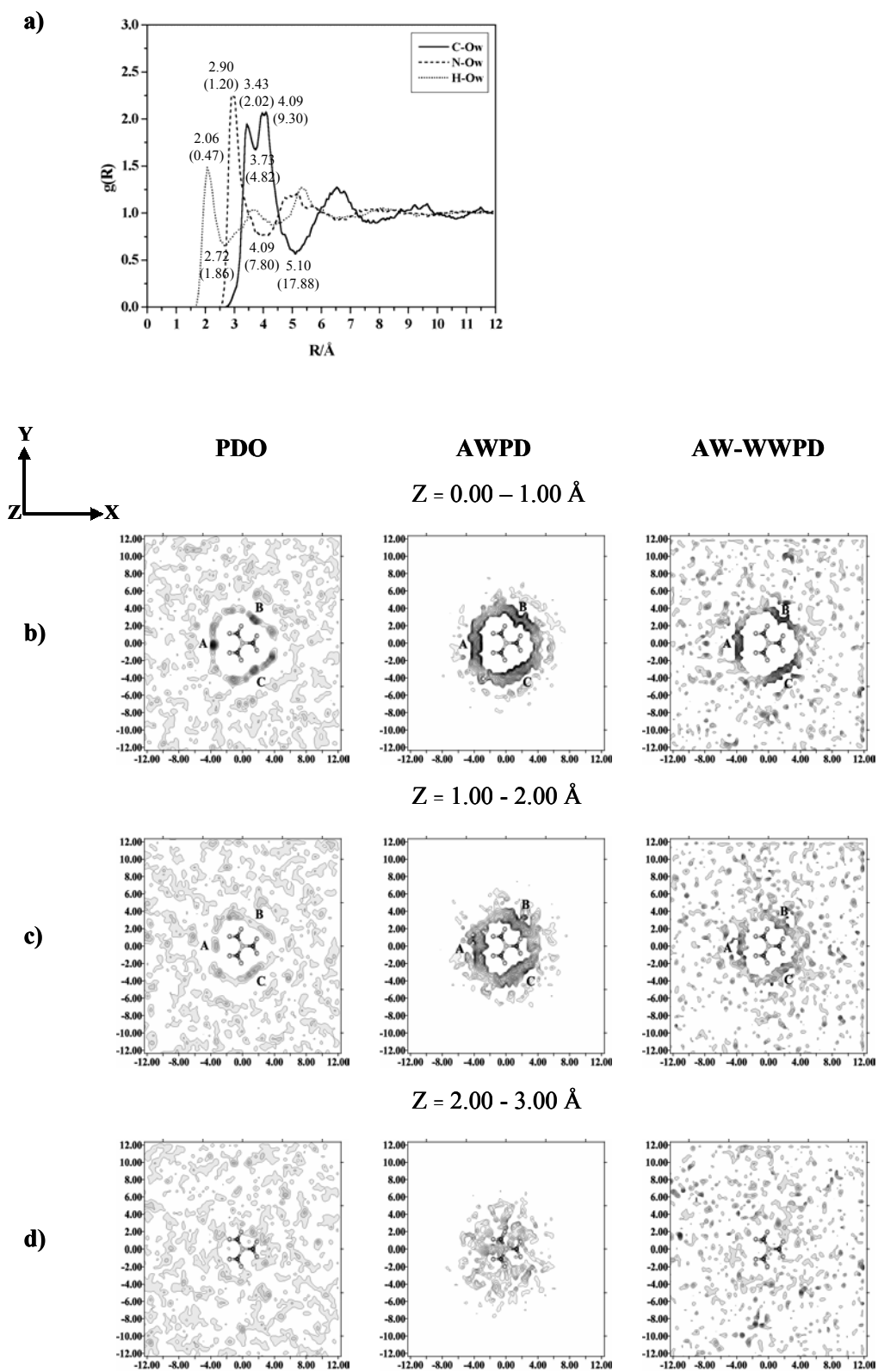


Figure 3.4

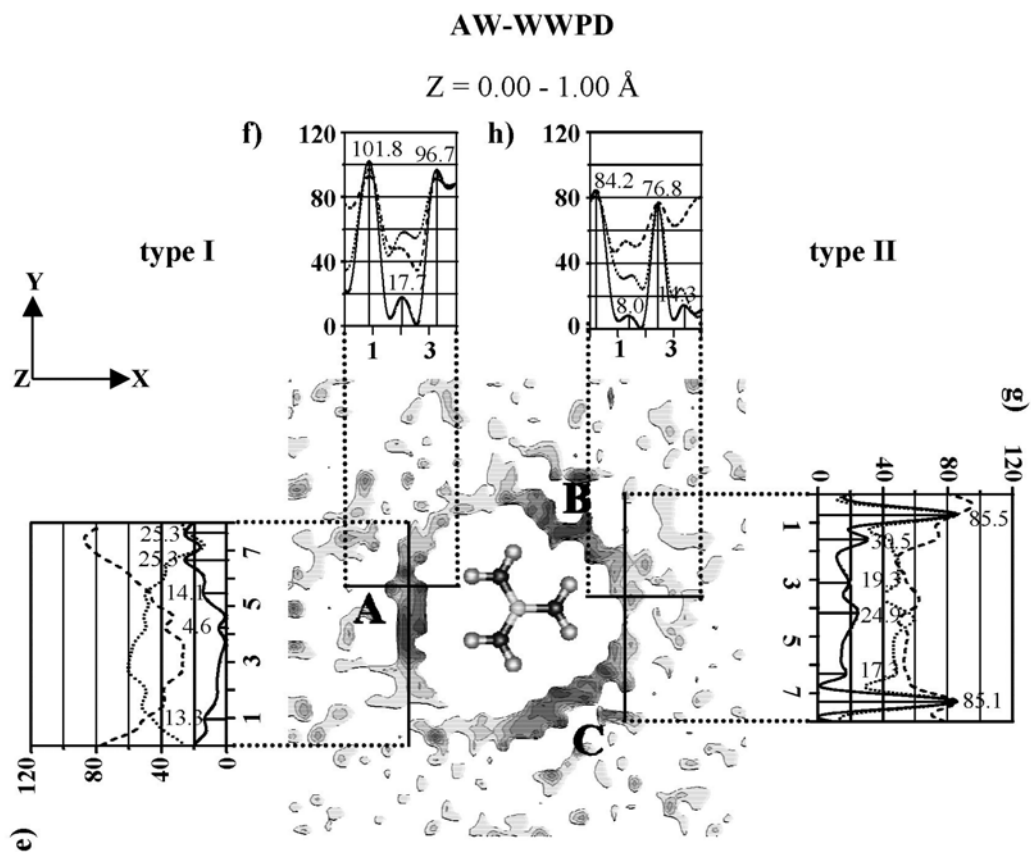


Figure 3.4 (continued)

The preferential hydration sites and the three-dimensional structures of the H-bond networks of water in $[\text{Gdm}^+]_{\text{aq}}$ are visualized and analyzed using the PDO, AWPD and AW-WWPD maps in Figures 3.4b to 3.4d. They are quite well-defined which support the results of $g(R)$ in general. The three most important H-bond networks seem to be all connected and located on the Gdm^+ molecular plane. The H-bonding features at these H-bond networks seem to include all structures in Figure 3.1. According to the contour densities on the PDO maps in Figures 3.4b and 3.4c, the H-bond network type **I** appeared with higher probability compared to the H-bond network type **II**. In other words, the H-bonding features in structures **a** and **b** were observed with higher frequencies in MD simulations, compared to structures **c**, **d** and **e**. Figure 3.4d suggests the boundary of the first hydration shell of Gdm^+ to be in the layer with $Z = 2$ to 3 \AA .

The structures of the average potential energy landscapes in Figures 3.4e to 3.4h show that the H-bond network types **I** and **II** are different in detail. The longitudinal AW-WWPD cross section plot of the H-bond network type **I** in Figure 3.4e reveals slightly smaller transition energy barriers ($\langle E_{\text{aq}}^{\text{L}} \rangle$) at the basin, compared to those of the H-bond network type **II** in Figure 3.4g. This suggests that water molecules could move or exchange easier within the H-bond network type **I**. It was also recognized in Figures 3.4e and 3.4f that, in the vicinity of the highest contour density of the H-bond network type **I**, the AWPD cross section plots are lower than the WWPD cross section plots and the structures of the AW-WWPD cross section plots are determined by the shape of the AWPD cross section plots. This is opposite to the situations in the H-bond network type **II**. These pieces of information will be used

to characterize the energy contributions to the stability of the close-contact Gdm^+ - FmO^- complex in aqueous solutions. The transverse AW-WWPD cross section plots in Figures 3.4f and 3.4h reveal that the motions of water molecules inside the H-bond network types **I** and **II** are confined in narrow interaction energy valleys of about 3 Å, with $\langle E_{\text{aq}}^{\text{T}} \rangle$ for the water exchange between the H-bond networks and the outsides of about 102 and 77 kJ/mol, respectively.

As mentioned earlier that the dynamic behavior of specific water molecules at the H-bond networks could be inferred from the average potential energy landscapes (Sagarik and Dokmaisrijan, 2005) and vice versa. Therefore, the detail information on the structures of the average potential energy landscapes could be useful to identify the paths taken by individual water molecules. It should also be emphasized that, based on the criteria adopted in the present work, the minima on the average potential energy landscapes, such as AW-WWPD maps, are associated with the low-lying interaction energy states, which were occupied by water molecules in the course of MD simulations. Furthermore, since the probability and the duration for a water molecule to occupy an interaction energy state depend upon the hydration dynamics of individual water molecule, as well as the transition energy barriers interconnecting the interaction energy states, it is reasonable to assume that the structures of the average potential energy landscapes define the H-bond lifetime. Since, by definition, $\tau_{\text{A-H}\cdots\text{B}, \text{max}}$ represents the longest H-bond lifetime, in which a specific water molecule is trapped inside the H-bond network of interest, one could identify the water molecule which takes the rate-determining water exchange path; by assuming that the water molecule with the highest $\tau_{\text{A-H}\cdots\text{B}, \text{max}}$ enters the H-bond

network by taking the path with the highest transition energy barriers. With this approach it is also possible to predict the rate-determining water exchange path at the H-bond networks. The assumption could be applied in the study of the reaction path, on which a reactive substrate is trapped long enough at functional group of receptor, in order that a specific chemical reaction could take place.

According to the above discussions on the AW-WWPD cross section plots, especially $\langle E_{\text{aq}}^{\text{T}} \rangle$, one could anticipate that $\tau_{\text{type I, max}}$ is larger than $\tau_{\text{type II, max}}$. In the present case, however, such a direct comparison is not appropriate. Since, based on the criteria for the bifurcated H-bond formation, the area occupied by the H-bond network type **II** is more than twice larger than that of the H-bond network type **I**. Attention was, therefore, focused on the effects of the ion-pair formation on the longest H-bond lifetimes at equivalent H-bond networks. In Table 3.2, $\tau_{\text{type I, max}}$ and $\tau_{\text{type II, max}}$ are about 9 and 11 ps, respectively, comparable with the approximated residence time of water at Na^+ in $[\text{NaCl}]_{\text{aq}}$ of 15 ps (Smith and Dang, 1994).

In order to obtain information on the accuracy of $\tau_{\text{A-H}\cdots\text{B, max}}$, additional comparisons have to be made. In the present case, MD analyses on pure water were performed and leading to some interesting results. It was noticed that, based on the same approach, the longest H-bond lifetime at the H atom of water was 8.7 ps, whereas the one at the O atom was 3.2 ps. These are compared well with the H-bond residence times reported based on NMR experiment of about 8 ps (Hertz, 1973) and MD simulations of 4.5 ps (Impey et al., 1983). The H-bond mean residence times of water within the first hydration shell of a water molecule were reported to be ranging from 2.5 to 10.0 ps (Brugè, Parisi, and Fornili, 1996). It should be added that, from

the literature survey (Impey et al.; Hertz, 1973; Brugè et al., 1996; Muegge and Knapp, 1995), the values of the H-bond lifetime or the H-bond residence time are sensitive to the definitions, as well as the methods employed in the investigations. It is, therefore, more appropriate to discuss and compare the results using pure water as a reference. In the present work, it is obvious that the reported values of $\tau_{A-H\cdots B, \max}$, are reasonable relative to the pure water, and the definition employed in the present work has been proved to be applicable.

3.2.2 $[\text{FmO}^-]_{\text{aq}}$

All the results on MD- $[\text{FmO}^-]_{\text{aq}}$ are displayed in Appendix C. Only important results on MD- $[\text{FmO}^-]_{\text{aq}}$ are summarized in Figure 3.5 for discussion. $g(\text{R}_{\text{C}\cdots\text{Ow}})$ in Figure 3.5a shows the main peak at $R_{\max} = 3.55 \text{ \AA}$, with $n(\text{R}_{\max}) = 4.15$. The latter suggests about four water molecules in close-contact with FmO^- . The position of the main peak of $g(\text{R}_{\text{C}\cdots\text{Ow}})$ is slightly too long to assign to structure **a** and slightly too short to be structure **b** in Figure 3.2. This makes believe that the average H-bonding feature in $[\text{FmO}^-]_{\text{aq}}$ lies between structures **a** and **b**. $g(\text{R}_{\text{O}\cdots\text{Ow}})$ in Figure 3.5a reveals about two (1.82) water molecules H-bonding directly to each oxygen atom of FmO^- , with the $\text{Ow-Hw}\cdots\text{O}$ H-bond distance of 2.96 \AA . The H-bond networks of water at the C-H group of FmO^- are less well-defined compared to the COO^- group, as seen from the size and shape of the main peak of $g(\text{R}_{\text{H}\cdots\text{Ow}})$ in Figure 3.5a.

Figure 3.5 Selected structure and energetic results obtained

from MD- $[\text{FmO}^-]_{\text{aq}}$.

a) $g(R)$; characteristic distances are given,
with $n(R)$ in parentheses.

b) – d) the PDO, AWPD and AW-WWPD maps.

e) – h) cross section plots computed from longitudinal and
transverse profile lines.

————— the AW-WWPD cross section plot.

----- the AWPD cross section plot.

..... the WWPD cross section plot.

X-, Y- and Z-axis in Å; energies in kJ/mol.

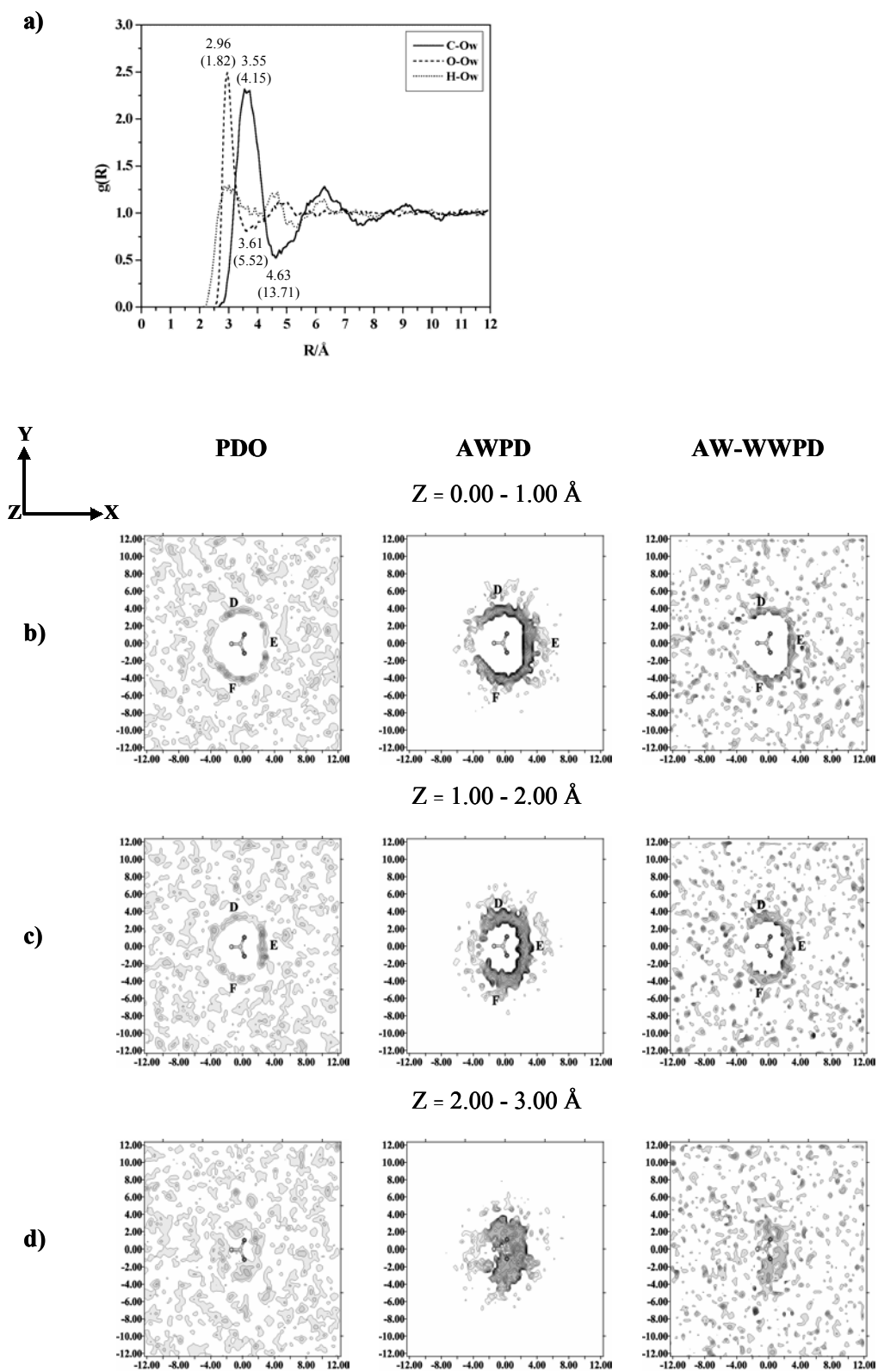


Figure 3.5

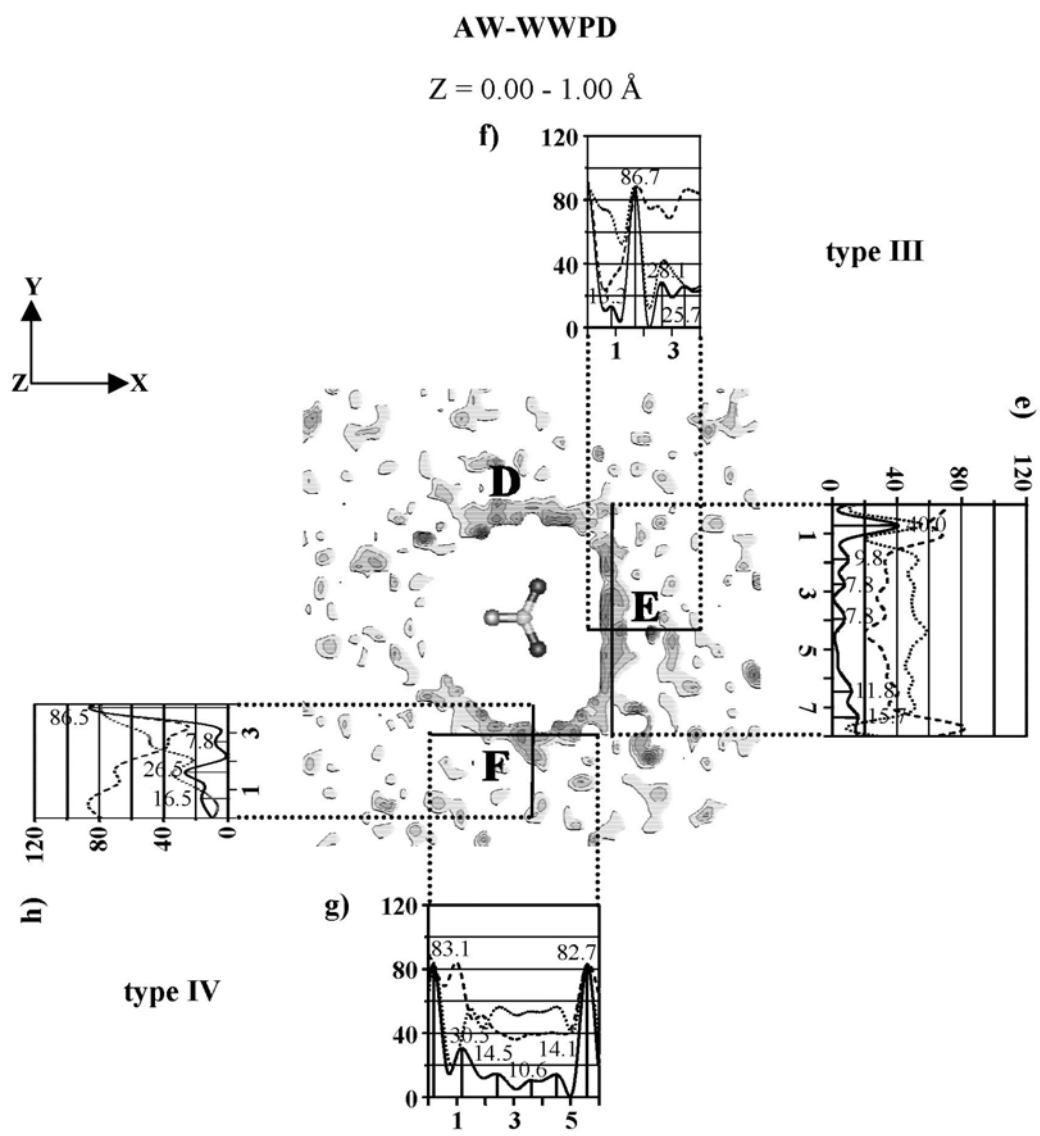


Figure 3.5 (continued)

For $[\text{FmO}^-]_{\text{aq}}$, three well-defined H-bond networks are seen on the PDO maps. They are labeled with **D**, **E** and **F** in Figures 3.5b and 3.5c. The H-bond network at **E** is located slightly above the FmO^- molecular plane, and is regarded as the H-bond network type **III** in the present study. The H-bond networks at **D** and **F** are equivalent. Both of them are seen on the FmO^- molecular plane, and are categorized as the H-bond network type **IV**. The H-bond network at **E** spans from the O1 to O2 atoms, with the contour density slightly higher than that at **D** and **F**. Figure 3.5d shows the boundary of the first hydration shell of FmO^- , in the layer with $Z = 2$ to 3 \AA .

The longitudinal AW-WWPD cross section plots in Figures 3.5e and 3.5g reveal that the H-bond networks at **D**, **E** and **F** are quite well-connected. Their structures suggest that, on average, water molecule in the H-bond network type **III** could move or exchange within a wider range, compared to the H-bond network type **IV**; $\langle E_{\text{aq}}^{\text{L}} \rangle$ inside the H-bond network type **III** in Figure 3.5e are on average smaller than those inside the H-bond network type **IV** in Figure 3.5g. However, the transverse AW-WWPD cross section plots in Figures 3.5f and 3.5h suggest faster water exchange between the H-bond network type **IV** and the outsides, compared to that between the H-bond network type **III** and the outsides. This is in line with the values of $\tau_{\text{type IV, max}}$ and $\tau_{\text{type III, max}}$ of about 1 and 2 ps, respectively. Figures 3.5e to 3.5h show that, in the vicinities of the highest contour densities of the H-bond network types **III** and **IV**, the AWPD cross section plots are lower than the WWPD cross section plots. They seem to define the shapes of the AW-WWPD cross section plots.

3.2.3 $[\text{Gdm}^+ - \text{FmO}^-]_{\text{aq}}$

All the structural and energetic results on $\text{MD}-[\text{Gdm}^+ - \text{FmO}^-]_{\text{aq, frozen}}^{\text{R}=\text{X}}$ and $\text{MD}-[\text{Gdm}^+ - \text{FmO}^-]_{\text{aq, free}}^{\text{R}=\text{X}}$ are summarized in Appendix C. Some characteristic results on $\text{MD}-[\text{Gdm}^+ - \text{FmO}^-]_{\text{aq, frozen}}^{\text{R}=3.9}$ and $\text{MD}-[\text{Gdm}^+ - \text{FmO}^-]_{\text{aq, free}}^{\text{R}=3.9}$ are displayed in Figure 3.6, whereas those of $\text{MD}-[\text{Gdm}^+ - \text{FmO}^-]_{\text{aq, frozen}}^{\text{R}=6.3}$ are illustrated in Figure 3.7. The MD results showed that the close-contact $\text{Gdm}^+ - \text{FmO}^-$ complex is associated in aqueous solutions at 298 K, and $g(\text{R})$ related to the hydration of the ion-pair complex, obtained from $\text{MD}-[\text{Gdm}^+ - \text{FmO}^-]_{\text{aq, free}}^{\text{R}=3.9}$ and $\text{MD}-[\text{Gdm}^+ - \text{FmO}^-]_{\text{aq, frozen}}^{\text{R}=3.9}$, are virtually the same. Therefore, only selected $g(\text{R})$ deduced from $\text{MD}-[\text{Gdm}^+ - \text{FmO}^-]_{\text{aq, free}}^{\text{R}=3.9}$ are displayed and discussed in details. This suggests further that the hydration structures obtained from these two MD conditions are similar and one could ascribe the three-dimensional structures of the H-bond networks of water for the freed close-contact ion-pair complex from $\text{MD}-[\text{Gdm}^+ - \text{FmO}^-]_{\text{aq, frozen}}^{\text{R}=3.9}$.

Figure 3.6 Selected structure and energetic results obtained

from MD- $[\text{Gdm}^+ - \text{FmO}^-]_{\text{aq, frozen}}^{\text{R}=3.9}$ and MD- $[\text{Gdm}^+ - \text{FmO}^-]_{\text{aq, free}}^{\text{R}=3.9}$.

a) – b) $g(\text{R})$; obtained from MD- $[\text{Gdm}^+ - \text{FmO}^-]_{\text{aq, free}}^{\text{R}=3.9}$;

characteristic distances are given, with $n(\text{R})$ in parentheses.

c) – e) the PDO, AWPD and AW-WWPD maps

computed from MD- $[\text{Gdm}^+ - \text{FmO}^-]_{\text{aq, frozen}}^{\text{R}=3.9}$.

f) – k) cross section plots computed

from MD- $[\text{Gdm}^+ - \text{FmO}^-]_{\text{aq, frozen}}^{\text{R}=3.9}$.

————— the AW-WWPD cross section plot.

----- the AWPD cross section plot.

..... the WWPD cross section plot.

X-, Y- and Z-axis in Å; energies in kJ/mol.

(see Figure 2.1 for atom numbering)

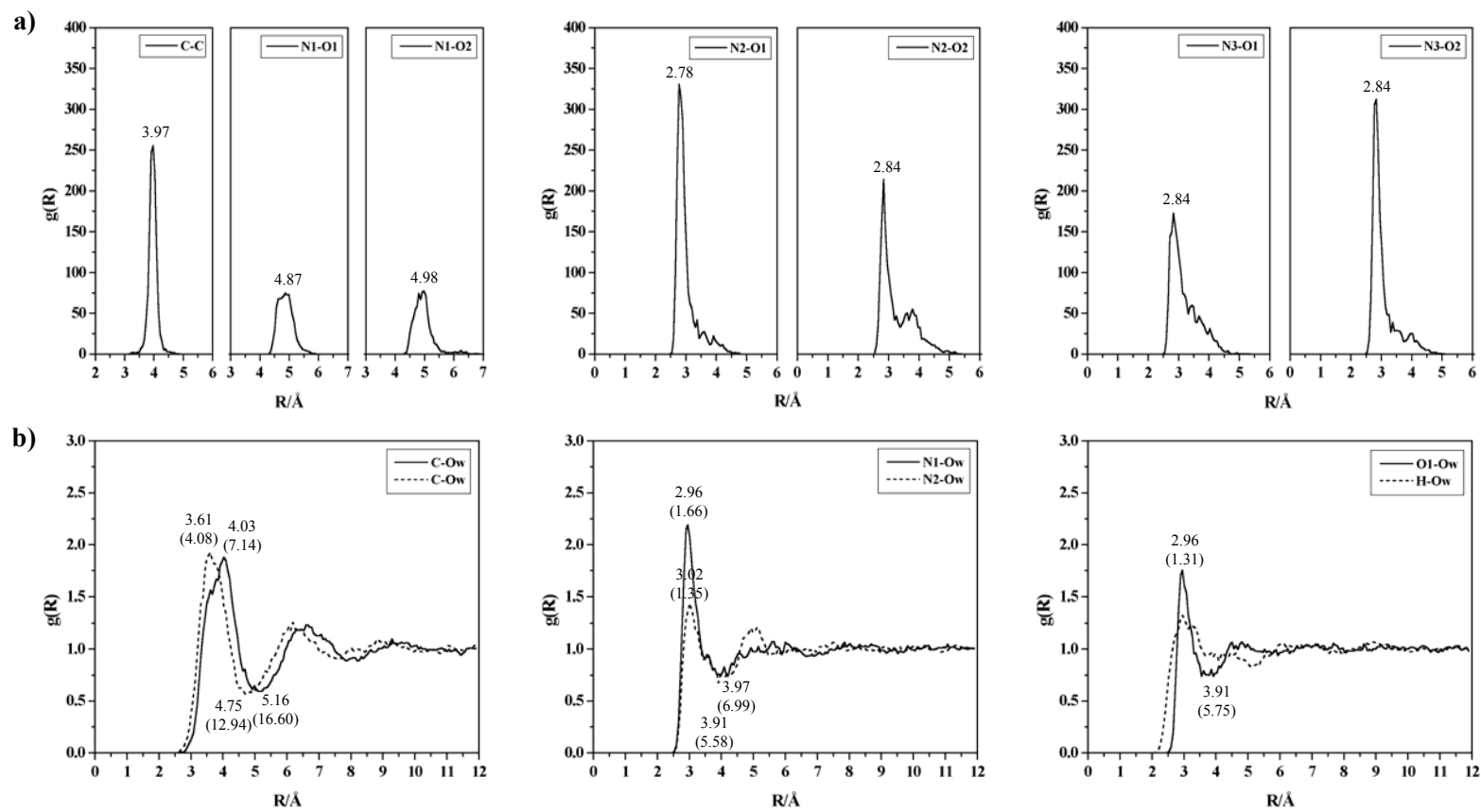


Figure 3.6

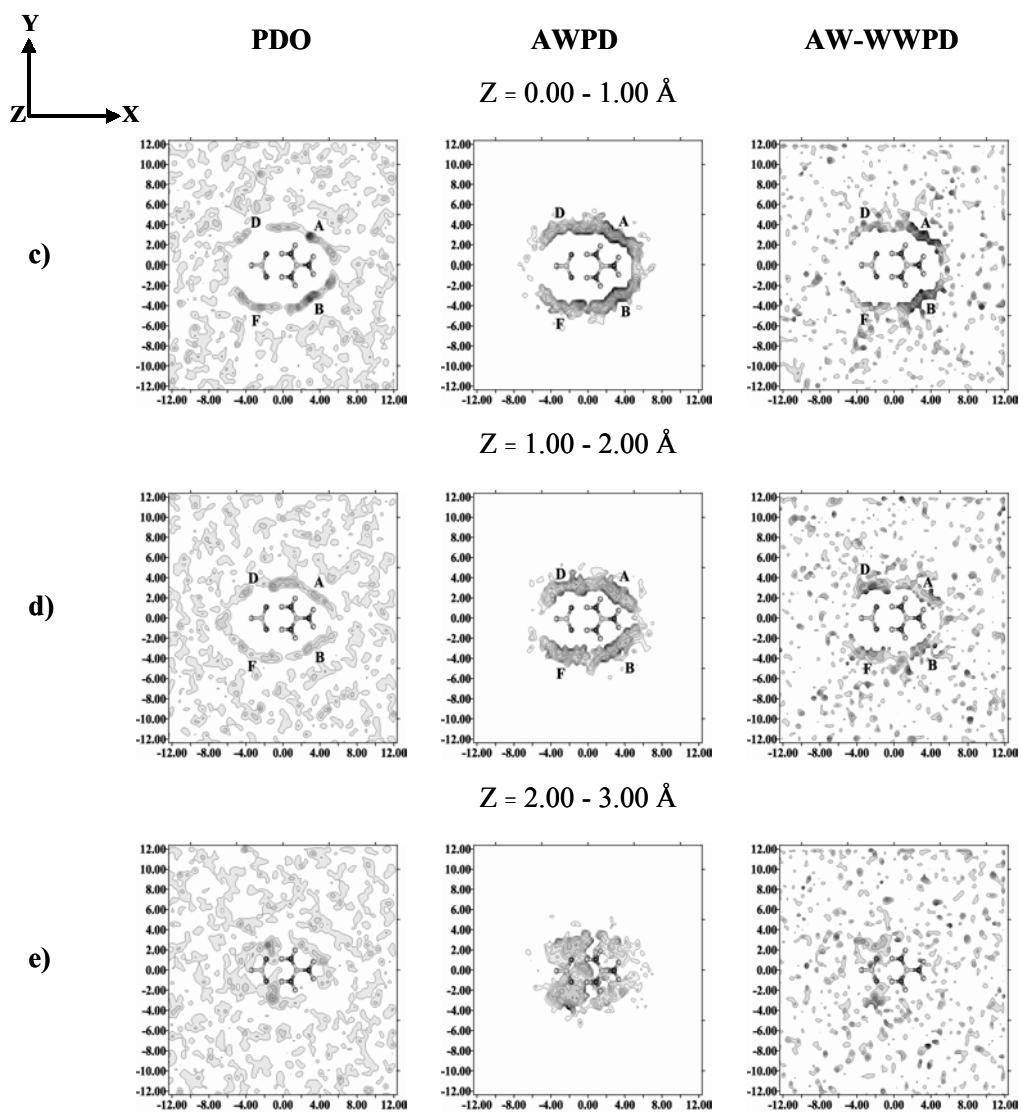


Figure 3.6 (continued)

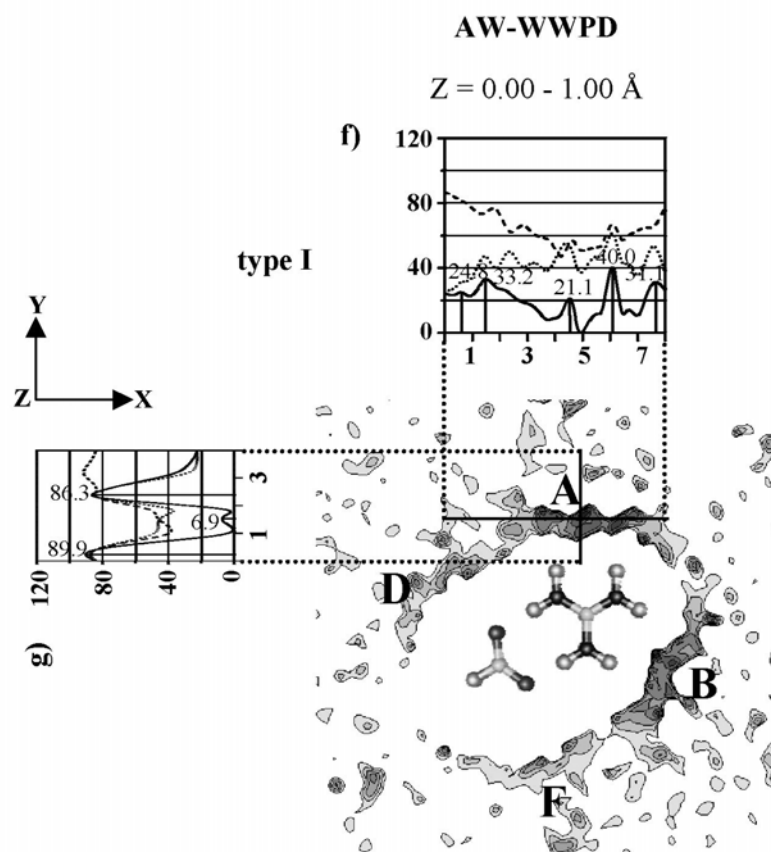


Figure 3.6 (continued)

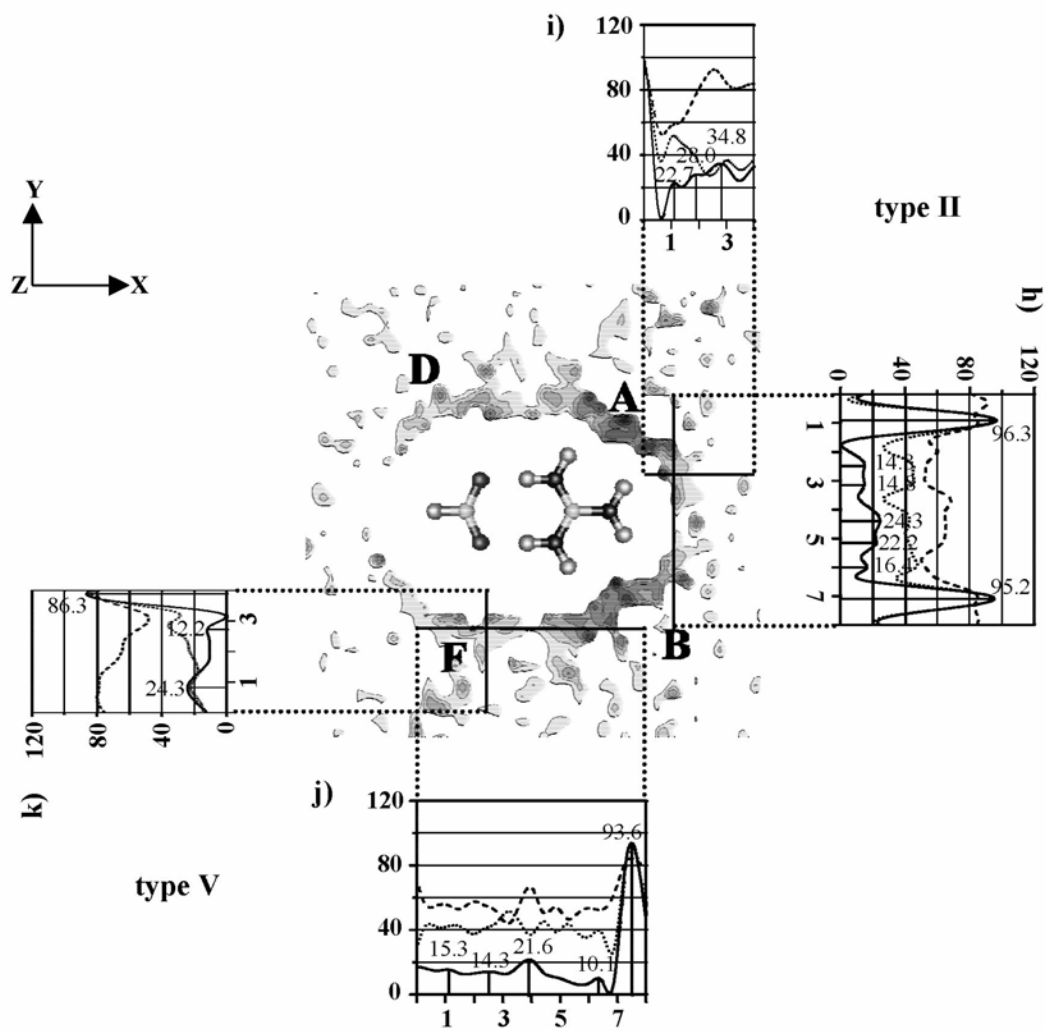


Figure 3.6 (continued)

Due to the symmetry of the close-contact Gdm^+ - FmO^- complex, the N2 and N3 atoms of Gdm^+ , as well as the O1 and O2 atoms of FmO^- , are equivalent. $g(R)$ illustrated in Figure 3.6a are related to the association of the close-contact Gdm^+ - FmO^- complex, whereas those in Figure 3.6b to its hydration. The primary evidence for the association of the close-contact Gdm^+ - FmO^- complex in aqueous solutions obtained from $g(R_{\text{C}\dots\text{C}})$ and $g(R_{\text{N}\dots\text{O}})$ in Figure 3.6a; all of which show single sharp peaks at the positions corresponding to the close-contact Gdm^+ - FmO^- complex in the gas phase. The main peak of $g(R_{\text{C}\dots\text{C}})$ at $R_{\text{max}} = 3.97 \text{ \AA}$ and those of $g(R_{\text{N}\dots\text{O}})$ at R_{max} between 2.78 and 2.84 \AA agree well with structure **a** in Figure 3.3. The N-H \dots O H-bond distances are in line with the results obtained from high-resolution protein structural analyses of the Arg-COO $^-$ complexes; the majority is within 2.6 and 3.0 \AA (Singh et al., 1987). The existence of $g(R_{\text{N2}\dots\text{O1}})$, $g(R_{\text{N2}\dots\text{O2}})$, $g(R_{\text{N3}\dots\text{O1}})$ and $g(R_{\text{N3}\dots\text{O2}})$ reflects the possibility for the H-bond donor-acceptor interchange between N2-H4 \dots O1 and N3-H5 \dots O2 H-bonds, by rotation of Gdm^+ and FmO^- about the C-N1 and C-H axes, respectively.

The formation of the close-contact Gdm^+ and FmO^- complex seems to block large part of the H-bond donor and acceptor functional groups, leading to remarkable changes in $g(R)$. As a consequence of the reduction of the H-bond network type **I**, the small peak of $g(R_{\text{C}\dots\text{Ow}})$ at $R_{\text{max}} = 3.43 \text{ \AA}$ in $[\text{Gdm}^+]_{\text{aq}}$ becomes a shoulder in Figure 3.6b. For MD- $[\text{Gdm}^+ - \text{FmO}^-]_{\text{aq, free}}^{R=3.9}$, the main peaks of $g(R_{\text{N2}\dots\text{Ow}})$, $g(R_{\text{H}\dots\text{Ow}})$ and $g(R_{\text{O1}\dots\text{Ow}})$ in Figure 3.6b are smaller and broader, compared to those in $[\text{Gdm}^+]_{\text{aq}}$ and $[\text{FmO}^-]_{\text{aq}}$, respectively. Since the N1-H1 and

N1-H2 groups are not directly involved in the ion-pair formation, $g(R_{N1...Ow})$ is not substantially changed. In comparison with $[Gdm^+]_{aq}$, the position of the main peak of $g(R_{N1...Ow})$ shifts slightly to longer distance, with a slight increase in the number of water molecules in close-contact with the N1-H1 and N1-H2 groups. The close-contact $Gdm^+ - FmO^-$ complex formation also reduces the possibility to form the H-bond network type **III**. In comparison to $[FmO^-]_{aq}$, the size of main peak of $g(R_{O...Ow})$ is considerably reduced, accompanied by a reduction of the number of water molecules in close-contact with the COO^- group, from about two (1.8) to about one (1.3).

The three-dimensional structures of the H-bond networks of water in the first hydration shell of the close-contact $Gdm^+ - FmO^-$ complex, derived from MD- $[Gdm^+ - FmO^-]_{aq, frozen}^{R=3.9}$, are displayed in Figures 3.6c to 3.6e. It appears that the H-bond networks at **A** and **D**, as well as **B** and **F**, are quite associated and well-connected. Both of them seem to help stabilize of the close-contact $Gdm^+ - FmO^-$ complex in aqueous solutions. The H-bond networks linking between the Gdm^+ and FmO^- ions will be regarded as the H-bond network type **V**, see Figures 3.6j and 3.6k. It seems that, within the H-bond network type **V**, water molecules could move or exchange in a wide range. $\tau_{type V, max}$ is only about 1 ps.

Figures 3.6f to 3.6k show in general that the WWPD cross section plots are lower than the AWPD cross section plots, and the structures of the AW-WWPD cross section plots are determined by the structures of the WWPD cross section plots. This suggests that the net stabilization effect of the close-contact

ion-pair complex arises partly from the H-bond networks caging around it. Similar conclusion was made based on calorimetric investigations on the binding affinities of the Gdm^+ derivatives and tetrabutylammonium acetate ($\text{TBA}^+ \cdot \text{AcO}^-$) in DMSO (Linton and Hamilton, 1999; Fan, Van Arman, Kincaid, and Hamilton, 1993). Under the experimental conditions (Linton and Hamilton, 1999), it was concluded that the H-bonds between the Gdm^+ and COO^- ions seems not enough to direct ion-pair formation, and the affinities between the substrates and receptors are facilitated by solvent reorganization. The same explanation was put forward by Laria and Fernández-Prini (1995), in which the solvent reactive field was pointed out to be the main reason for the association of pairs of monovalent ions over a wide range of interionic distances.

The close-contact $\text{Gdm}^+ \cdot \text{FmO}^-$ complex formation leads to considerable changes in the structures of the longitudinal AW-WWPD cross section plot of the H-bond network type **I**, see Figure 3.6f. The transition energy barriers to water exchange within the H-bond network type **I** ($\langle E_{\text{aq}}^{\text{L}} \rangle$) are increased, compared to $[\text{Gdm}^+]_{\text{aq}}$; whereas the transition energy barrier to water exchange between the H-bond network type **I** and the outsides ($\langle E_{\text{aq}}^{\text{T}} \rangle$) is decreased to about 86 kJ/mol, see Figure 3.6g. As a consequence, $\tau_{\text{type I, max}}$ is reduced to 6.9 ps, see Table 3.2 for comparison. The transverse AW-WWPD cross section plot in Figure 3.6i also shows a decrease in the transition energy barrier to the water exchange between the H-bond network type **II** and the outsides; while the longitudinal AW-WWPD cross section plot is not much different. This leads to a decrease of $\tau_{\text{type II, max}}$ to about 7 ps.

The formation of the interstitial H-bond network of water between the Gdm^+ and FmO^- ions brings about changes in the structures and energetic of the H-bond network types **I**, **II** and **V**. The results from MD- $[\text{Gdm}^+ - \text{FmO}^-]_{\text{aq, frozen}}^{\text{R}=6.3}$ in Figures 3.7a and 3.7b illustrated that water molecules in the interstitial H-bond network, regarded as the H-bond network type **VI**, are very localized, especially in the layer with $Z = 1 - 2 \text{ \AA}$. The longitudinal and transverse WWPD cross section plots in Figures 3.7h and 3.7i clearly show that the H-bonds between water molecules in the H-bond network type **VI** are very weak, as a consequence of strong H-bond interactions between the water molecules and the solute ions. The difference between the solute-solvent and solvent-solvent interaction energies amounts approximately to 100 kJ/mol, see Figure 3.7h. In the interstitial H-bond network, the mobility of water molecules is rather restricted, only within a small and narrow energy valley of about 2 \AA width, see Figures 3.7h and 3.7i. This is in accordance with $\tau_{\text{type VI, max}}$ of about 18 ps. The shapes of the transverse and longitudinal AW-WWPD cross section plots of the H-bond network types **I** and **II**, obtained from MD- $[\text{Gdm}^+ - \text{FmO}^-]_{\text{aq, frozen}}^{\text{R}=6.3}$, are resemble those from MD- $[\text{Gdm}^+]_{\text{aq}}$; whereas the H-bond network type **V** seems to be less connected compared to MD- $[\text{Gdm}^+ - \text{FmO}^-]_{\text{aq, frozen}}^{\text{R}=3.9}$.

Figure 3.7 Selected structure and energetic results obtained

from MD- $[\text{Gdm}^+ - \text{FmO}^-]_{\text{aq, frozen}}^{\text{R} = 6.3}$.

a) – c) the PDO, AWPD and AW-WWPD maps.

d) – k) cross section plots.

————— the AW-WWPD cross section plot.

----- the AWPD cross section plot.

..... the WWPD cross section plot.

X-, Y- and Z-axis in Å; energies in kJ/mol.

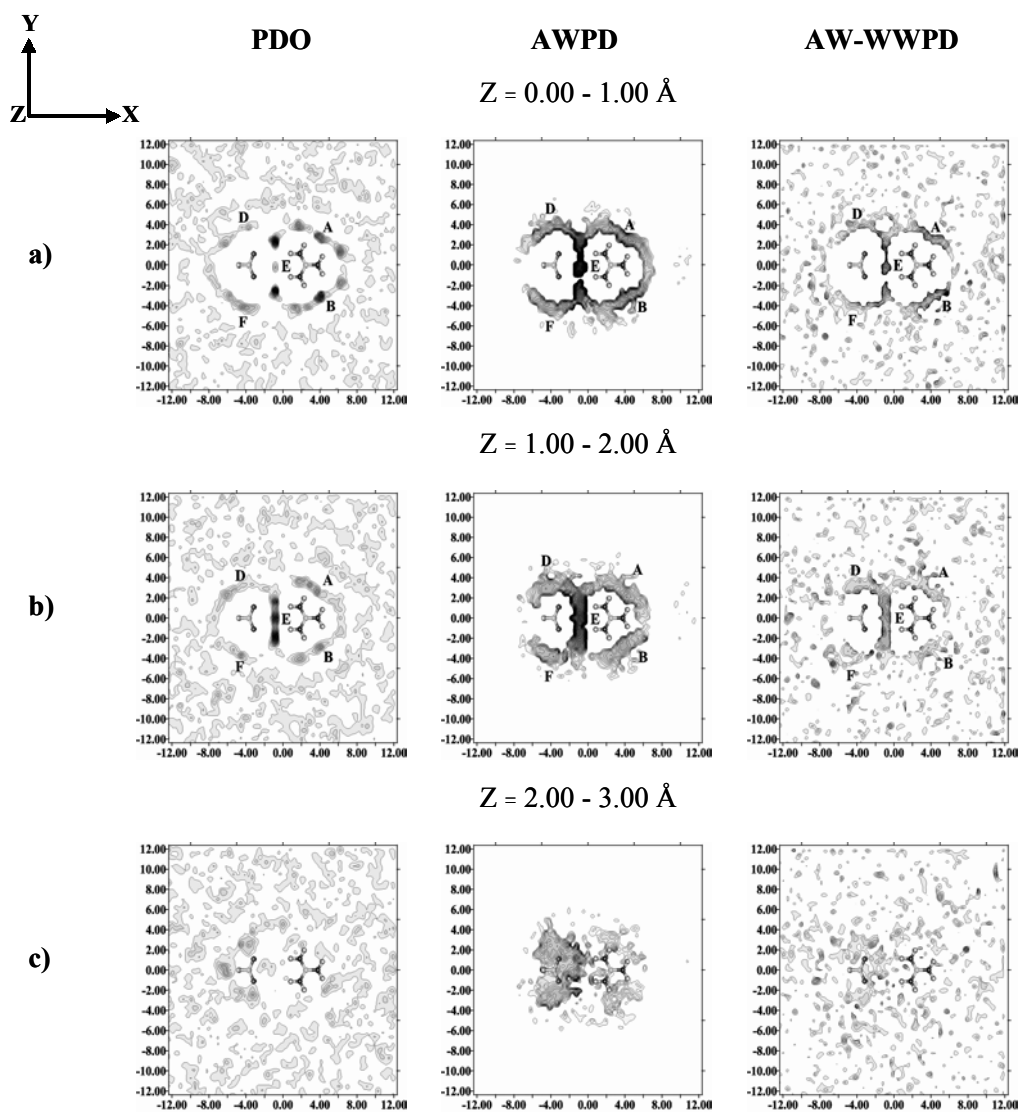


Figure 3.7

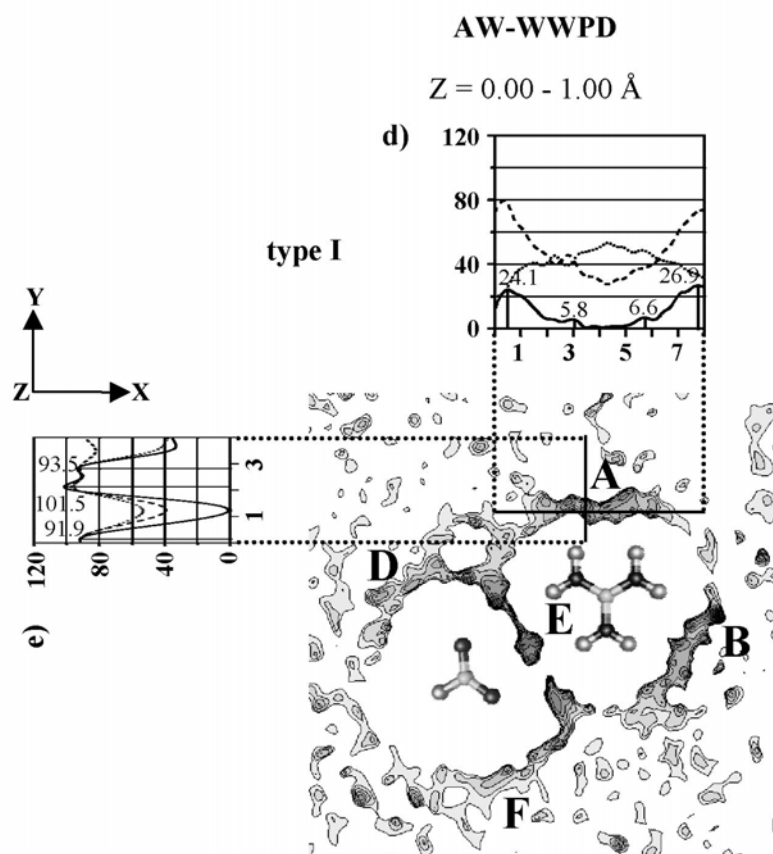


Figure 3.7 (continued)

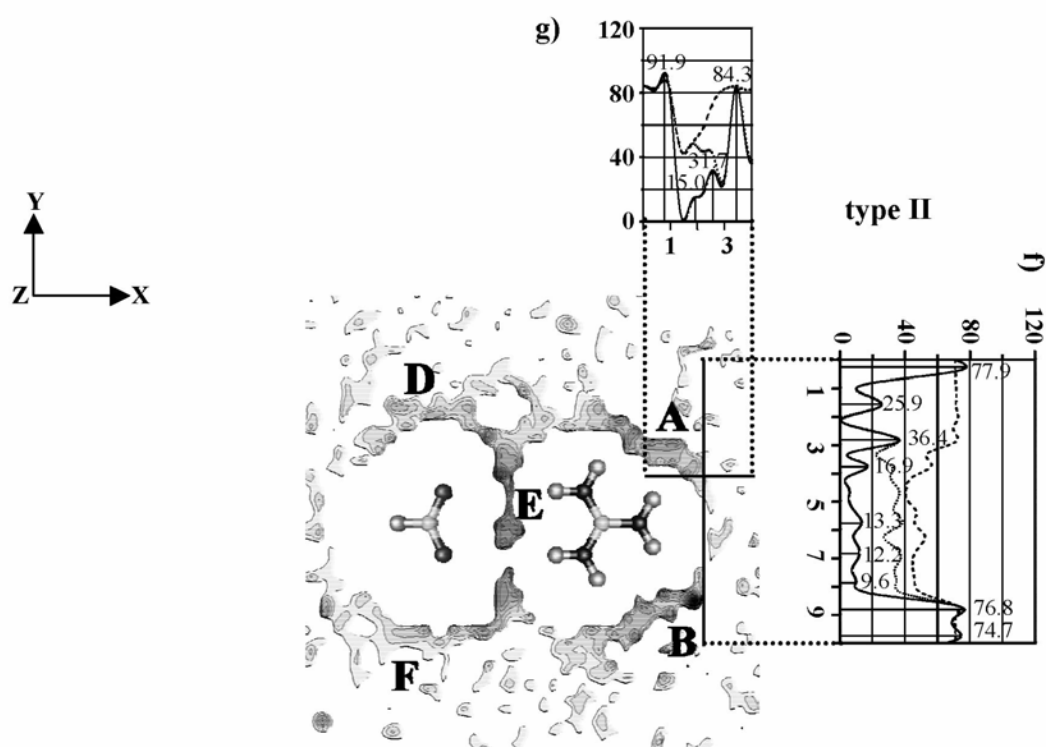


Figure 3.7 (continued)

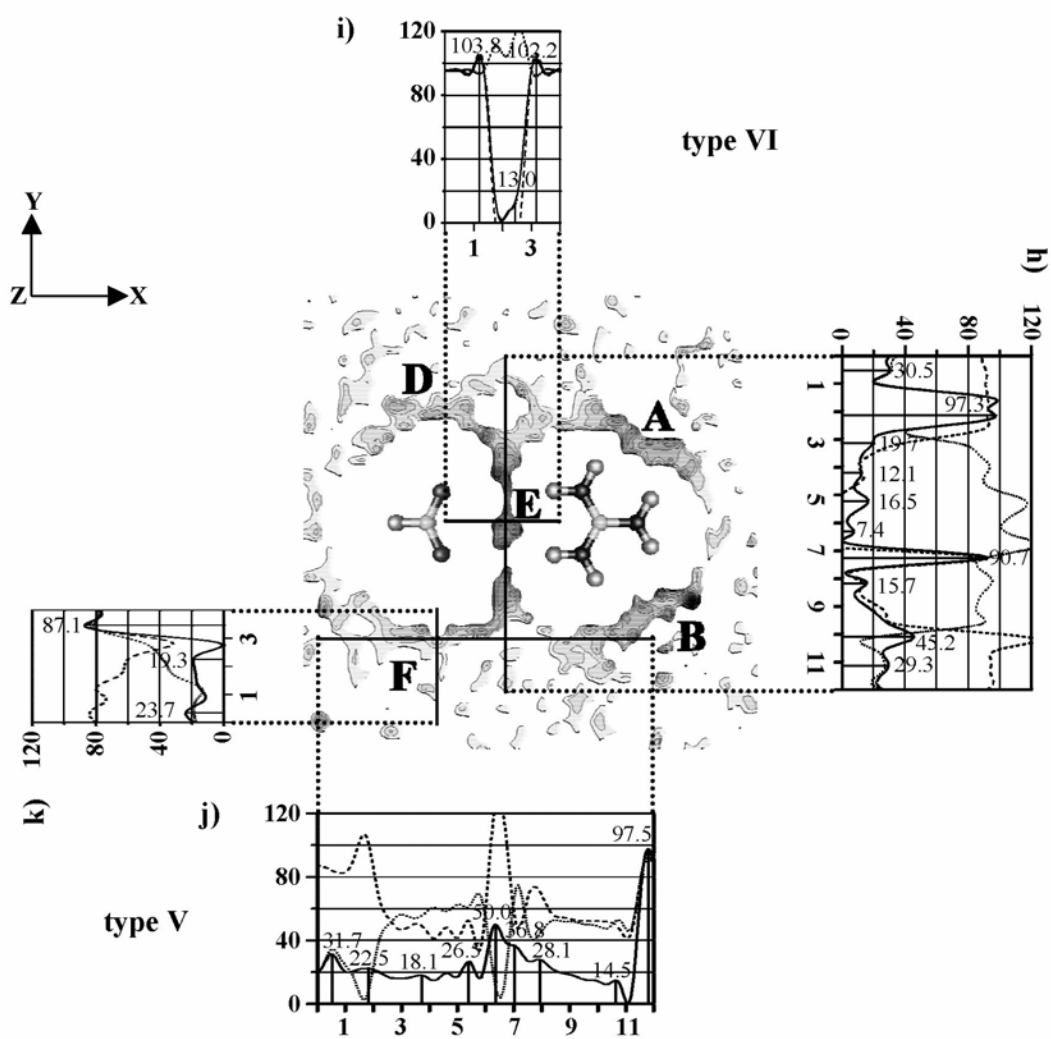


Figure 3.7 (continued)

Under the present MD simulations conditions, the solvent-separated $\text{Gdm}^+ - \text{FmO}^-$ complex seems not favorable in aqueous solutions. When all molecules were allowed to move in MD- $[\text{Gdm}^+ - \text{FmO}^-]_{\text{aq, free}}^{\text{R}=6.3}$, $g(\text{R}_{\text{C}\dots\text{C}})$ and $g(\text{R}_{\text{N}\dots\text{O}})$, (see in Appendix C), revealed that the solvent-separated $\text{Gdm}^+ - \text{FmO}^-$ complex was disrupted, due mainly to strong solute-solvent and weak solvent-solvent H-bond interactions within the interstitial H-bond network. This is different from the results of the PMF calculations (Saigal and Pranata, 1997; Rozanska and Chipot, 2000; Sagarik and Chaiyapongs, 2004), in which the second minimum, corresponding to the solvent-separated ion-pairs, was observed on the free energy profiles at the interionic distances approximately between 6 and 7 Å. A plausible explanation for the discrepancy was given in details by Chipot, Maigret, Pearlman, and Kollman (1996); Saigal and Pranata (1997), in which an artifact of the relative orientation constraint imposed in the PMF calculations was pointed out to be one of the main reasons. The applicability and shortcomings of theoretical methods for free energy calculations have been addressed in details (Kollman, 1993; Leach, 1996) and will not be repeated here.

It should be mentioned that the theoretical results reported in the present work are based on a pair-wise additive scheme, in which the many-body or polarization effects are not included in the model calculations. Based on MD simulations on $[\text{NaCl}]_{\text{aq}}$, with polarizable and nonpolarizable water models, the dependence of some ionic-solution properties on the polarizability was found to be moderate (Smith and Dang, 1994), with slightly larger effects at the highly polarizable Cl^- ion. Since the ions and the ion-pair considered in the present work are

considerably larger than monovalent ions, the polarization effects could be expected to be smaller; due to lower charge densities on atoms. Additionally, it was reported by Laria and Fernández-Prini (1995) that, when polarization effects were introduced to a model calculation, the ion clusters exhibited less structure, with lower degree of ionic hydrations; due to the destabilization of the solute-solvent interactions in the first hydration shell. Since a destabilization of the solute-solvent interactions is usually accompanied by a stabilization of the solvent-solvent interactions (Clementi, 1980), and the MD results in this present study suggested that the associations of water molecules in the first hydration shell are partly responsible for the net stabilization of the close-contact ion-pair, one could anticipate that the close-contact ion-pair will become more associated if polarization effects are included in this model calculation. The results on the solvent-separated ion-pair are also expected to remain the same; due to the fact that the solute-solvent interactions in the interstitial H-bond network are considerably stronger than the solvent-solvent interactions.

CHAPTER IV

CONCLUSION

Structures and stability of salt-bridge in aqueous solution were studied using a complex formed from the Gdm^+ and FmO^- ions as a model system. The theoretical investigations were started with construction of intermolecular potentials to describe the interactions in $[\text{Gdm}^+]_{\text{aq}}$, $[\text{FmO}^-]_{\text{aq}}$ and $[\text{Gdm}^+ - \text{FmO}^-]_{\text{aq}}$, using the T-model. The T-model potentials were tested in the calculations of equilibrium structures and interaction energies of the $\text{Gdm}^+ - \text{H}_2\text{O}$, $\text{FmO}^- - \text{H}_2\text{O}$ and $\text{Gdm}^+ - \text{FmO}^-$ 1 : 1 complexes in the gas phase. The lowest-lying minimum energy geometries of these 1 : 1 complexes were examined using *ab initio* calculations at MP2 levels of theory. It appeared that, cyclic–bifurcated H-bond complexes represent the most stable structures in the gas phase. The structural and energetic results obtained from the T-model potentials agreed well with *ab initio* calculations at the MP2 levels.

Based on the computed T-model potentials, the three-dimensional structures and energetic of the H-bond networks of water in the first hydration shell of the Gdm^+ and FmO^- ions, as well as the $\text{Gdm}^+ - \text{FmO}^-$ complex, were investigated, by conducting series of MD simulations. The PDO maps obtained from the analyses of MD results suggested two types of the H-bond networks in the first hydration shell of $[\text{Gdm}^+]_{\text{aq}}$, regarded as the H-bond network types **I** and **II** in the present study. Both of them are located on the Gdm^+ molecular plane and seem to be quite well-

connected. The analyses of the cross section plots revealed that the solute-solvent interactions dominate the solvent-solvent interactions for the H-bond network type **I**, whereas the situation is opposite for the H-bond network type **II**. The structures of the average potential energy landscapes in $[\text{Gdm}^+]_{\text{aq}}$ suggested further that water molecules inside the H-bond network type **I** should have higher mobility compare to the H-bond network type **II**.

Due to the fact that the FmO^- ion is a strong proton acceptor, the three-dimensional structures and energetic of the H-bond networks in the first hydration in $[\text{FmO}^-]_{\text{aq}}$ are different from $[\text{Gdm}^+]_{\text{aq}}$. The PDO maps showed that the H-bond network at the COO^- group is located slightly above the FmO^- plane; the longitudinal cross section plots revealed that water molecules could move or exchange in a wider range, especially in the H-bond network type **III**. The detail structures of the longitudinal and transverse cross section plots suggested that, near the energy minima in the H-bond network types **III** and **IV**, the solute-solvent interactions dominate the solvent-solvent interactions.

The MD results on $[\text{Gdm}^+ - \text{FmO}^-]_{\text{aq}}$ revealed that the close-contact ion-pair formation leads to considerable changes in the hydration structures and energetic of the aqueous solutions. In the first hydration shell, the longitudinal and transverse cross section plots indicated stronger solvent-solvent H-bond interactions compared to the solute-solvent H-bond interactions. This suggested that water molecules in the first hydration shell form solvent cages around the ion-pair complex, leading to a net stabilization effect to the close-contact ion-pair complex. Similar conclusions were put forward in the cases of $[\text{Gdm}^+ - \text{TBA} \cdot \text{AcO}^-]_{\text{DMSO}}$ and the aqueous solutions of

ion-pairs formed from monovalent ions. The solvent reorganization and solvent reactive field were pointed out to be responsible for the ion-pair associations in the solutions, respectively. Due to strong solute-solvent and weak solvent-solvent H-bond interactions in the interstitial H-bond network, the present MD simulations predicted that the solvent-separated $\text{Gdm}^+ - \text{FmO}^-$ complex are disrupted in aqueous solutions.

Attempt has been made in the present work to account for the dynamic behavior of water molecules in the first hydration shell of solutes, using the structures of the average potential energy landscapes and the longest H-bond lifetime defined in the previous investigation. Although the average potential energy landscapes in $[\text{Gdm}^+]_{\text{aq}}$, $[\text{FmO}^-]_{\text{aq}}$ and $[\text{Gdm}^+ - \text{FmO}^-]_{\text{aq}}$ are rather complicated and irregular, the computed longest H-bond lifetimes are reasonable, compared with the residence times obtained from other MD simulations and NMR experiments. The longest H-bond lifetime could be associated with the water molecule which takes the rate-determining water exchange path; by assuming that the water molecule with the longest H-bond lifetime enters the first hydration shell by taking the path with the highest transition energy barriers. The longest H-bond lifetime, therefore, represents a simple and reasonable alternative to introduce the dynamic behavior of water molecules in definition of the first hydration shell; a specific water molecule is considered to reside in the first hydration shell of solute only when it is trapped long enough in it.

Finally, it should be mentioned that the present theoretical results were based on a pair-wise additive scheme, in which the many-body or polarization effects were not included in the model calculations. However, based on the MD simulations on ion-pairs of monovalent ions in aqueous solutions, and the fact that the ions and ion-pairs considered here possess lower charge densities on atoms, compared to the

monovalent ions, it is reasonable to believe that the present results will not be substantially changed if cooperative effects are included in the model calculations.

REFERENCES

REFERENCES

- Ahlrichs, R., et al. (1985). Implementation of an electronic structure program system on the CYBER 205. **Journal of Computational Chemistry**. 6: 200-208.
- Allen, M. P., and Tildesley, D. J. (1994). **Computer simulations of liquids**. New York: Clarendon Press.
- Barlow, D. J., and Thornton, J. M. (1983). Ion-pairs in proteins. **Journal of Molecular Biology**. 168: 867-885.
- Barril, X., Alemán, C., Orozco, M., and Luque, F. J. (1998). Salt bridge interactions: Stability of the ionic and neutral complexes in the gas phase, in solution, and in proteins. **Proteins: Structure, Function, and Genetics**. 32: 67-79.
- Böhm, H. J., and Ahlrichs, R. (1982). A study of short-range repulsions. **Journal of Chemical Physics**. 77: 2028-2034.
- Böhm, H. J., and Ahlrichs, R. (1985). Molecular dynamics simulation of liquid CH_2Cl_2 and CHCl_3 with new pair potentials. **Molecular Physics**. 54: 1261-1274.
- Böhm, H. J., Ahlrichs, R., Scharf, P., and Schiffer, H. (1984). Intermolecular potentials for CH_4 , CH_3F , CHF_3 , CH_3Cl , CH_2Cl_2 , CH_3CN and CO_2 . **Journal of Chemical Physics**. 81: 1389-1395.
- Böhm, H. J., Meissner, C., and Ahlrichs, R. (1984). Molecular dynamics simulation of liquid CH_3F , CHF_3 , CH_3Cl , CH_2Cl_2 , CH_3CN , CO_2 and CS_2 with new pair potentials. **Molecular Physics**. 53: 651-672.

- Boys, S. F., and Bernardi, F. (1970). The calculation of small molecular interactions by the differences of separate total energies. Some procedures with reduced errors. **Molecular Physics**. 19: 553-566.
- Breneman, C. M., and Wiberg, K. B. (1990). Determining atom-centered monopoles from molecular electrostatic potentials. The need for high sampling density in formamide conformational analysis. **Journal of Computational Chemistry**. 11: 361-373.
- Brugè, F., Parisi, E., and Fonili, S. L. (1996). Effects of simple model solutes on water dynamics: residence time analysis. **Chemical Physics Letters**. 250: 443-449.
- Brunne, R. M., Liepinsh, E., Otting, G., Wüthrich, K., and van Gunsteren, W. F. (1993). Hydration of proteins: A comparison of experimental residence times of water molecules solvating the bovine pancreatic trypsin inhibitor with theoretical model calculations. **Journal of Molecular Biology**. 231: 1040-1048.
- Case, D. A., et al. (1999). **AMBER** (version 6) [computer software]. San Francisco: University of California.
- Chipot, C., Maignet, B., Pearlman, D. A., and Kollman, P. A. (1996). Molecular dynamics potential of mean force calculations: A study of the toluene-ammonium π -cation interactions. **Journal of the American Chemical Society**. 118: 2998-3005.
- Clementi, E. (1980). **Lecture notes in chemistry 19: Computational aspects for large chemical systems**. Berlin: Springer-Verlag.
- Cummins, P. L., and Gready, J. E. (1994). The electrostatic potential in the

- semiempirical molecular orbital approximation. **Chemical Physics Letters**. 225: 11-17.
- Fan, E., Van Arman, S. A., Kincaid, S., and Hamilton, A. D. (1993). Molecular recognition: Hydrogen-bonding receptors that function in highly competitive solvents. **Journal of the American Chemical Society**. 115: 369-370.
- Field, M. J., Baas, P. A., and Karplus, M. (1990). A combined quantum mechanical and molecular mechanical potential for molecular dynamics simulations. **Journal of Computational Chemistry**. 11: 700-733.
- Frisch, M. J., et al. (1998). **Gaussian 98** package (revision A.7) [Computer software]. Pittsburgh, PA, USA: Gaussian.
- Fülscher, M. P., and Mehler, E. L. (1988). Ab initio interaction potentials of guanidine-formic acid in neutral and charged states. **Journal of Molecular Structure (THEOCHEM)**. 165: 319-327.
- Gandini, D., Gogioso, L., Bolognesi, M., and Bordo, D. (1996). Pattern of ionizable sidechains interactions in protein structures. **Proteins: Structure, Function, and Genetics**. 24: 439-449.
- Gao, J. (1994). Computation of intermolecular interactions with a combined quantum mechanical and classical approach. In D. A. Smith (ed.). **Modeling the hydrogen bond**. (ACS Symposium Series 569, pp. 8-21). Washington, DC: American Chemical Society.
- Gao, J., Garner, D. S., and Jorgensen, W. L. (1986). Ab initio study of structures and binding energies for anion-water complexes. **Journal of the American Chemical Society**. 108: 4784-4790.
- Hertz, H. G. (1973). **Water**. In F. Franks (ed.). (A Comprehensive Treatise vol. 3.).

New York: Plenum Press.

- Hoinkis, J., Ahlrichs, R., and Böhm, H. J. (1983). A simple treatment of intermolecular interactions: Synthesis of ab initio calculations and combination rules. **International Journal of Quantum Chemistry**. 23: 821-834.
- Impey, R. W., Madden, P. A., and McDonald, I. R. (1983). Hydration and mobility of ions in solution. **The Journal of Physical Chemistry**. 87: 5071-5083.
- Ippolito, J. A., Alexander, R. S., and Christianson, D. W. (1990). Hydrogen bond stereochemistry in protein structure and function. **Journal of Molecular Biology**. 215: 457-471.
- Jorgensen, W. L., and Gao, J. (1986). Monte Carlo simulations of the hydration of ammonium and carboxylate ions. **The Journal of Physical Chemistry**. 90: 2174-2182.
- Jorgensen, W. L., and Tirado-Rives, J. (1988). The OPLS potential functions for proteins. Energy minimizations for crystals of cyclic peptides and crambin. **Journal of the American Chemical Society**. 110: 1657-1666.
- Keith, T. A., and Frisch, M. J. (1994). Inclusion of explicit solvent molecules in a self-consistent-reaction field model of solvation. In D. A. Smith (ed.). **Modeling the hydrogen bond**. (ACS Symposium Series 569, pp. 22-35). Washington, DC: American Chemical Society.
- Kirsch, J. F., et al. (1984). Mechanism of action of aspartate aminotransferase proposed on the basis of its spatial structure. **Journal of Molecular Biology**. 174: 497-525.
- Kollman, P. (1993). Free energy calculations: Applications to chemical and biological

- phenomena. **Chemical Reviews**. 93: 2395-2417.
- Laria, D., and Fernández-Prini, R. (1995). Molecular dynamics study of water clusters containing ion pairs: From contact to dissociation. **Journal of Chemical Physics**. 102: 7664-7673.
- Leach, A. R. (1996). **Molecular modelling: Principle and applications**. Singapore: Longman.
- Linton, B., and Hamilton, A. D. (1999). Calorimetric investigation of guanidinium-carboxylate interactions. **Tetrahedron**. 55: 6027-6038.
- Lukovits, I., Karpfen, A., Lischka, H., and Schuster, P. (1979). Ab initio LCMO studies on the hydration of formate ion. **Chemical Physics Letters**. 63: 151-154.
- Luque, F. J., Reuter, N., Cartier, A., and Ruiz-López, M. F. (2000). Calibration of the quantum/classical Hamiltonian in semiempirical QM/MM AM1 and PM3 methods. **The Journal of Physical Chemistry A**. 104: 10923-10931.
- Melo, A., et al. (1999). Theoretical study of arginine-carboxylate interactions. **Journal of Molecular Structure (THEOCHEM)**. 463: 81-90.
- Mitchell, J. B. O., Thornton, J. M., Singh J., and Price, S. L. (1992). Towards an understanding of the arginine-aspartate interaction. **Journal of Molecular Biology**. 226: 251-262.
- Moran, L. A., and Scrimgeour, K. G. (1994). **Biochemistry resource book**. London: Prentice Hall.
- Muegge, I., and Knapp, E. W. (1995). Residence times and lateral diffusion of water at protein surfaces: Application to BPTI. **The Journal of Physical Chemistry**. 99: 1371-1374.

- Nakamura, H. (1999). Salt bridge (Salt linkage, Ionic bond). In T. E. Creighton (ed.). **Encyclopedia of molecular biology**. (Vol. 4, p. 2266). New York: John Wiley & Son.
- Odelius, M., and Laaksonen, A. (1999). Combined MD simulation-NMR relaxation studies of molecular motion and intermolecular interactions. In P. B. Baluena and J. M. Seminario (eds.). **Molecular dynamics from classical to quantum methods**. (Theoretical and computational chemistry, Vol. 7, pp. 281-324). Amsterdam: Elsevier.
- Refson, K. (1996). **Moldy** (revision 2.20 for release 2.14) [Computer software]. Oxford UK: Department of Earth Sciences, Oxford University.
- Riordan, J. F., McElvany, K. D., and Borders, C. L. (1977). Arginyl residues: Anion recognition sites in enzymes. **Science**. 195: 884-886.
- Rozanska, X., and Chipot, C. (2000). Modeling ion-ion interaction in proteins: A molecular dynamics free energy calculation of the guanidinium-acetate association. **Journal of Chemical Physics**. 112: 9691-9694.
- Sagarik, K. (1999). Theoretical studies on hydrogen bonding in hydroxylamine clusters and liquid. **Journal of Molecular Structure (THEOCHEM)**. 465: 141-155.
- Sagarik, K., and Asawakun, P. (1997). Intermolecular potential for phenol based on the test particle model. **Chemical Physics**. 219: 173-191.
- Sagarik, K., Chaiwongwattana, S., and Sisot, P. A theoretical study on clusters of benzoic acid-water in benzene solutions. (2004). **Chemical Physics**. 306: 1-12.
- Sagarik, K., and Chaiyapongs, S. (2004). Structures and stability of model salt-bridge

- interaction in aqueous solution. In **Proceedings of the 8 th Annual National Symposium on Computational Science and Engineering (ANSCSE-8)**. (pp. 9-12). Nakhon Ratchasima, Thailand: Suranaree University of Technology.
- Sagarik, K., and Dokmaisrijan, S. (2005). A theoretical study on hydration of alanine zwitterions. **Journal of Molecular Structure (THEOCHEM)**. 718: 31-47.
- Sagarik, K., and Rode, B. M. (2000). Intermolecular potential for benzoic acid-water based on the test-particle model and statistical mechanical simulations of benzoic acid in aqueous solutions. **Chemical Physics**. 260: 159-182.
- Sagarik, K., and Spohr, E. (1995). Statistical mechanical simulations on properties of liquid pyridine. **Chemical Physics**. 199: 73-82.
- Sagarik, K. P., and Ahlrichs, R. (1986). Molecular dynamics simulations of liquid CHClF_2 with a test-particle model potential. **Chemical Physics Letters**. 131: 74-81.
- Sagarik, K. P., and Ahlrichs, R. (1987). A test particle model potential for formamide and molecular dynamics simulations of the liquid. **Journal of Chemical Physics**. 86: 5117-5126.
- Sagarik, K. P., Ahlrichs, R., and Brode, S. (1986). Intermolecular potentials for ammonia based on the test particle model and the coupled pair functional method. **Molecular Physics**. 57: 1247-1264.
- Sagarik, K. P., Pongpituk, V., Chaiyapongs, S., and Sisot, P. (1991). Test-particle model potentials for hydrogen-bonded complexes: complexes formed from HCN, HF, H_2O , NH_3 , HCONH_2 , HCONHCH_3 , guanine and cytosine. **Chemical Physics**. 156: 439-456.

- Saigal, S., and Pranata, J. (1997). Monte Carlo simulations of guanidinium acetate and methylammonium acetate ion pairs in water. **Bioorganic Chemistry**. 25: 11-21.
- Shimoni, L., Glusker, J. P., and Bock, C. W. (1996). Energies and geometries of isographic hydrogen-bonded networks. 1. The $R_2^2(8)$ graph set. **The Journal of Physical Chemistry**. 100: 2957-2967.
- Singh, J., Thornton, J. M., Snarey, M., and Campbell, S. F. (1987). The geometries of interacting arginine-carboxyls in proteins. **FEBS Letters**. 224: 161-171.
- Smith, D. E., and Dang, L. X. (1994). Computer simulations of NaCl association in polarizable water. **Journal of Chemical Physics**. 100: 3757-3766.
- Su, Y., and Gallicchio, E. (2004). The non-polar solvent potential of mean force for the dimerization of alanine dipeptide: the role of solute-solvent van der Waals interactions. **Biophysical Chemistry**. 109: 251-260.
- SURFER** for window (version 6.04) [Computer software]. (1997). USA: Golden Software.
- Tormo, J., et al. (1994). Crystal structure of a human rhinovirus neutralizing antibody complexed with a peptide derived from viral capsid protein VP2. **The EMBO Journal**. 13: 2247-2256.
- Van Holde, K. E., Johnson, W. C., and Ho, P. S. (1998). **Principle of physical biochemistry**. New Jersey: Prentice-Hall.
- Wüthrich, K. (1995) Hydration of biological macromolecules in solution: Surface structure and molecular recognition. In K. Wüthrich (ed.). **NMR in structural biology**. (World Scientific Series in 20 th Century Chemistry, Vol. 5, pp. 647-655). Singapore: World Scientific.

Zheng, Y-J., and Ornstein, R. L. (1996). What happens to salt-bridges in nonaqueous environments: Insights from quantum mechanics calculations. **Journal of the American Chemical Society**. 118: 11237-11243.

APPENDICES

APPENDIX A

TWENTY COMMON AMINO ACIDS

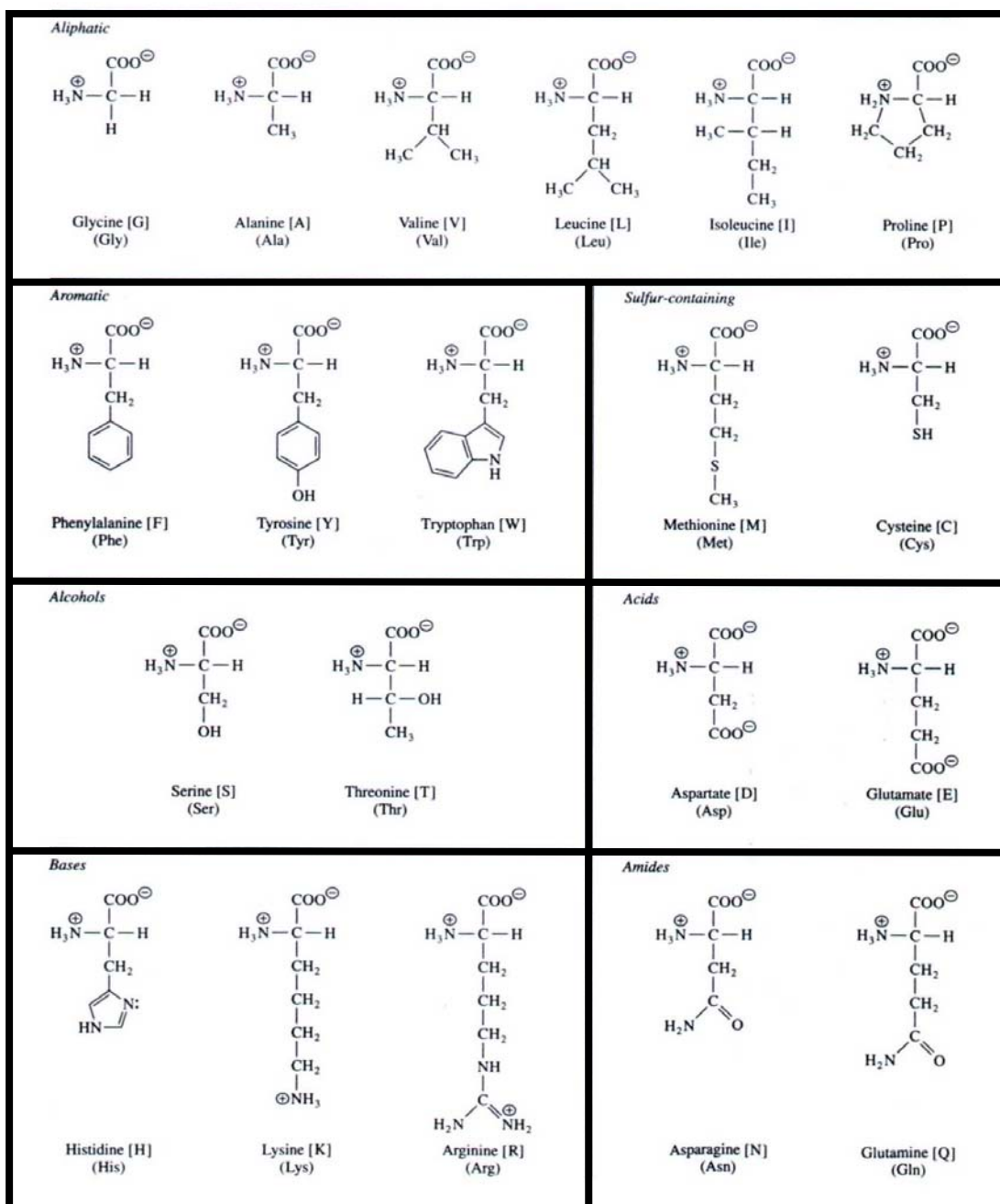


Figure A.1 Twenty common amino acids (Moran and Scrimgeour, 1994).

APPENDIX B

SUPPLEMENTARY DIAGRAMS FOR

RESEARCH METHODOLOGY

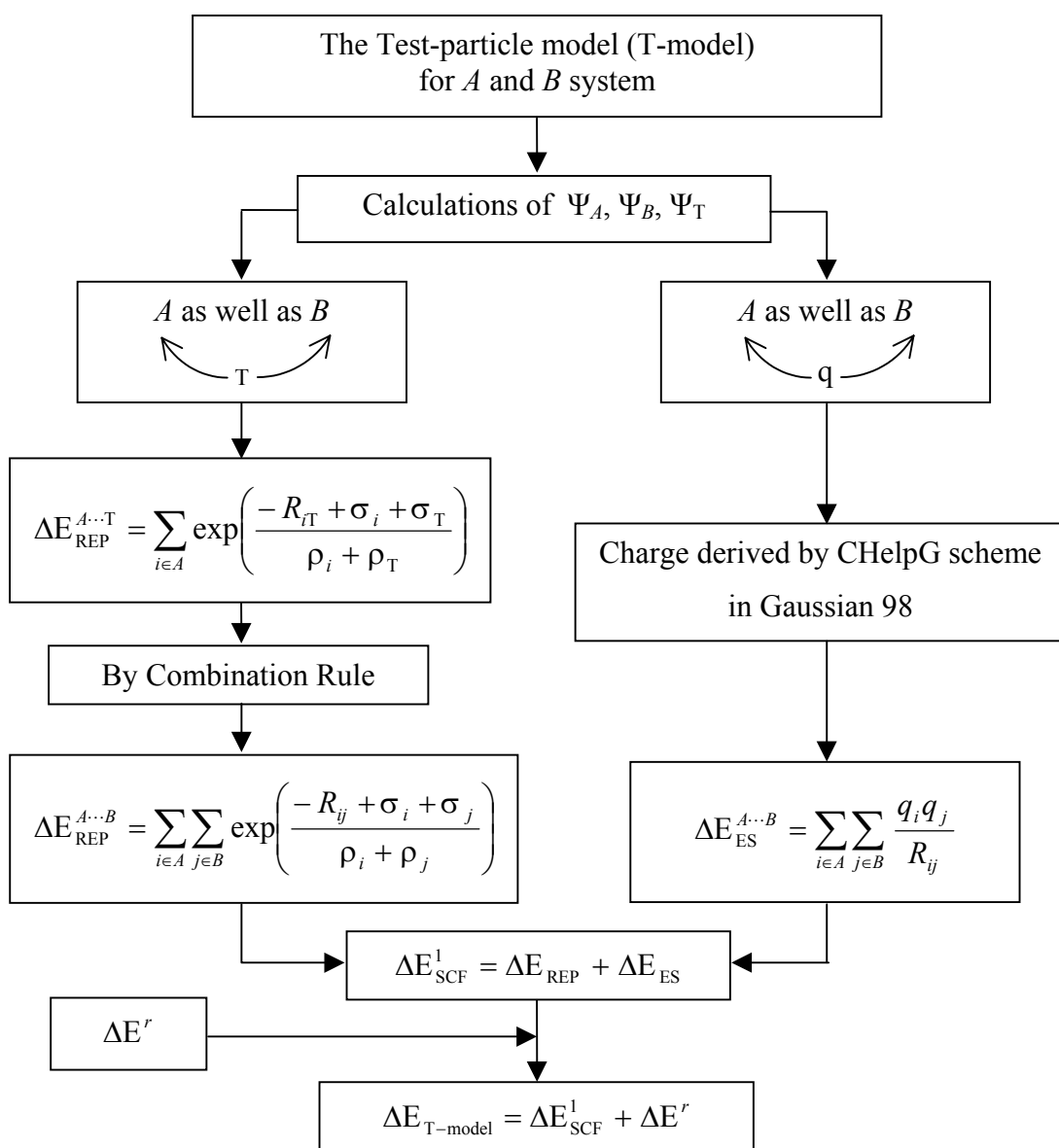


Figure B.1 Basic steps in the construction of T-model potential.

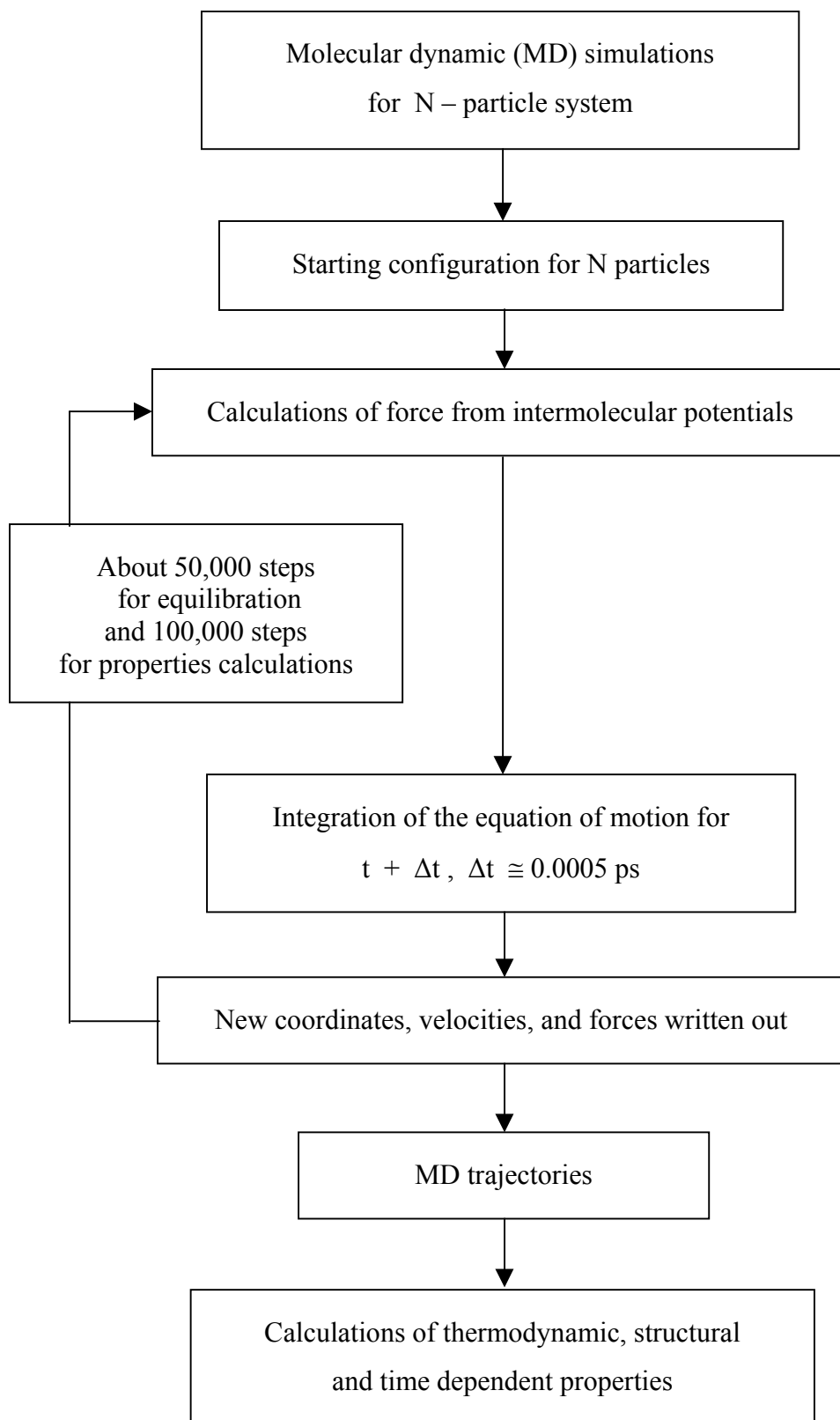


Figure B.2 Schematic diagram for MD simulations of N-particle system.

APPENDIX C
SUPPLEMENTARY RESULTS

Table C.1 Optimized geometries of the Gdm^+ , and FmO^- ions.

Ion	Bond length (Å)	Bond angle (degree)
Gdm^+	C-N = 1.334 N-H = 1.009	N-C-N = 120.00 C-N-H = 121.05 H-N-H = 117.90
FmO^-	C-O = 1.254 C-H = 1.127	O-C-O = 130.32 H-C-O = 114.84

Table C.2 The T-model parameters for Gdm^+ , FmO^- and water. All parameters are in atomic unit.

	Atom	σ_i	ρ_i	q_i
Gdm^+	C	0.041671	0.507268	1.306000
	N	1.294571	0.241744	-1.100000
	H	-0.080972	0.245387	0.499000
FmO^-	C	0.829235	0.328076	0.977705
	O	1.160264	0.239856	-0.889574
	H	0.165060	0.289490	-0.198557
$\text{H}_2\text{O}^{(1)}$	O	1.284091	0.200370	-0.451660
	H	-0.318644	0.331849	0.514110
	D ⁽²⁾	-	-	-0.576560

⁽¹⁾ Data taken from Sagarik et al. (1991).

⁽²⁾ Dummy center for electrostatic point charge.

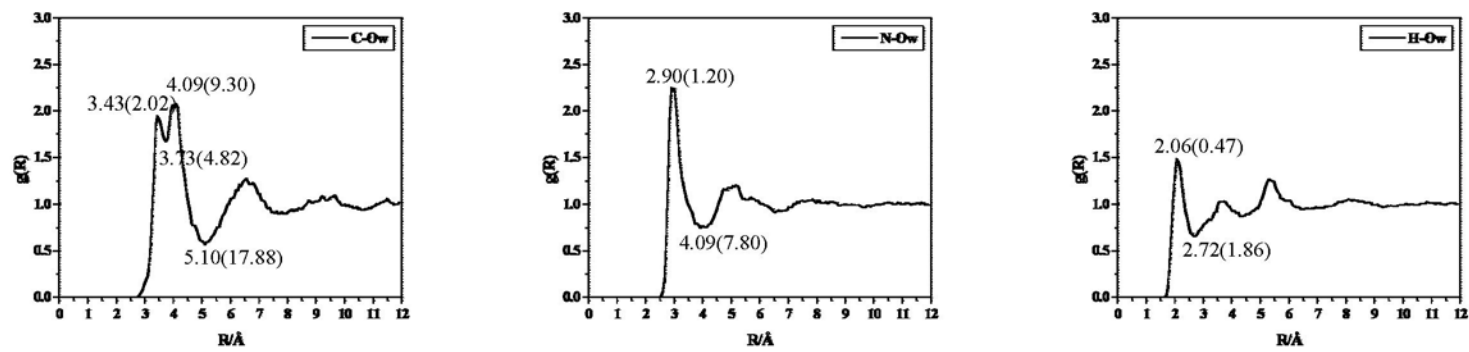
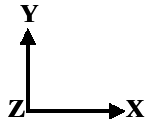
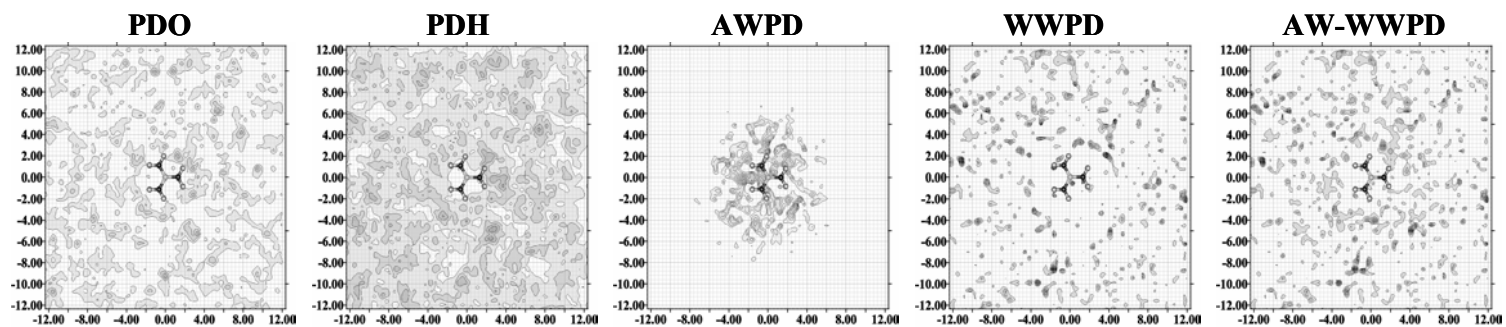


Figure C.1 $g(R)$ obtained from MD- $[\text{Gdm}^+]_{\text{aq}}$; characteristic distances are given, with $n(R)$ in parentheses.



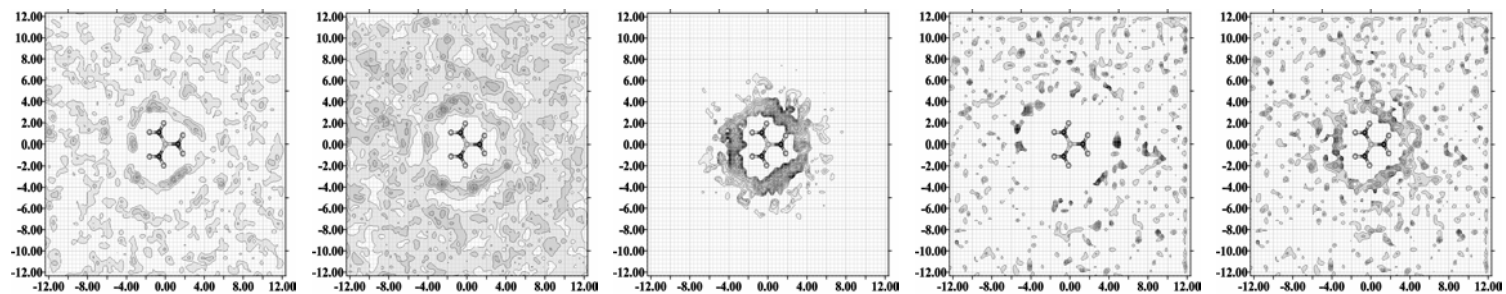
a)

 $Z = 2.00 - 3.00 \text{ \AA}$



b)

 $Z = 1.00 - 2.00 \text{ \AA}$



c)

 $Z = 0.00 - 1.00 \text{ \AA}$

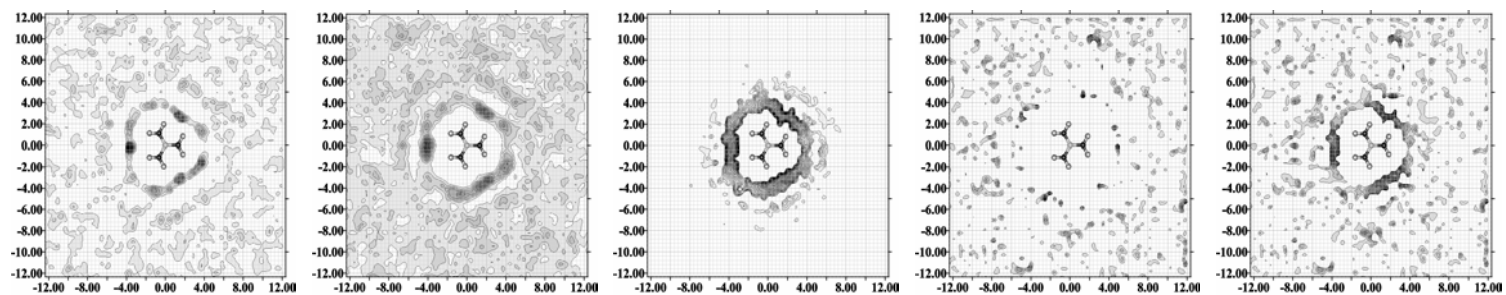
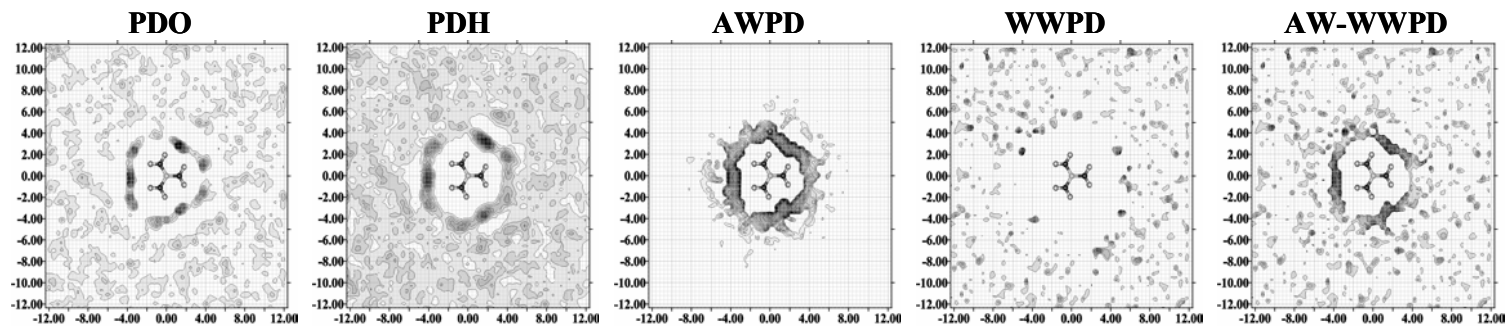
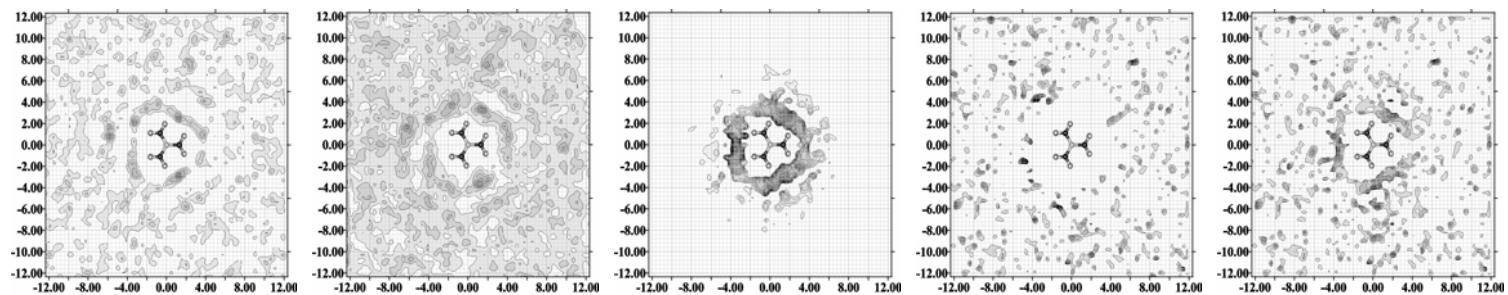


Figure C.2 The PDO, PDH, AWP, WWPD and AW-WWPD maps obtained from MD-[Gdm⁺]_{aq}.

Y
↑
Z ← **X** →
d)
 $Z = -1.00 - 0.00 \text{ \AA}$



e)
 $Z = -2.00 - -1.00 \text{ \AA}$



f)
 $Z = -3.00 - -2.00 \text{ \AA}$

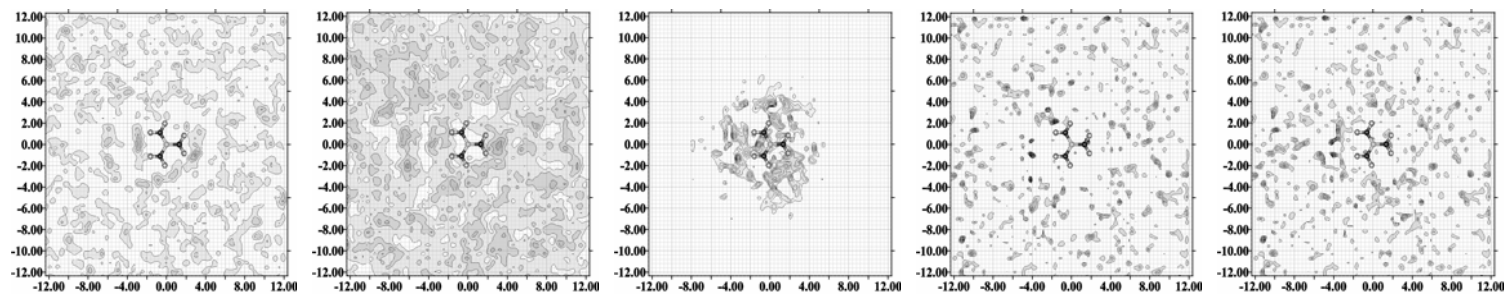


Figure C.2 (continued)

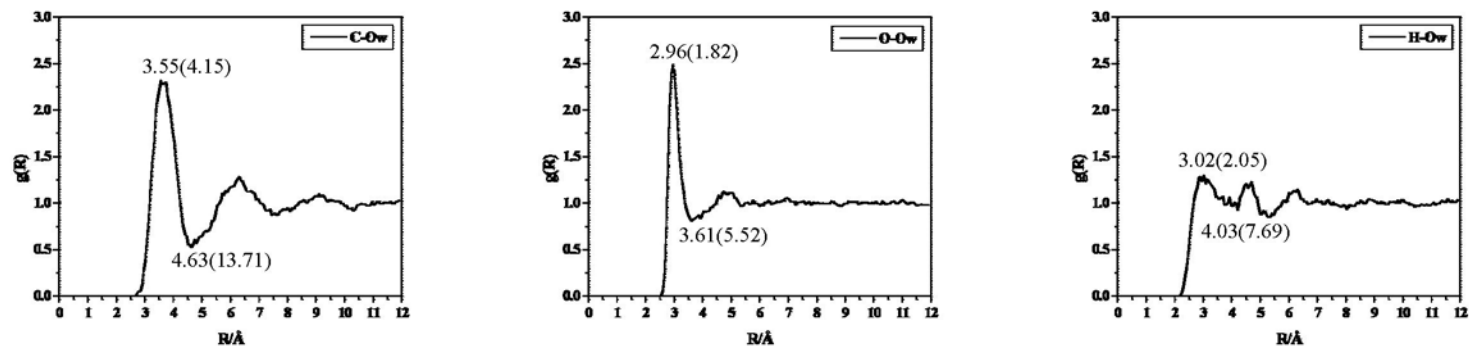
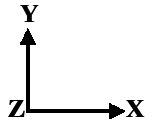
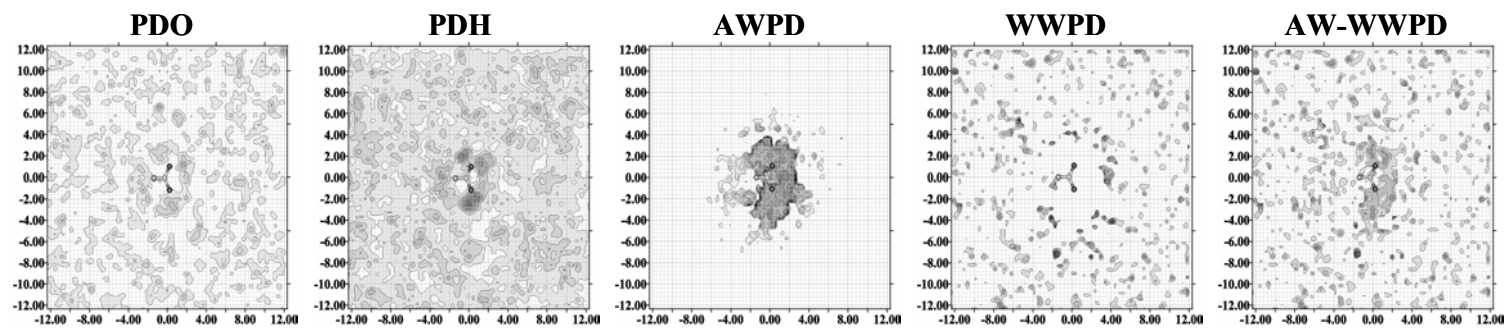


Figure C.3 $g(R)$ obtained from MD- $[\text{FmO}^-]_{\text{aq}}$; characteristic distances are given, with $n(R)$ in parentheses.



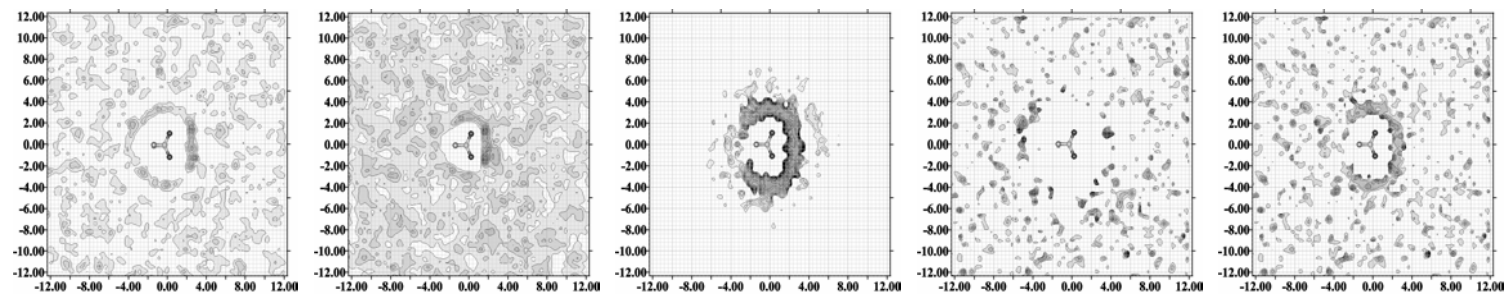
a)

 $Z = 2.00 - 3.00 \text{ \AA}$



b)

 $Z = 1.00 - 2.00 \text{ \AA}$



c)

 $Z = 0.00 - 1.00 \text{ \AA}$

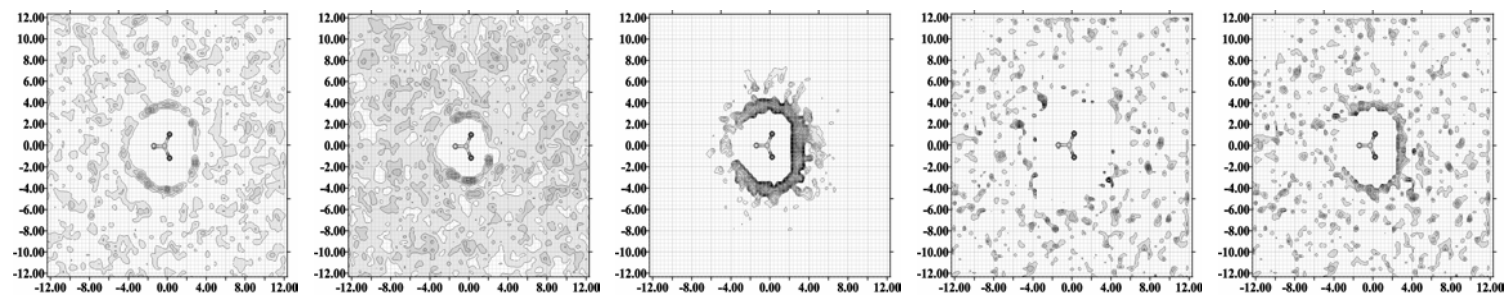
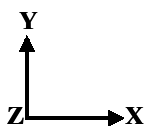
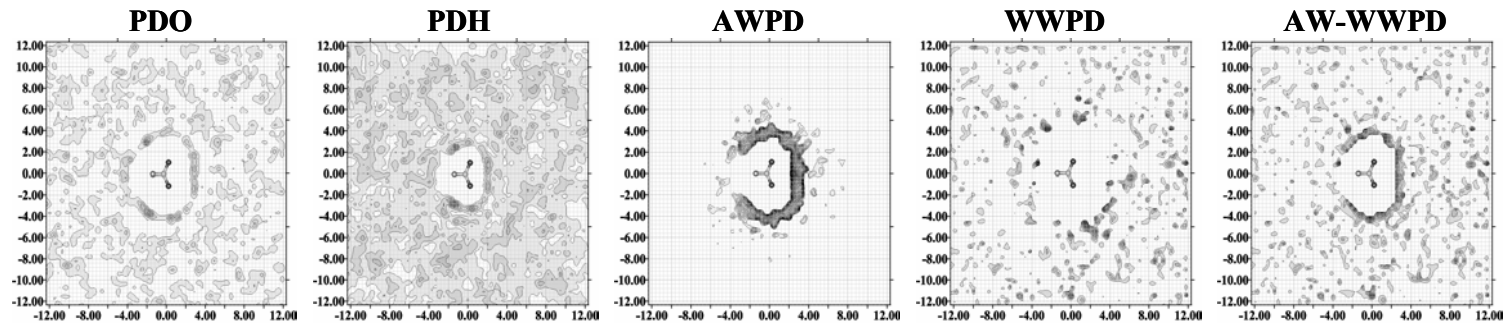


Figure C.4 The PDO, PDH, AWP, WWPD and AW-WWPD maps obtained from MD- $[\text{FmO}^-]_{\text{aq}}$.



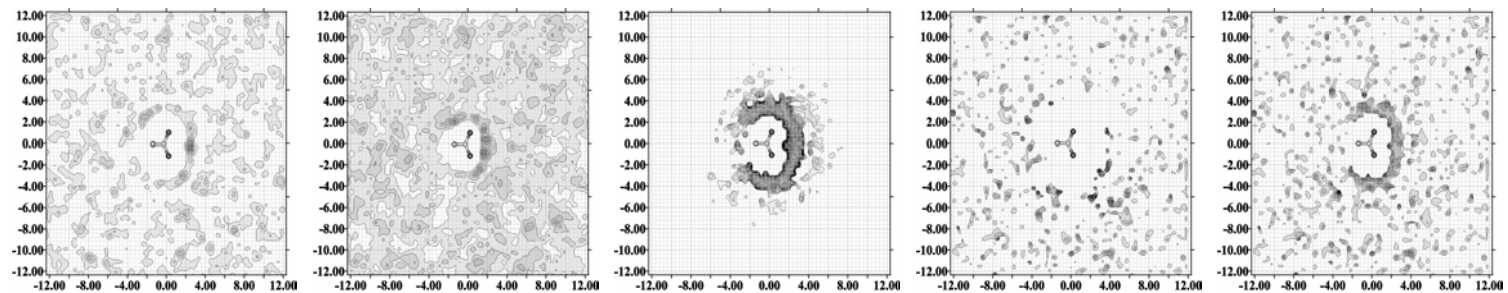
d)

 $Z = -1.00 - 0.00 \text{ \AA}$



e)

 $Z = -2.00 - -1.00 \text{ \AA}$



f)

 $Z = -3.00 - -2.00 \text{ \AA}$

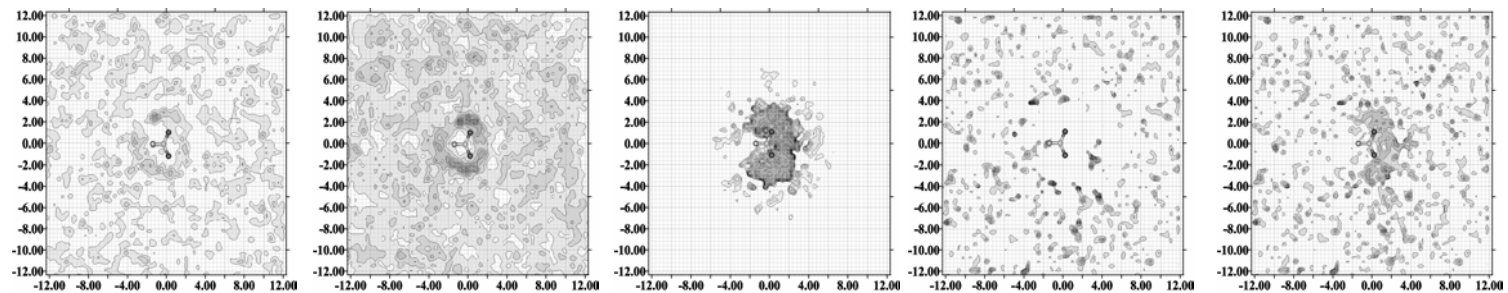


Figure C.4 (continued)

Figure C.5 $g(R)$ obtained from MD- $[\text{Gdm}^+ - \text{FmO}^-]_{\text{aq, frozen}}^{R=3.9}$;

characteristic distances are given, with $n(R)$ in parentheses.

(see Figure 2.1 for atom numbering)

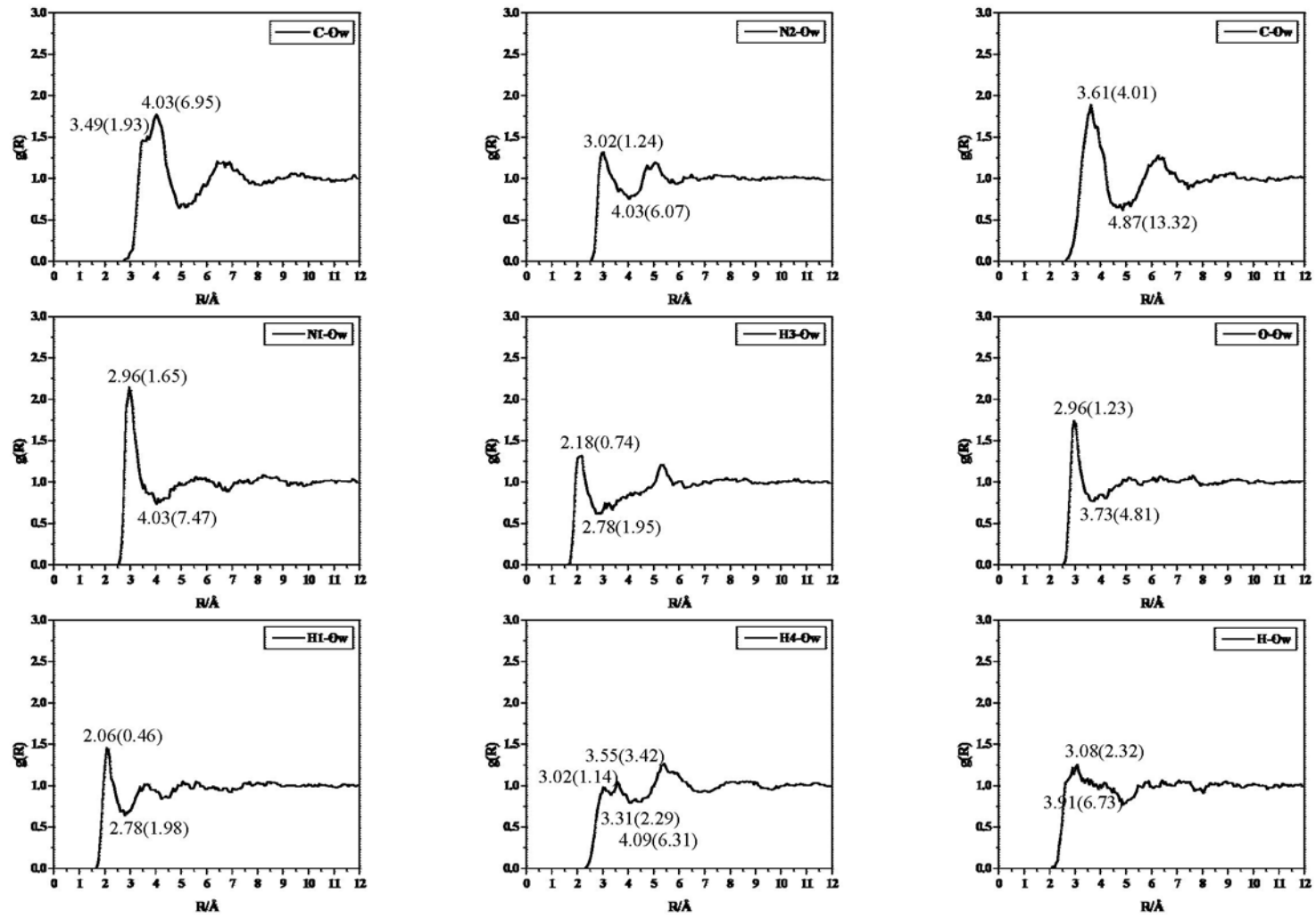


Figure C.5

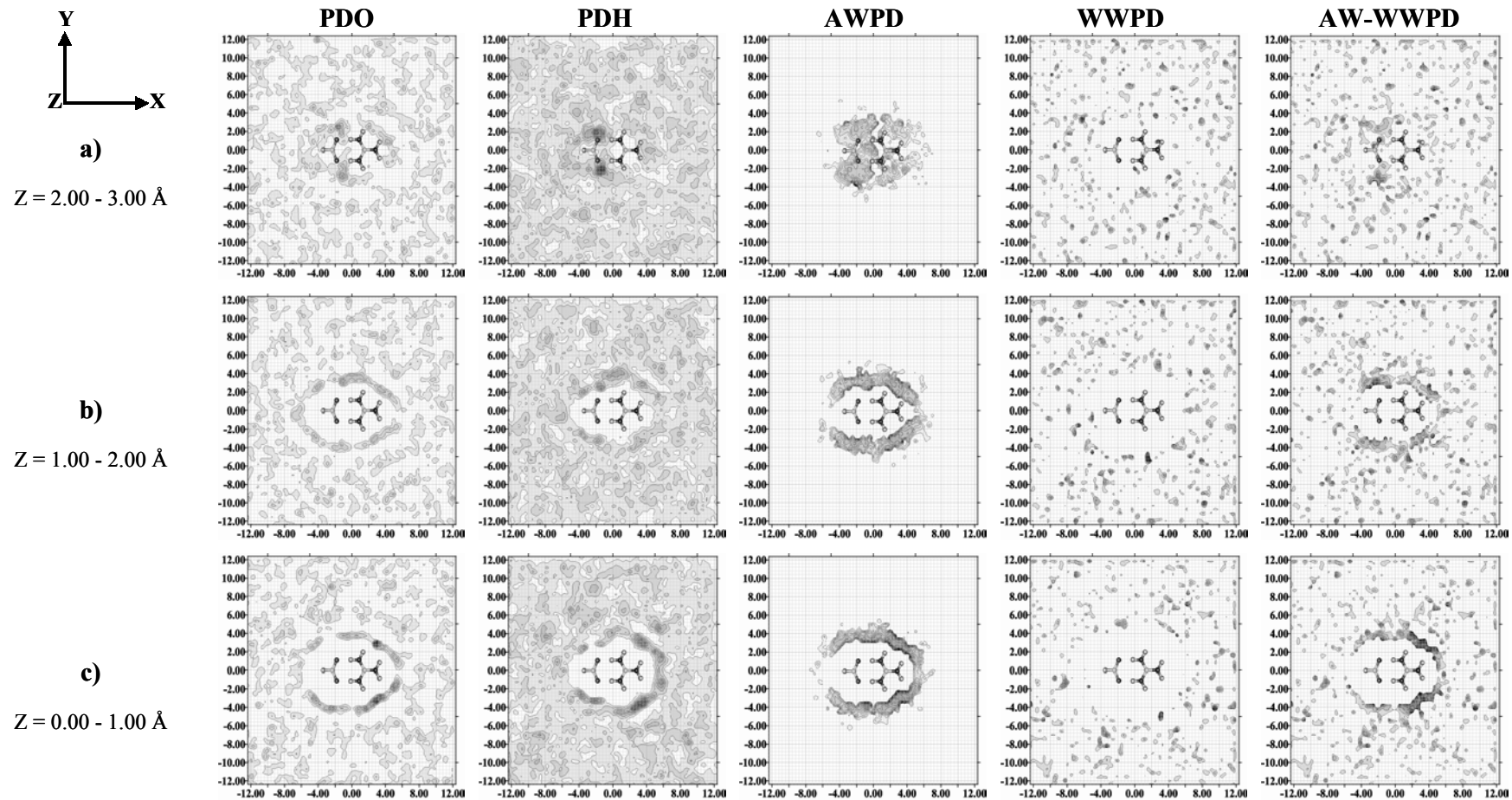
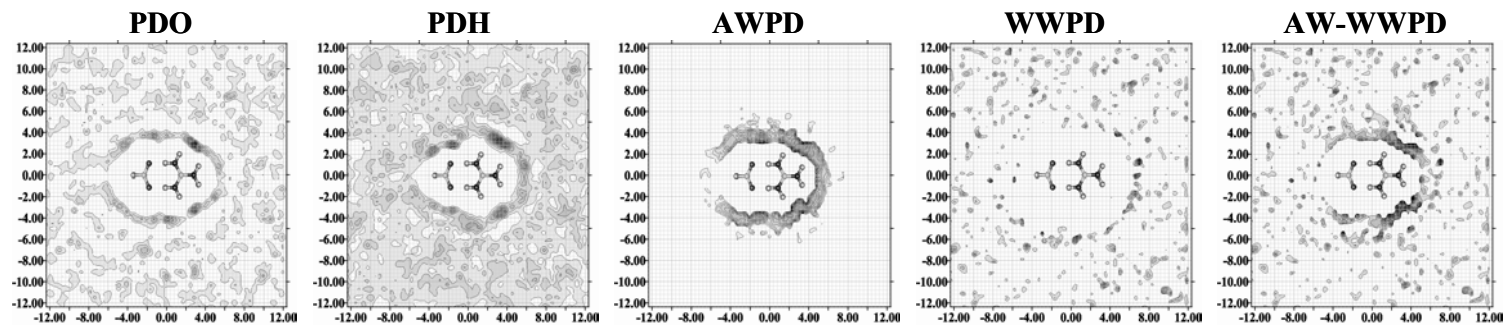
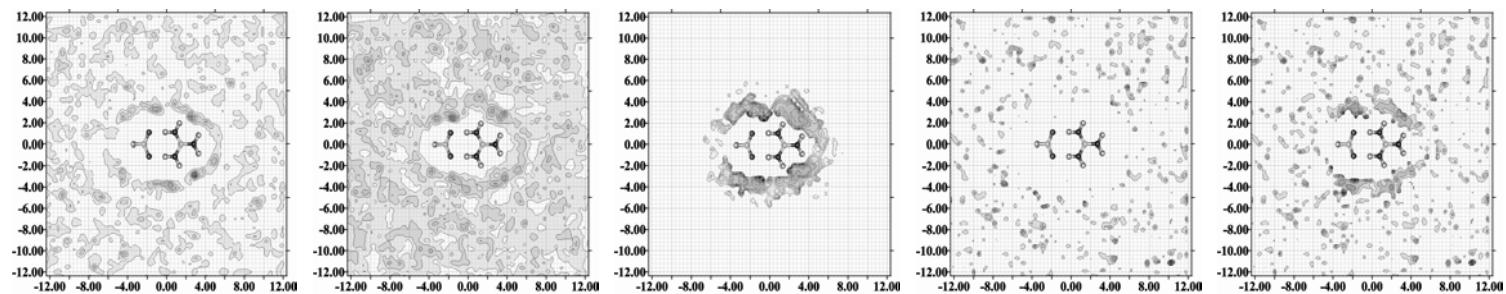


Figure C.6 The PDO, PDH, AWPD, WWPD and AW-WWPD maps obtained from MD-[Gdm⁺ - FmO⁻]_{aq, frozen}^{R=3.9}.

Y
↑
Z ← **X** →
d)
 $Z = -1.00 - 0.00 \text{ \AA}$



e)
 $Z = -2.00 - -1.00 \text{ \AA}$



f)
 $Z = -3.00 - -2.00 \text{ \AA}$

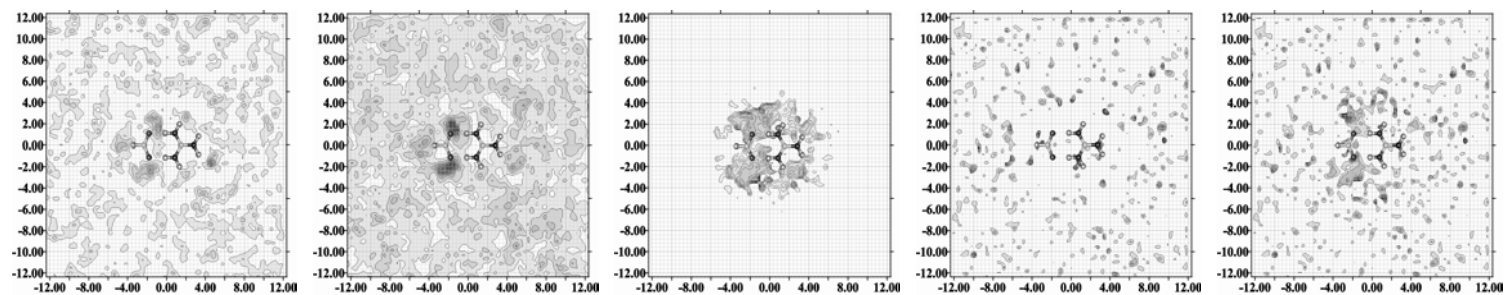


Figure C.6 (continued)

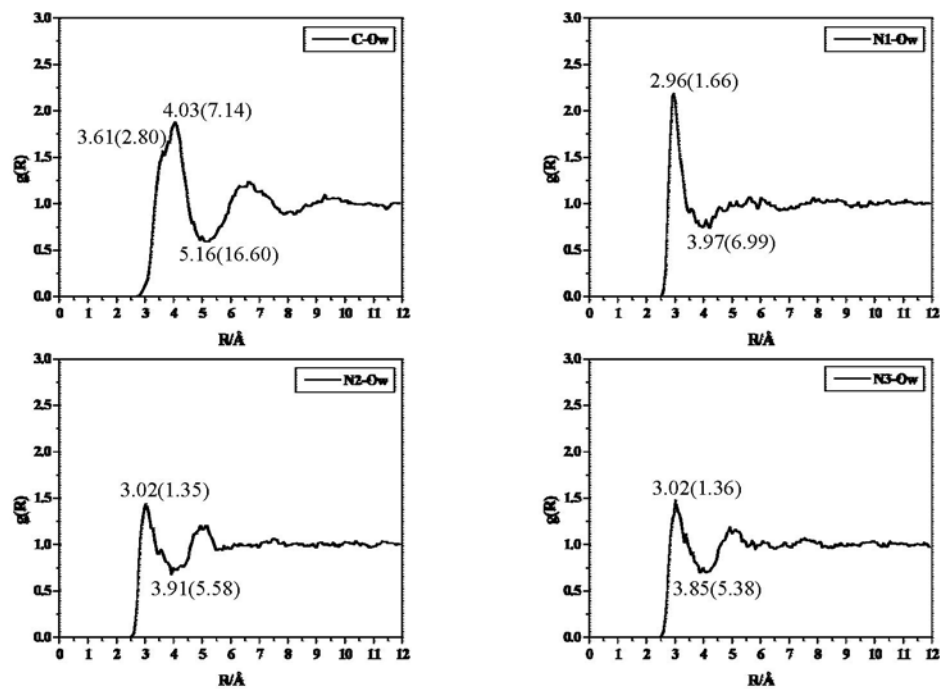


Figure C.7 $g(R)$ obtained from MD-[Gdm⁺ – FmO⁻]_{aq, free}^{R=3.9}; characteristic distances are given, with $n(R)$ in parentheses.

(see Figure 2.1 for atom numbering)

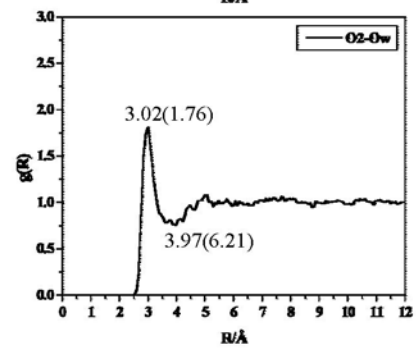
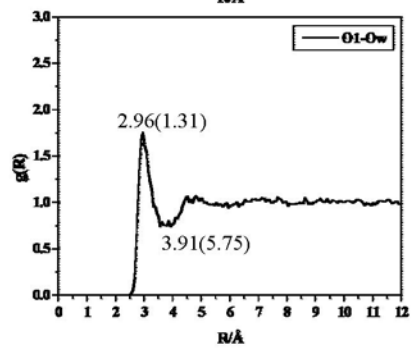
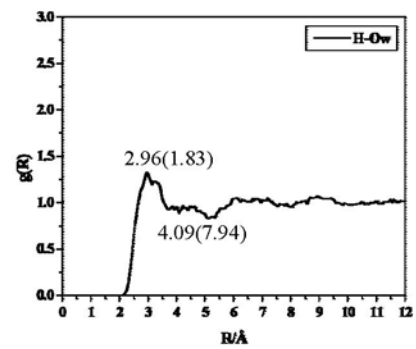
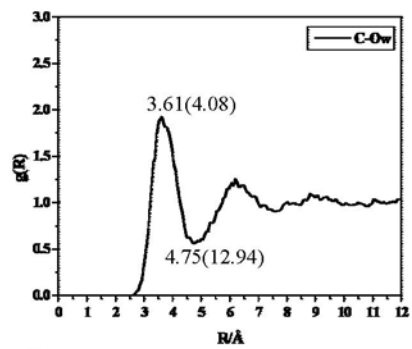


Figure C.7 (continued)

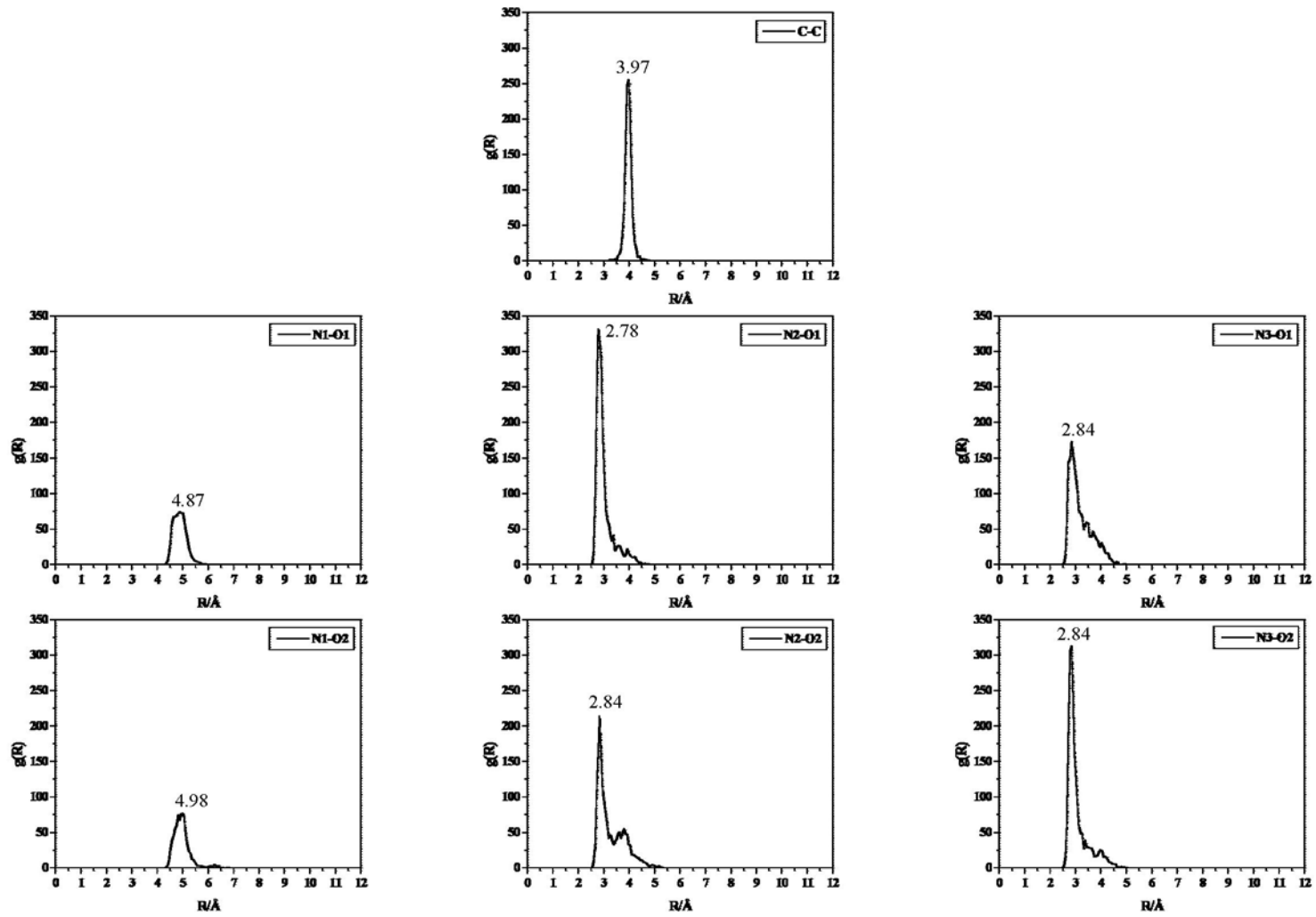


Figure C.7 (continued)

Figure C.8 $g(R)$ obtained from MD- $[\text{Gdm}^+ - \text{FmO}^-]_{\text{aq, frozen}}^{R=6.3}$;

characteristic distances are given, with $n(R)$ in parentheses.

(see Figure 2.1 for atom numbering)

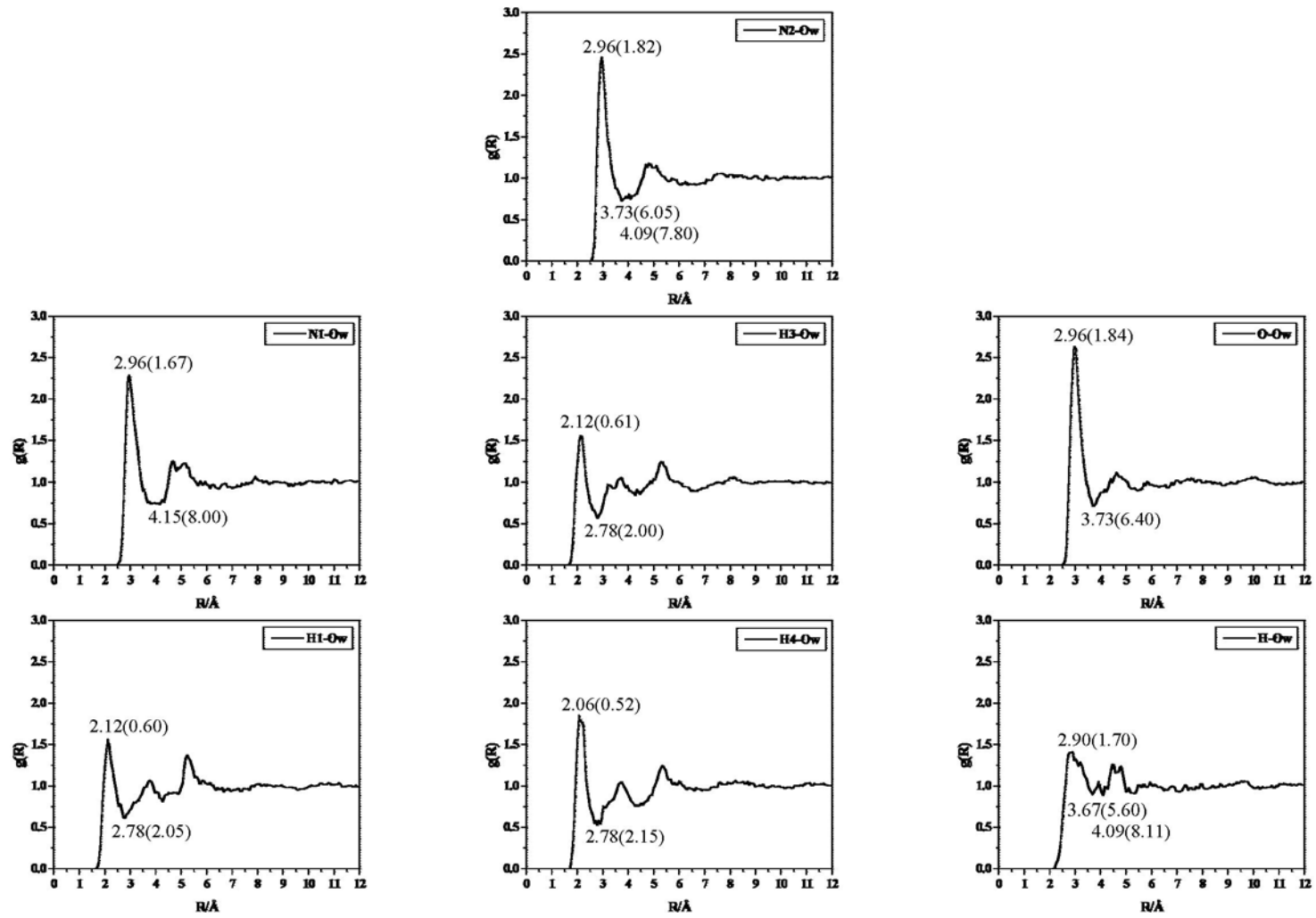


Figure C.8

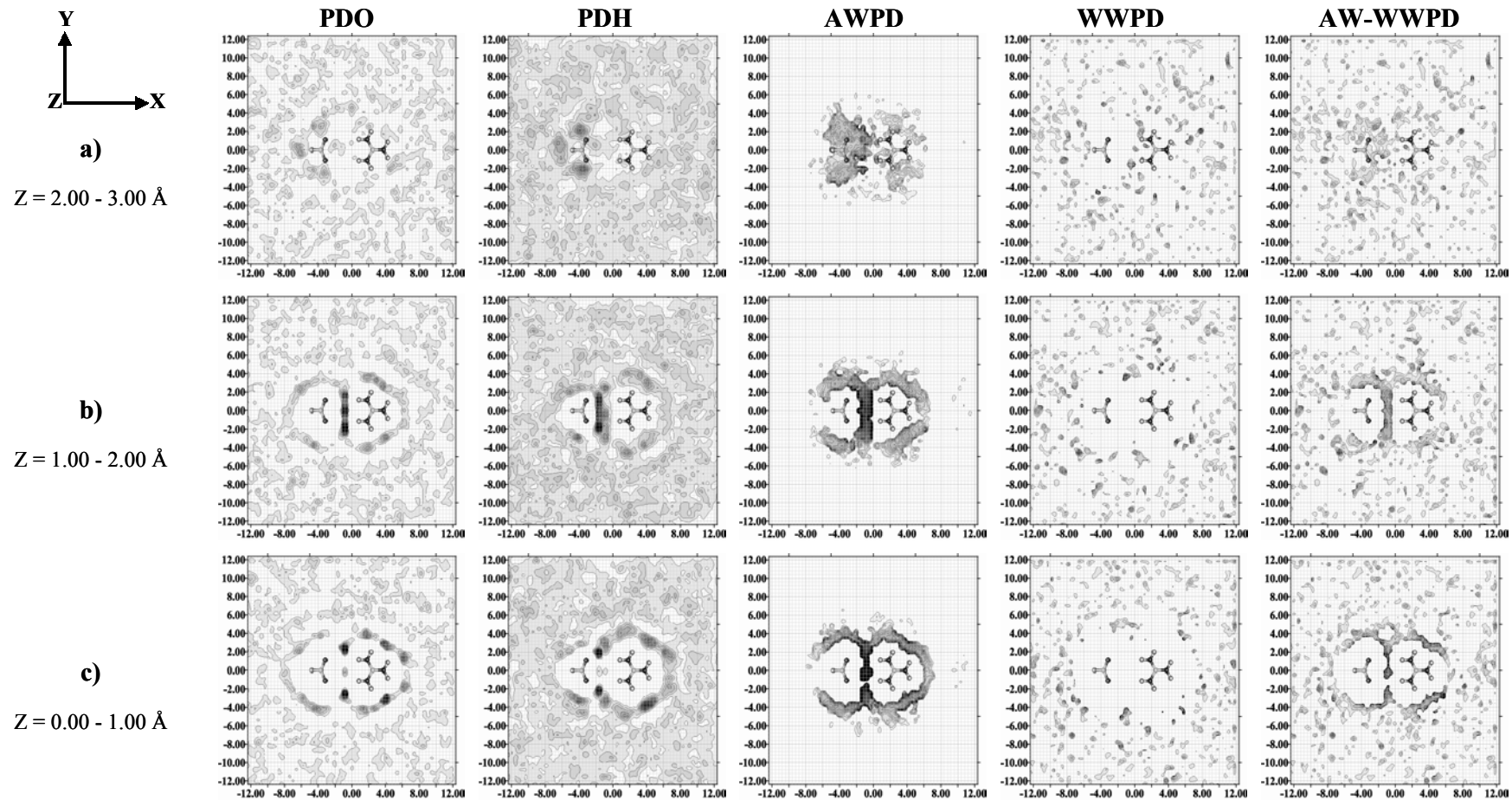


Figure C.9 The PDO, PDH, AWPD, WWPD and AW-WWPD maps obtained from MD-[Gdm⁺ - FmO⁻]_{aq, frozen}^{R = 6.3}.

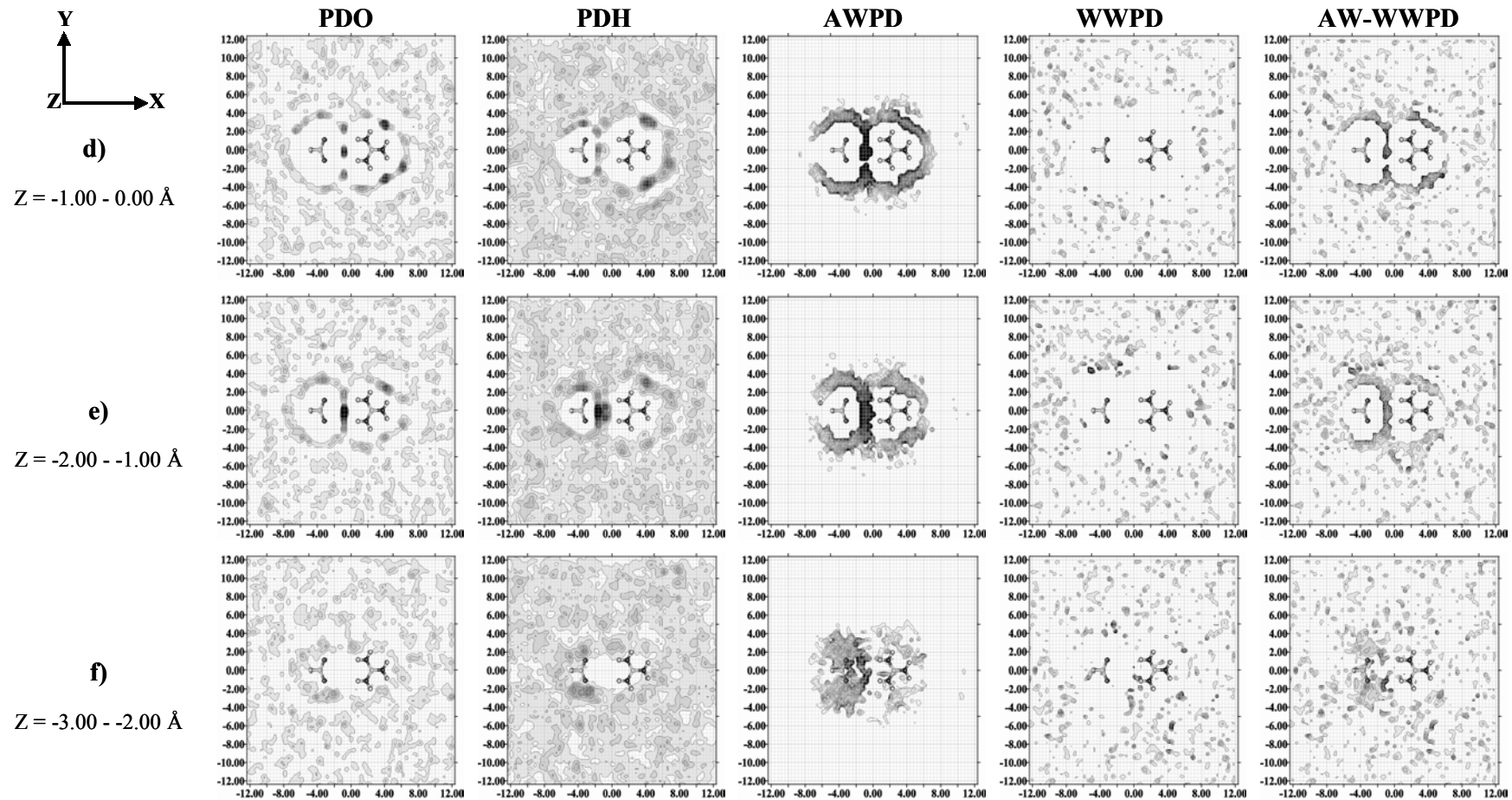


Figure C.9 (continued)

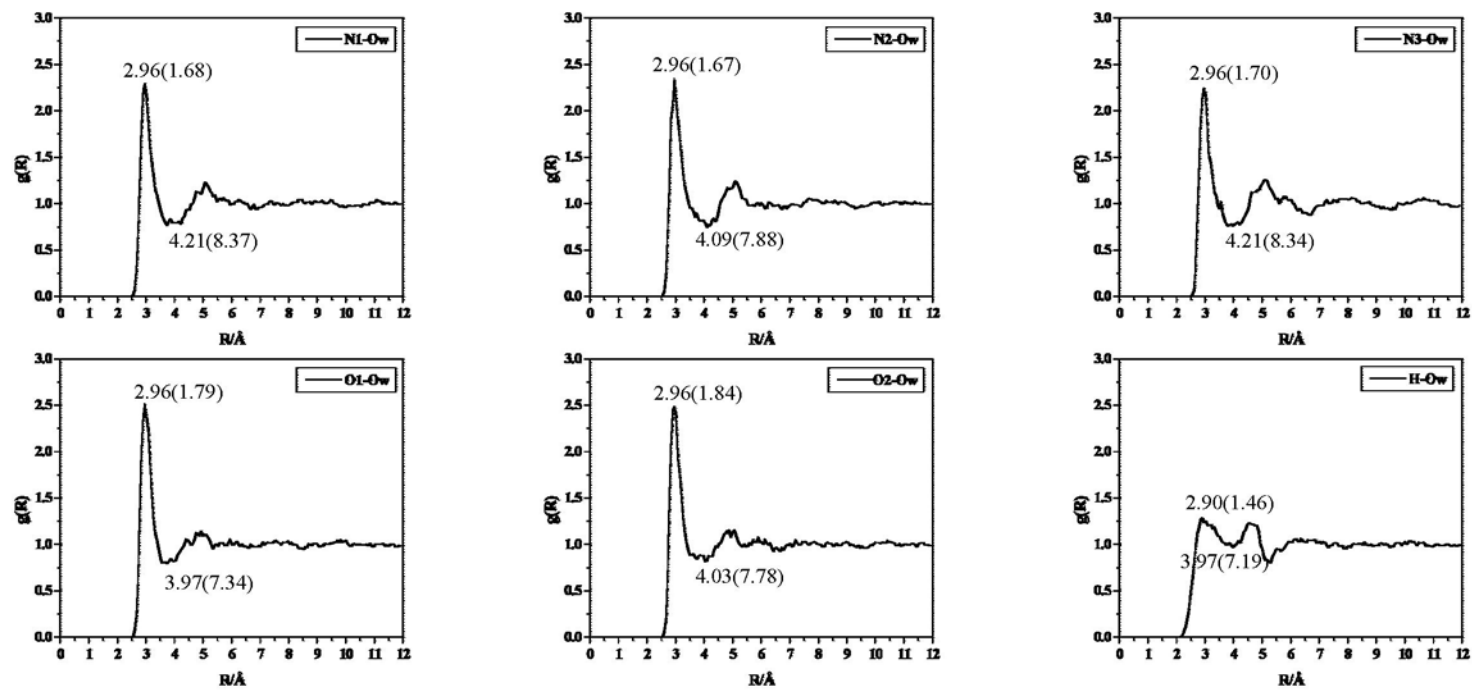


Figure C.10 $g(R)$ obtained from MD-[Gdm⁺ - FmO⁻]_{aq, free}^{R=6.3}; characteristic distances are given, with $n(R)$ in parentheses.

(see Figure 2.1 for atom numbering)

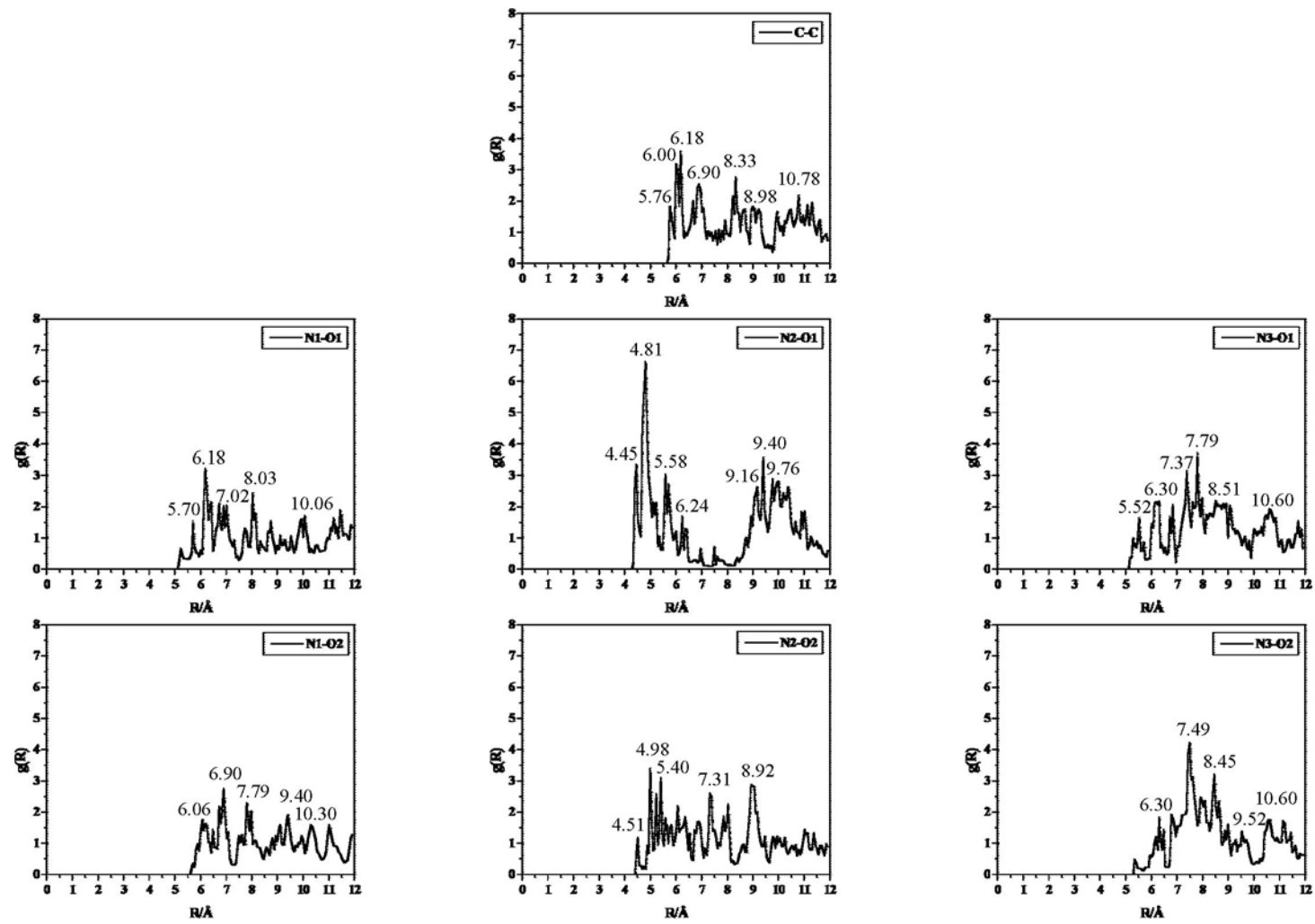


Figure C.10 (continued)

APPENDIX D

ARTICLE IN PROCEEDING OF ANSCSE-8

Additional results presented in the 8th Annual National Symposium on Computational Science and Engineering (ANSCSE-8), 21-23 July 2004, Suranaree University of Technology (SUT), Nakhon Ratchasima, Thailand.

STRUCTURES AND STABILITY OF MODEL SALT-BRIDGE INTERACTION IN AQUEOUS SOLUTION

Kritsana Sagarik¹ and Supaporn Chaivapongs²

¹*School of Chemistry, Institute of Science, Suranaree University of Technology,
Nakhon Ratchasima 30000, Thailand*

²*Department of Chemistry, Faculty of Science, Ramkhamhaeng University,
Bangkok 10240, Thailand*

ABSTRACT: Structures and stability of model salt-bridge interaction in aqueous solution were investigated using complex formed from guanidinium (GN) and formate (FM) ions. The intermolecular potentials to describe the GN-H₂O, FM-H₂O and GN-FM interactions were constructed using the Test-particle model (T-model) and applied in Molecular Dynamics (MD) simulations of the aqueous solutions at 298 K. Although the charged hydrogen bonds (H-bonds) between GN and FM are quite strong, the hydration free-energy calculations showed the possibility for the solvent-separated structure in the aqueous solutions. The structures and energetic of the H-bond networks in the vicinities of the GN-FM complex were visualized and discussed based on probability distribution (PD) maps and the average potential energy landscapes.

KEYWORDS: T-model, guanidinium, formate, salt bridge, aqueous solution

1. INTRODUCTION

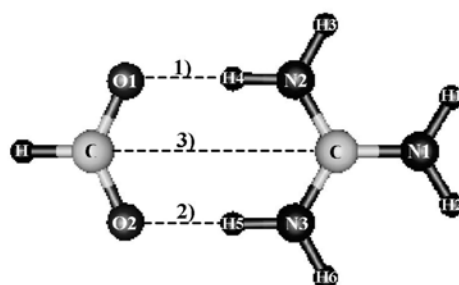
Structures and interaction energies of ion-pairs in proteins have been of interest since on average one-third of the charged residues in proteins involved in ion-pairs and 76 % of these are concerned with stabilizing the protein tertiary structures (Barlow 1983). Interaction among water, formate (FM), and guanidinium (GN) ions has been selected as model system in the study of salt-bridge interactions (Zheng 1996). In the present study, structures and energetic of the aqueous solutions of FM, GN and GN-FM complexes were investigated using MD simulations. The structures of the H-bond networks at the functional groups were displayed using various PD maps. The stability of the GN-FM complex in aqueous solution was anticipated from the free energy profile for hydration, inferred from the MD simulations.

2. COMPUTATIONAL METHODS

The T-model potentials to describe the GN-H₂O, FM-H₂O and GN-FM interactions were applied in NVE-MD simulations of the GN-FM complex in aqueous solution ($[(GN-FM)]_{aq}$) at 298 K. A GN-FM complex and 500 water molecules were put in a cubic box subject to periodic boundary conditions. The GN-FM complex was positioned at the center of the simulation box. The density of the aqueous solution was kept constant at 1 g ml⁻¹. Fifty thousand MD steps of 0.0005 ps were devoted to equilibration and another one hundred thousand steps to property calculation. Based on specified conditions, three series of MD simulations were performed on $[(GN-FM)]_{aq}$. The calculation of free energy of hydration was made using MD simulations in combination with the Thermodynamic Integration (TI) method (Meizei 1986). In order to ensure the reversible path in the free energy calculation, the distance between the center of mass of FM and GN was varied from 3 Å to 9 Å.

3. RESULTS AND DISCUSSION

The gas-phase equilibrium structure and interaction energy of the GN-FM complex, obtained from the T-model (Böhm 1984) are shown in Figure 1. The oxygen probability distribution (PDO) maps in Figure 2a show well defined H-bond networks in the vicinities of GN compared to FM. They are labeled with **G**, **D**, **A** and **C**, respectively. The shapes of the average potential energy landscapes in Figure 3 reveal that the motions of water molecules are confined in long and narrow energy valleys, spanning from O1 to H4 to H3 as well as from O2 to H5 to H6. This suggests that water molecules could move or exchange easier within the H-bond networks, compared to the water exchange between the first hydration shell and outside. The AWPDP and AW-WWPD maps show that the GN-FM complex is quite stable in aqueous solutions. In the course of MD simulations, the H-bond lifetime ($\langle t_{N-H...O} \rangle$) in Table 1 amounts on average to 88 %. The relative free energy profile in Figure 4 shows two possible thermodynamic states which correspond to the ion-pair and solvent-separated structures. The solvent-separated structure is about 73 kJ mol⁻¹ more stable than the ion-pair structure. The free energy barrier to the conversion from the ion-pair to solvent-separated structures is about 5 kJ mol⁻¹, whereas from the solvent-separated to ion-pair is about 78 kJ mol⁻¹.



$$\Delta E^{\text{T-model}} = -480.765 \text{ kJ mol}^{-1}$$

- 1) H4...O1 = 1.73 Å 2) H5...O2 = 1.73 Å
 N2...O1 = 2.74 Å 3) N3...O2 = 2.74 Å
 N2-H4...O1 = 177.67° N3-H5...O2 = 177.86°
 3) C...C = 3.93 Å

Figure 1. Equilibrium geometry of GN-FM computed from T-model potential.

Table 1. Some average H-bond distances ($\langle R_{N-H...O} \rangle$) and angles ($\langle \theta_{N-H...O} \rangle$) as well as the H-bond lifetimes ($\langle t_{N-H...O} \rangle$) derived from MD simulations.

SD = Standard Deviation.

Distance and angle are in Å and degree, respectively.

H-bond		SD	H-bond		SD
N2-H4...O1	$\langle R_{N2-H4...O1} \rangle$	3.02	N3-H5...O1	$\langle R_{N3-H5...O1} \rangle$	3.20
	$\langle \theta_{N2-H4...O1} \rangle$	23.27		$\langle \theta_{N3-H5...O1} \rangle$	30.02
	$\langle t_{N2-H4...O1} \rangle$	93.45		$\langle t_{N3-H5...O1} \rangle$	87.16
N2-H4...O2	$\langle R_{N2-H4...O2} \rangle$	3.24	N3-H5...O2	$\langle R_{N3-H5...O2} \rangle$	3.06
	$\langle \theta_{N2-H4...O2} \rangle$	30.69		$\langle \theta_{N3-H5...O2} \rangle$	23.17
	$\langle t_{N2-H4...O2} \rangle$	80.94		$\langle t_{N3-H5...O2} \rangle$	88.64

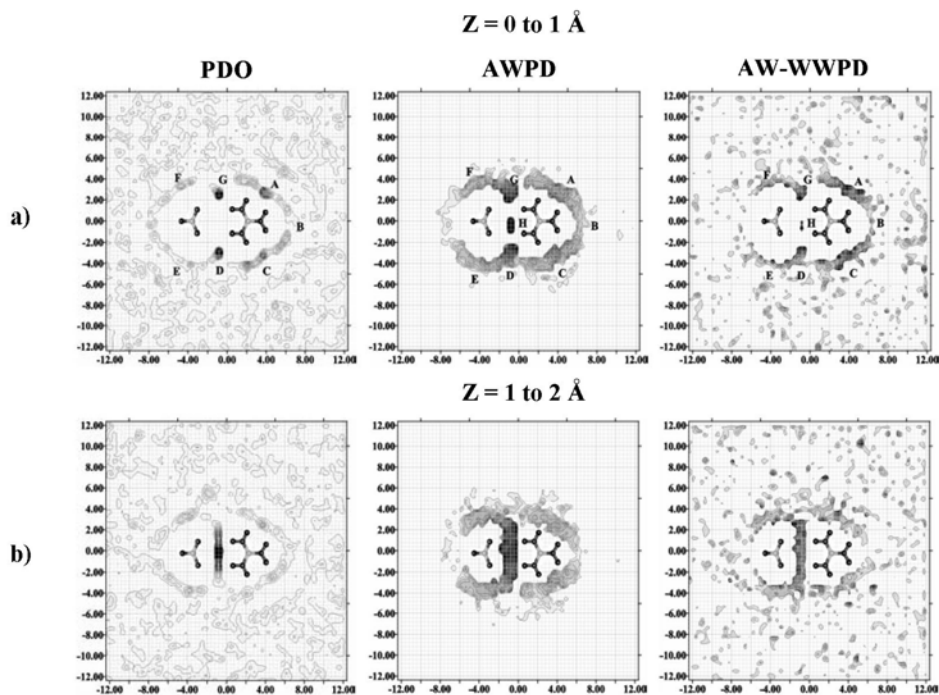


Figure 2. PDO, AWPD and AW-WWPD derived from MD simulations.

PDO = the oxygen probability distribution map.
AWPD = the average solute-solvent interaction energy probability distribution map.
AW-WWPD = total-average interaction energy probability distribution map.

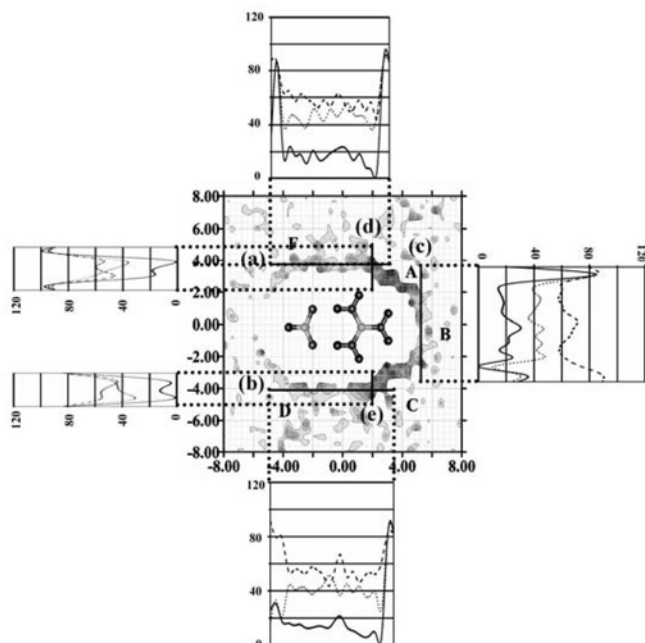


Figure 3. Average potential energy landscapes derived from MD simulations.

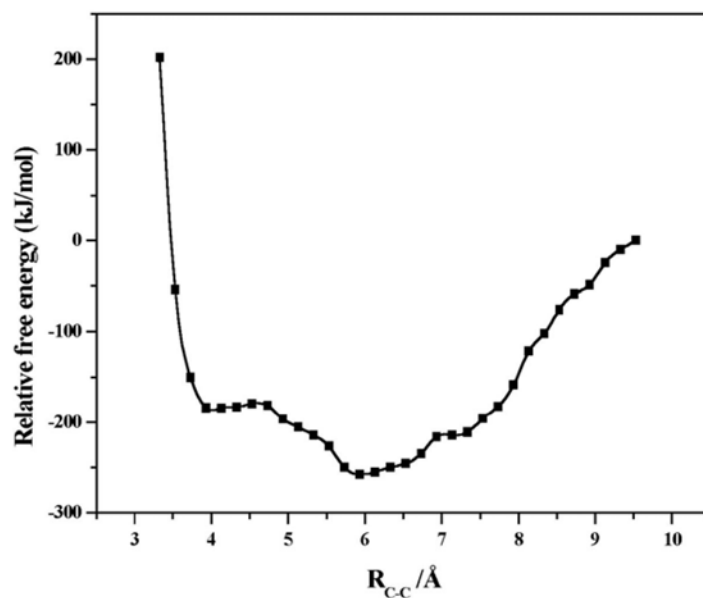


Figure 4. Free energy profile for [(GN-FM)]_{aq}.

4. REFERENCES

- Barlow, D.J., and Thornton, J.M. (1983). " Ion-pairs in proteins." *Journal of Molecular Biology*. Vol. 168, 867-885.
- Böhm, H.J., Ahlrichs, R., Scharf, P., and Schiffer, H. (1984). " Intermolecular potentials for CH₄, CH₃F, CHF₃, CH₃Cl, CH₂Cl₂, CH₃CN and CO₂." *Journal of Chemical Physics*. Vol.81, No.3, 1389-1395.
- Meizei, M. and Beveridge, D. L. (1986). " Computer Simulation of Chemical and Biomolecular Systems. " *Free Energy Simulations*. Annals of the New York Academy of Sciences. Vol.482, 1-26.
- Zheng, Y-J., and Ornstein, R.L. (1996). " What happens to salt-bridges in nonaqueous environment: Insights from quantum mechanics calculations. " *Journal of American Chemical Society*. Vol.118, 11237-11243.

CURRICULUM VITAE

POL. CAPT. SUPAPORN CHAIYAPONGS

Born : February 11, 1960, Bangkok

Citizenship : Thailand

Education :

1982 B.Sc. (Chemistry), Silpakorn University, Nakhonpathom, Thailand

1994 M.S. (Applied Chemistry), Ramkhamhaeng University, Bangkok, Thailand

2004 Ph.D. (Chemistry), Suranaree University of Technology,

Nakhon Ratchasima, Thailand

Experience :

1983-1992 Sub-Inspector, Toxicology Sub-Division,
Institute of Forensic Medicine, Police Department,
Bangkok, Thailand

1996-present Lecturer, Department of Chemistry, Faculty of Science,
Ramkhamhaeng University, Bangkok, Thailand

Publications :

1. Sagarik, K., and Chaiyapongs, S. (2004). Structures and stability of model salt-bridge interaction in aqueous solution. In **Proceedings of the 8th Annual National Symposium on Computational Science and Engineering (ANSCSE-8)**. (pp. 9-12) Nakhon Ratchasima, Thailand: Suranaree University of Technology.
2. Sagarik, K., and Chaiyapongs, S. (2005). Structures and stability of salt-bridge in aqueous solution. **Biophysical Chemistry**. accepted for publication.